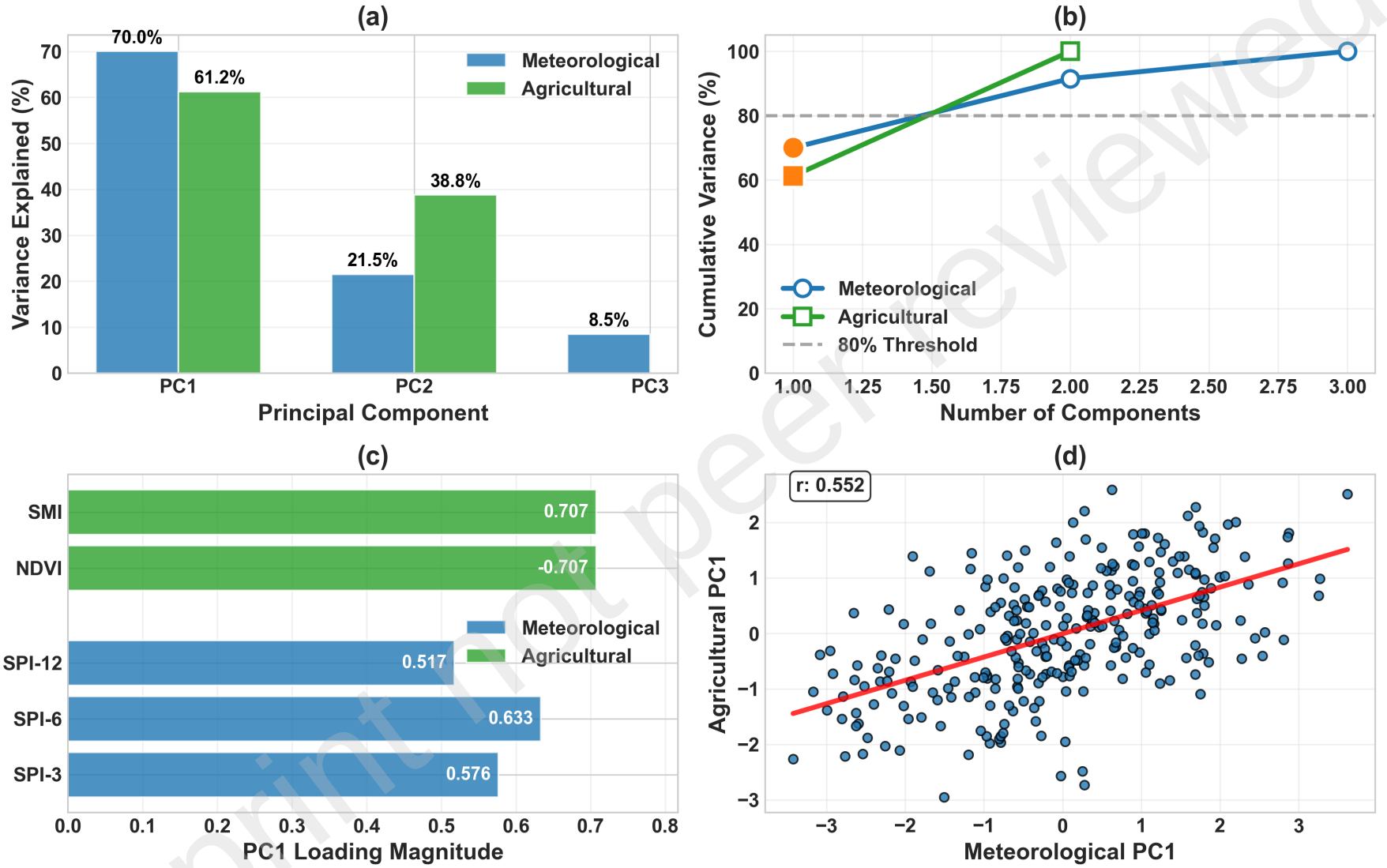

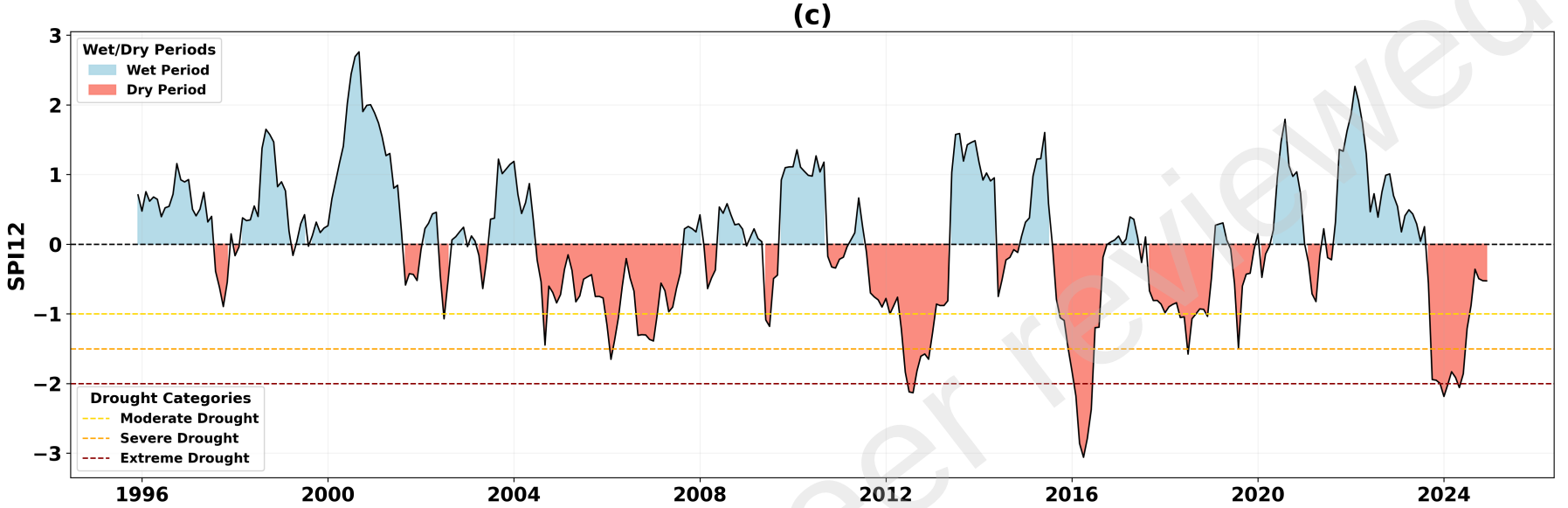

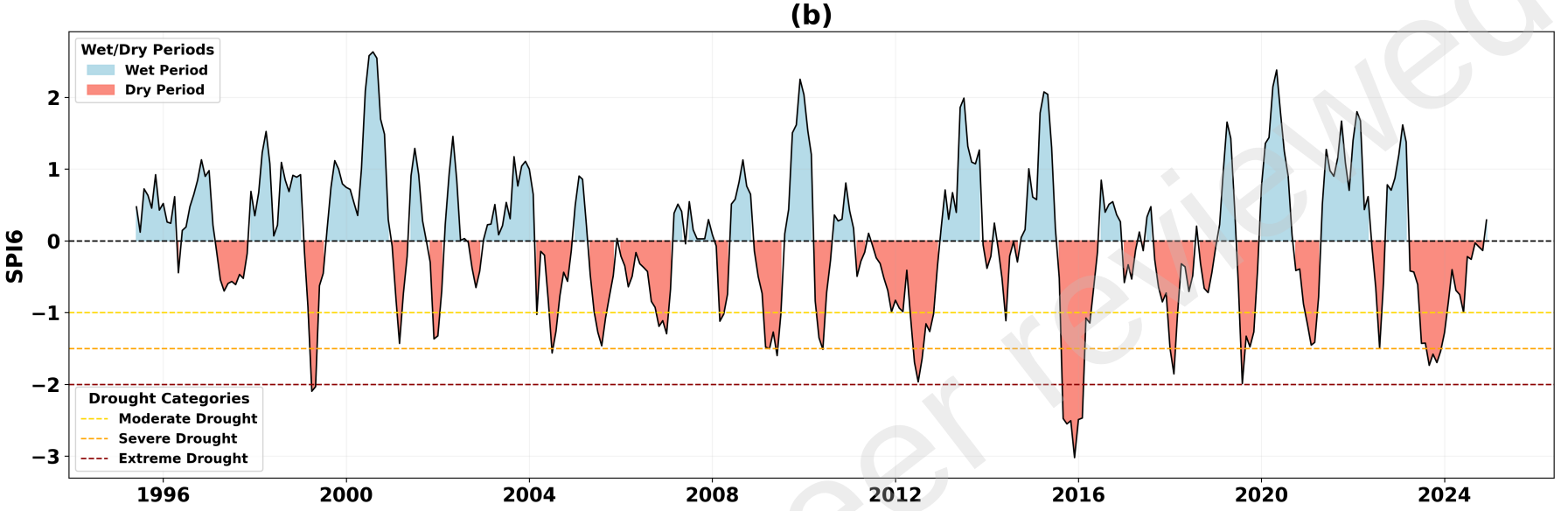

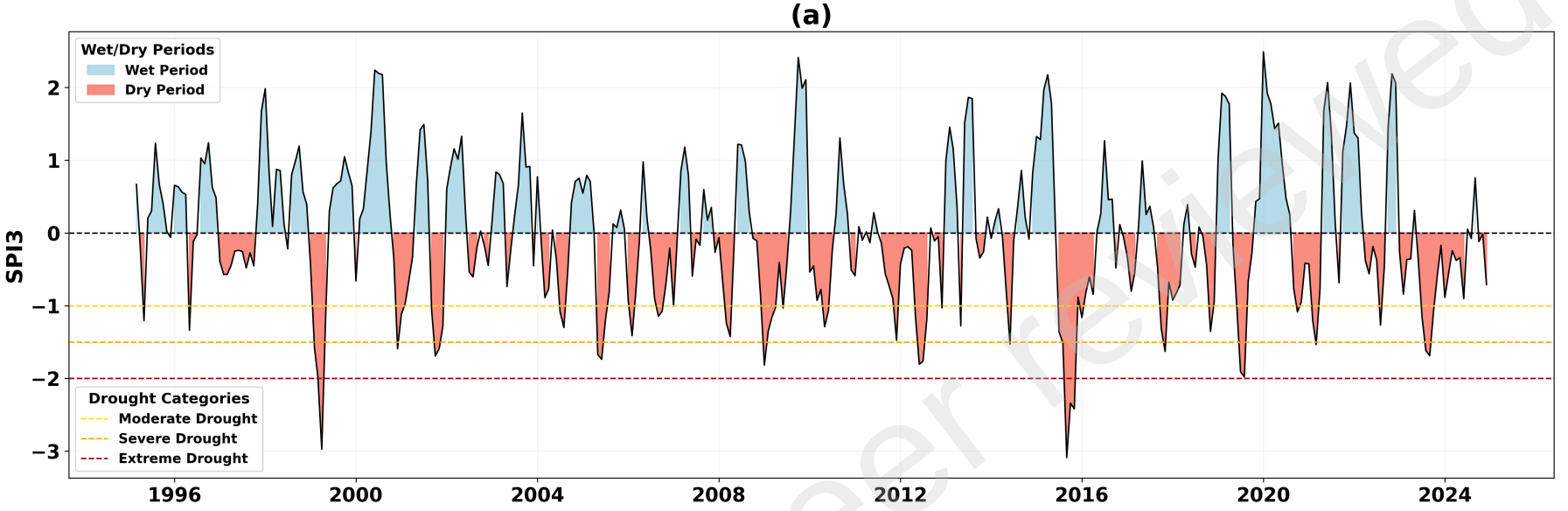

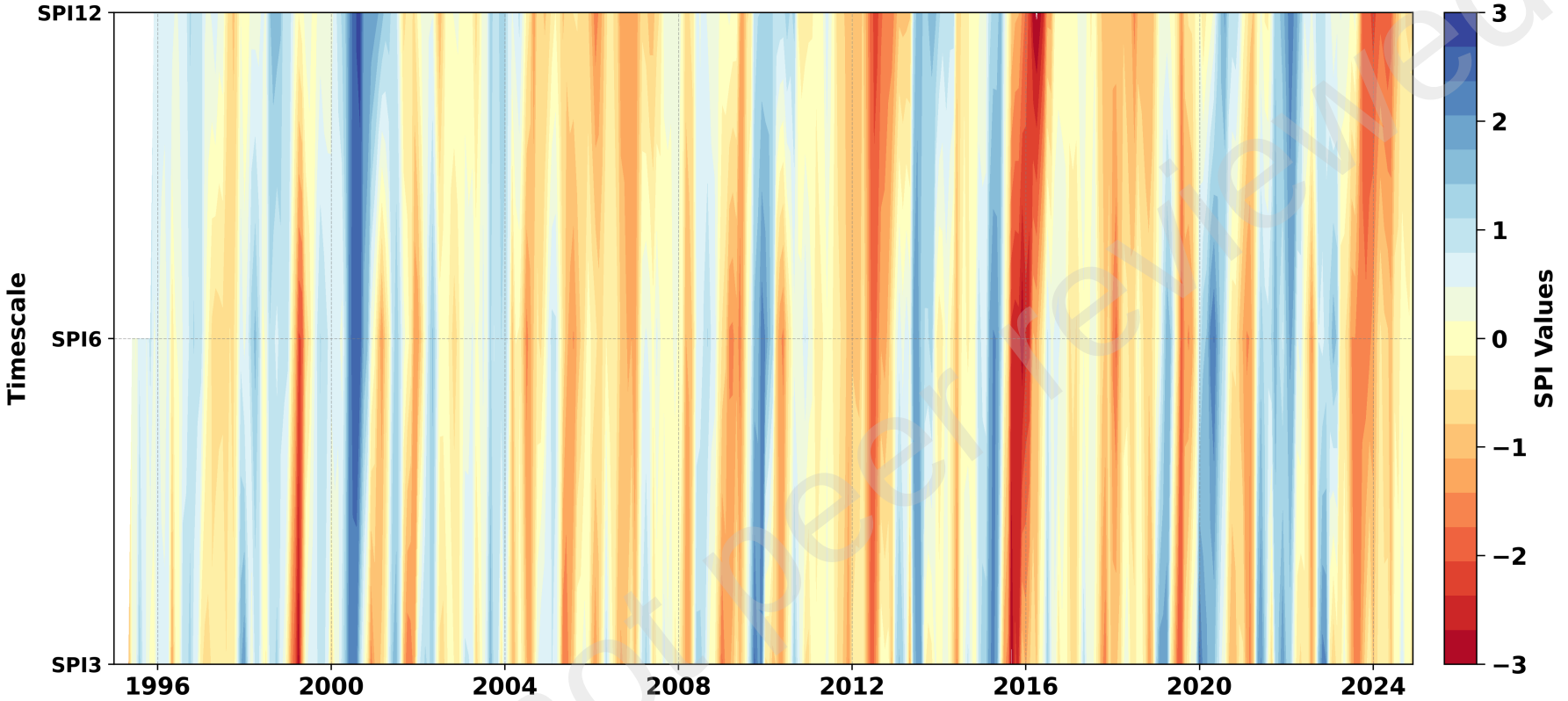

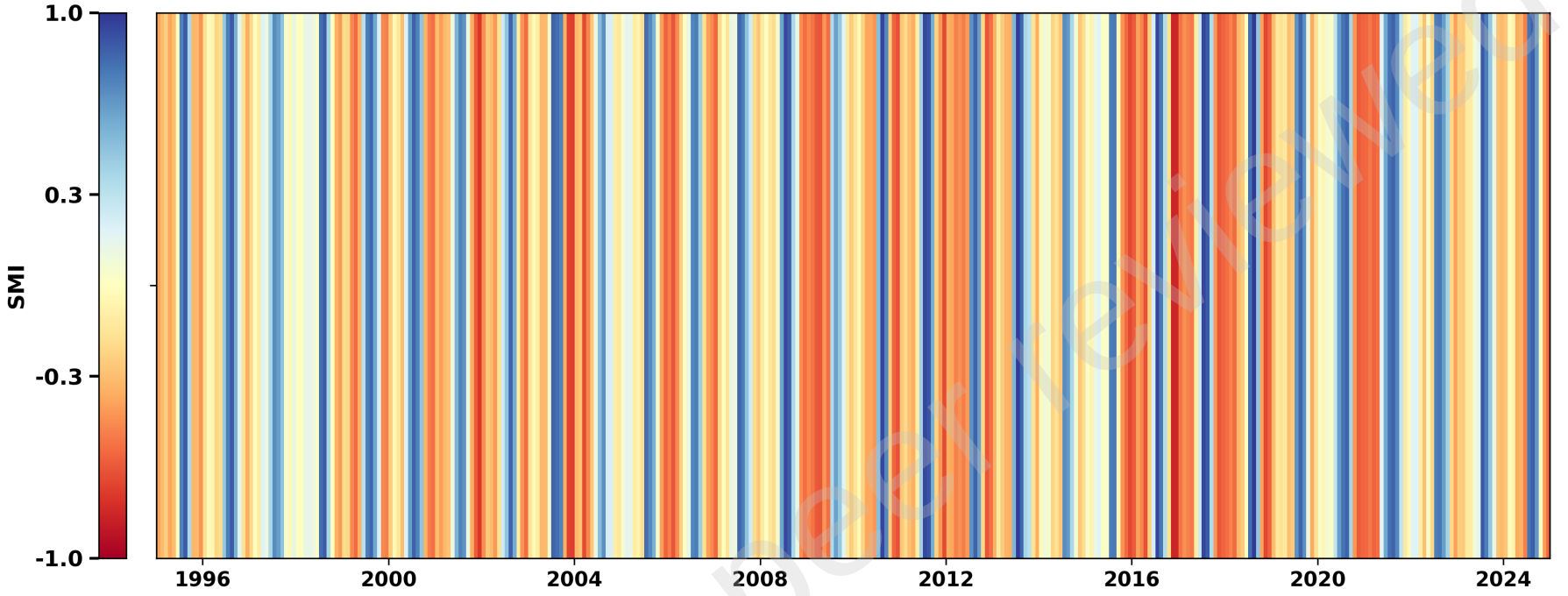

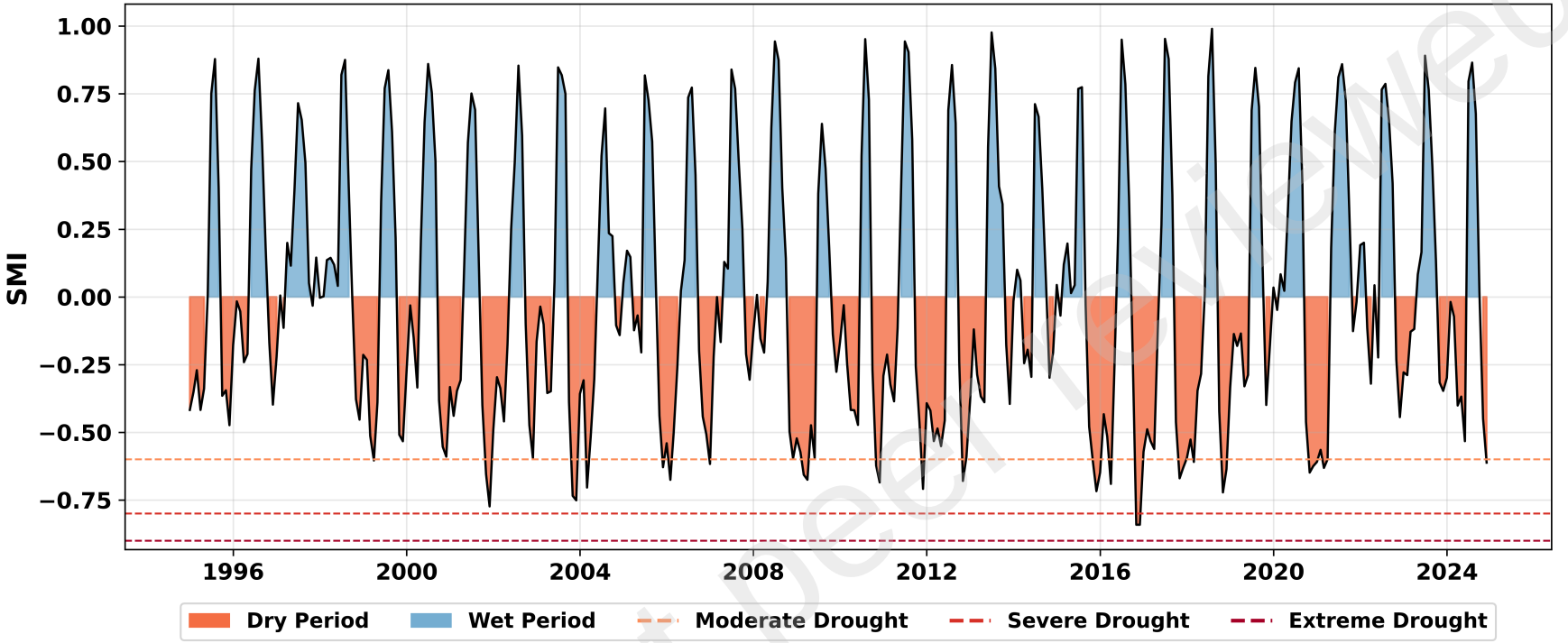

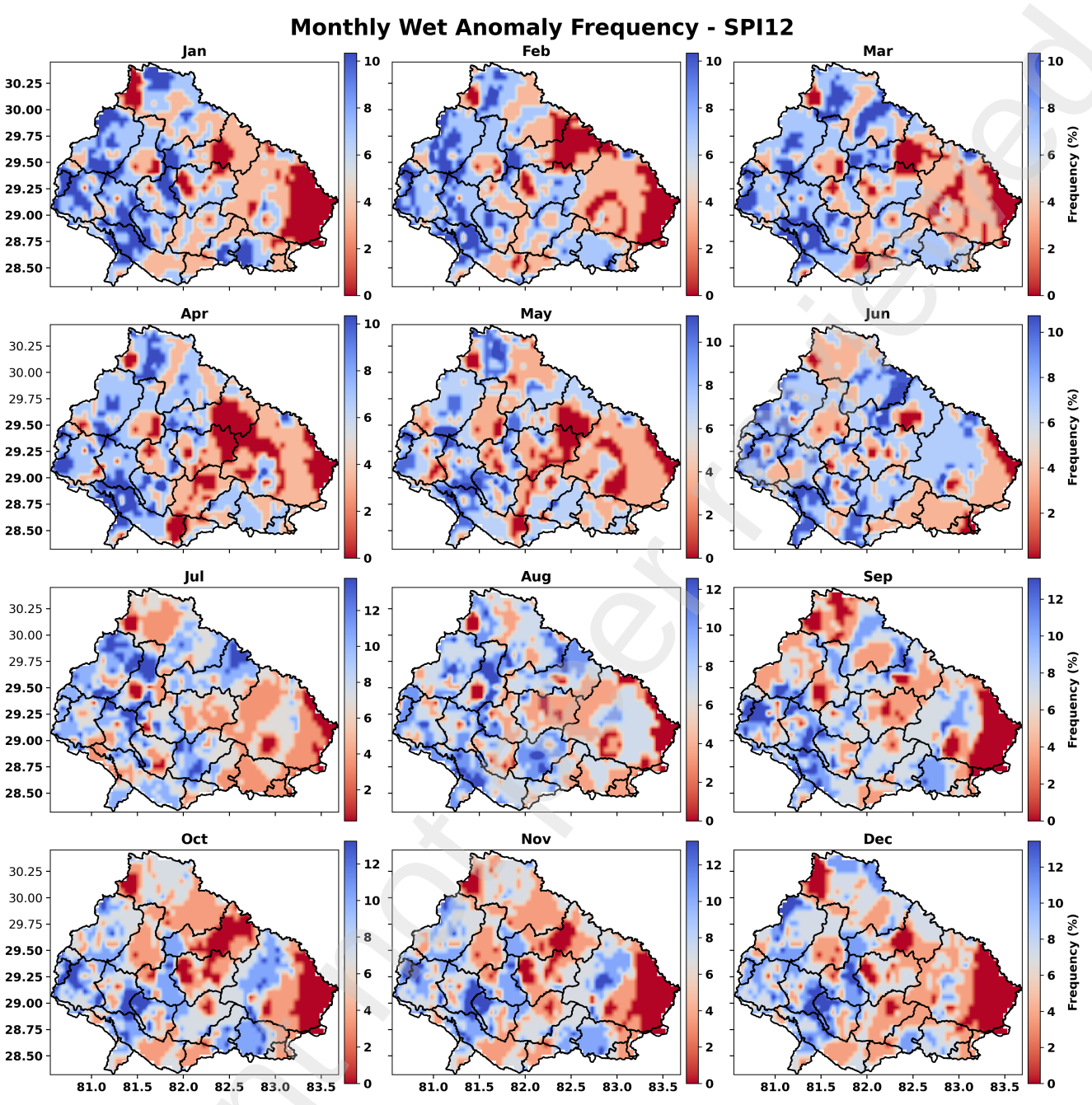

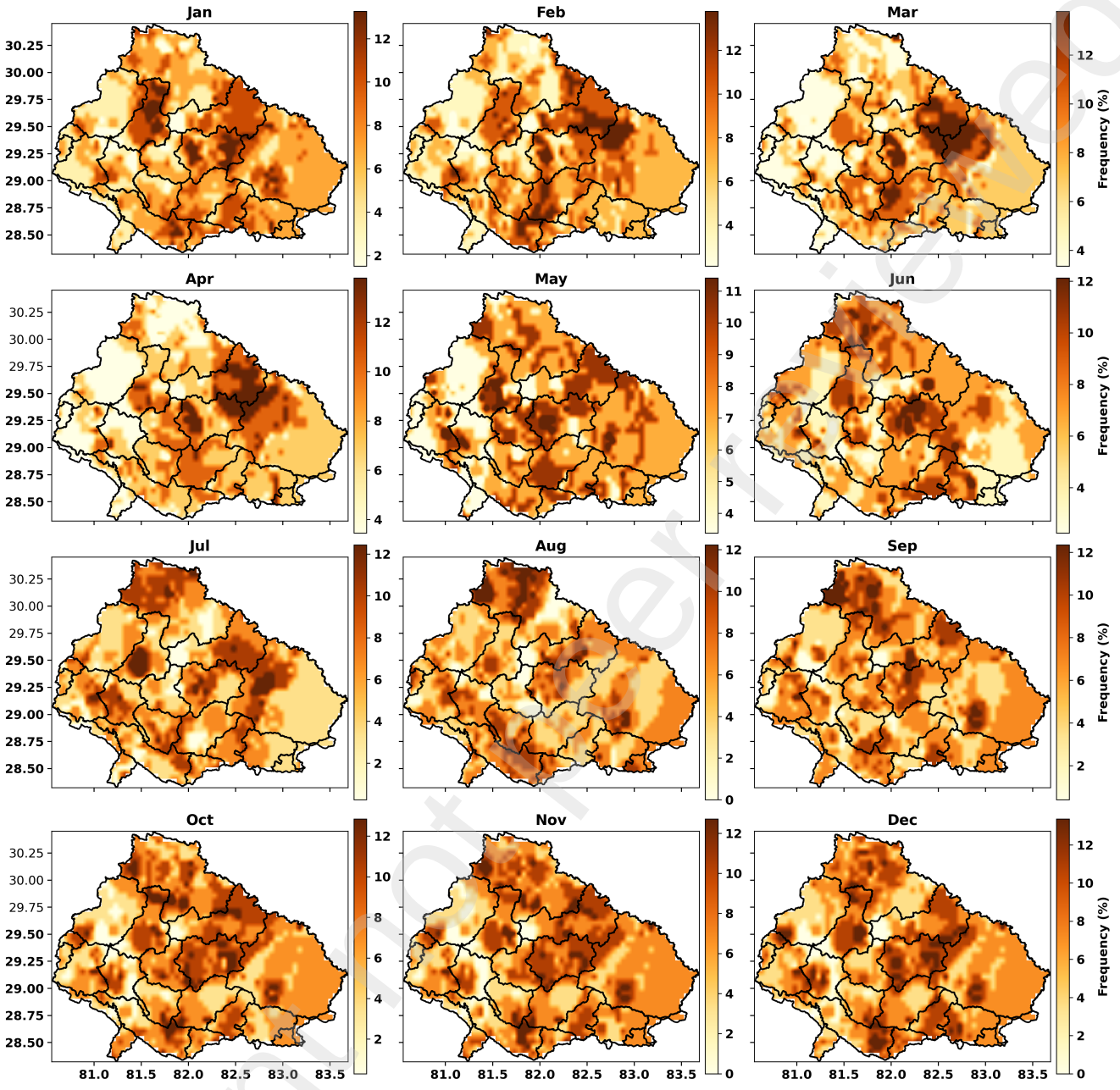

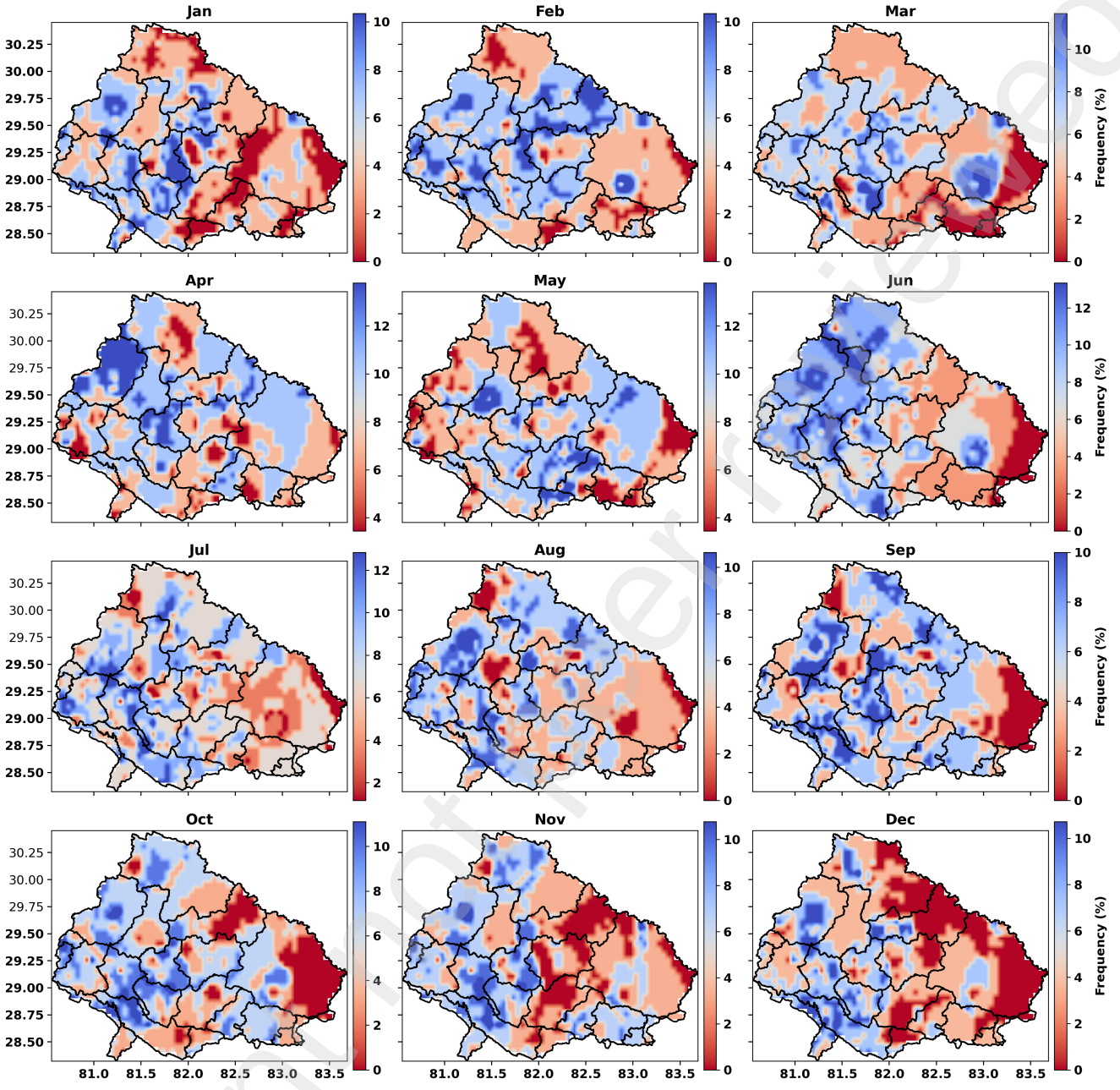

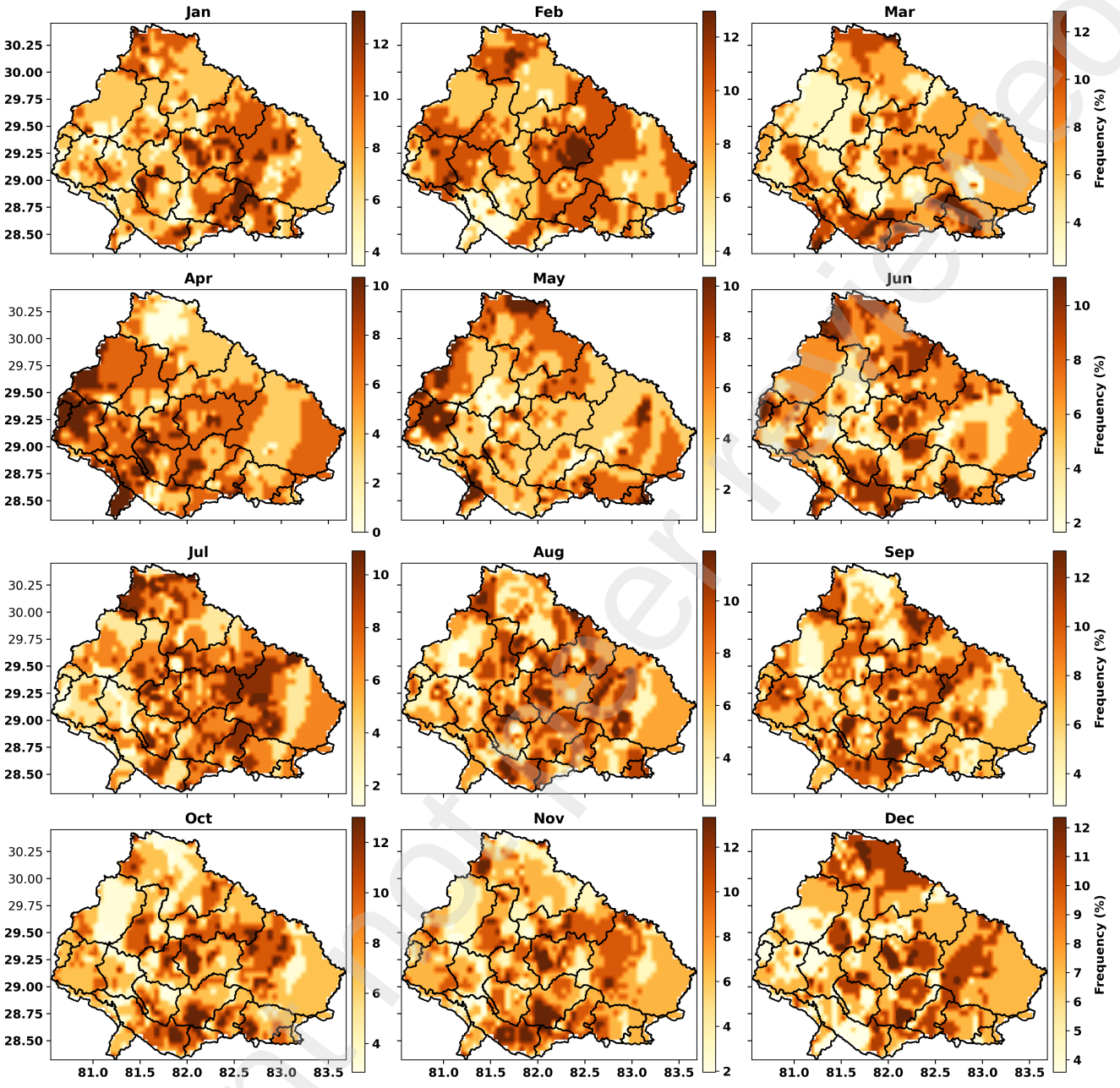

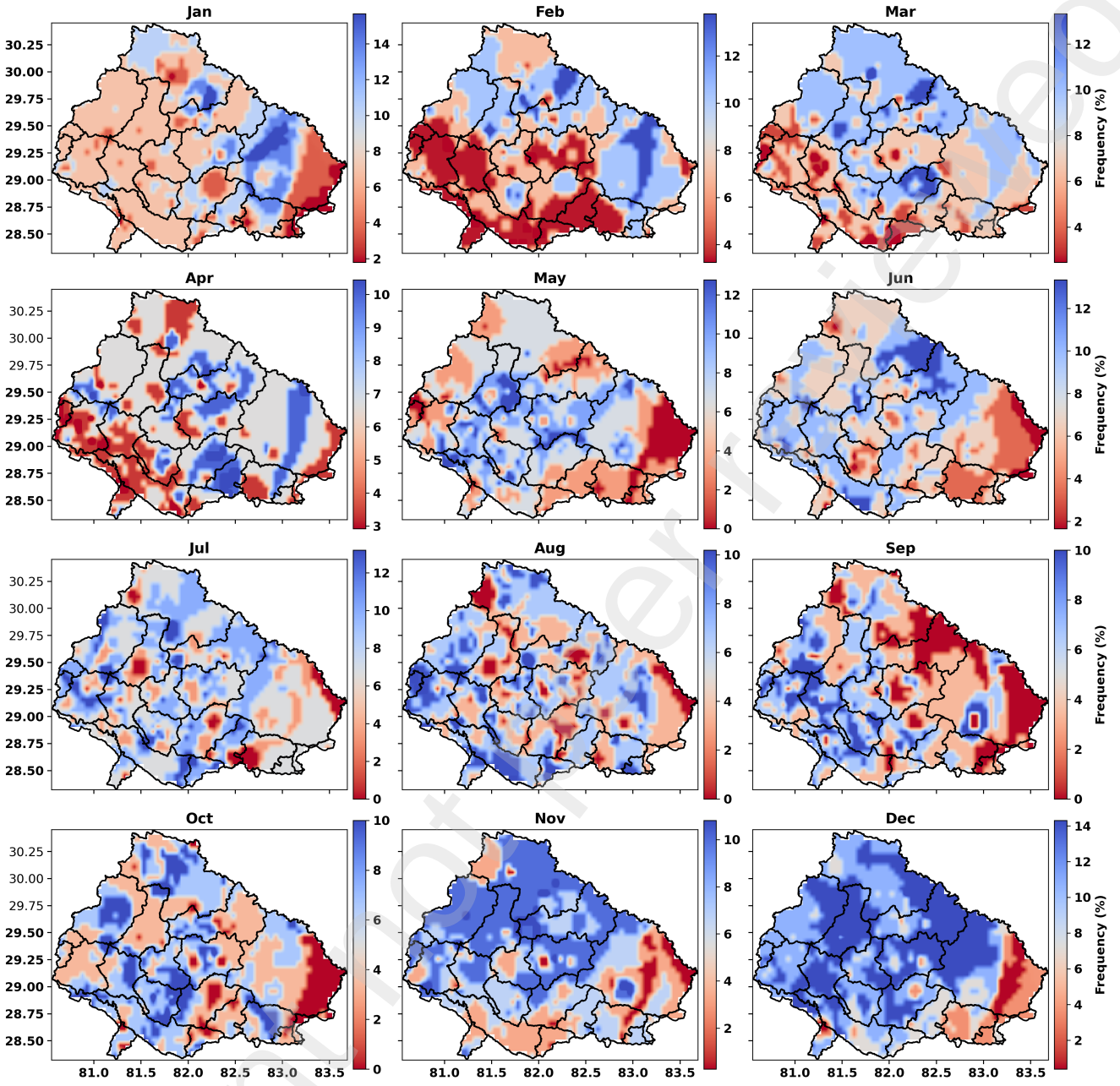

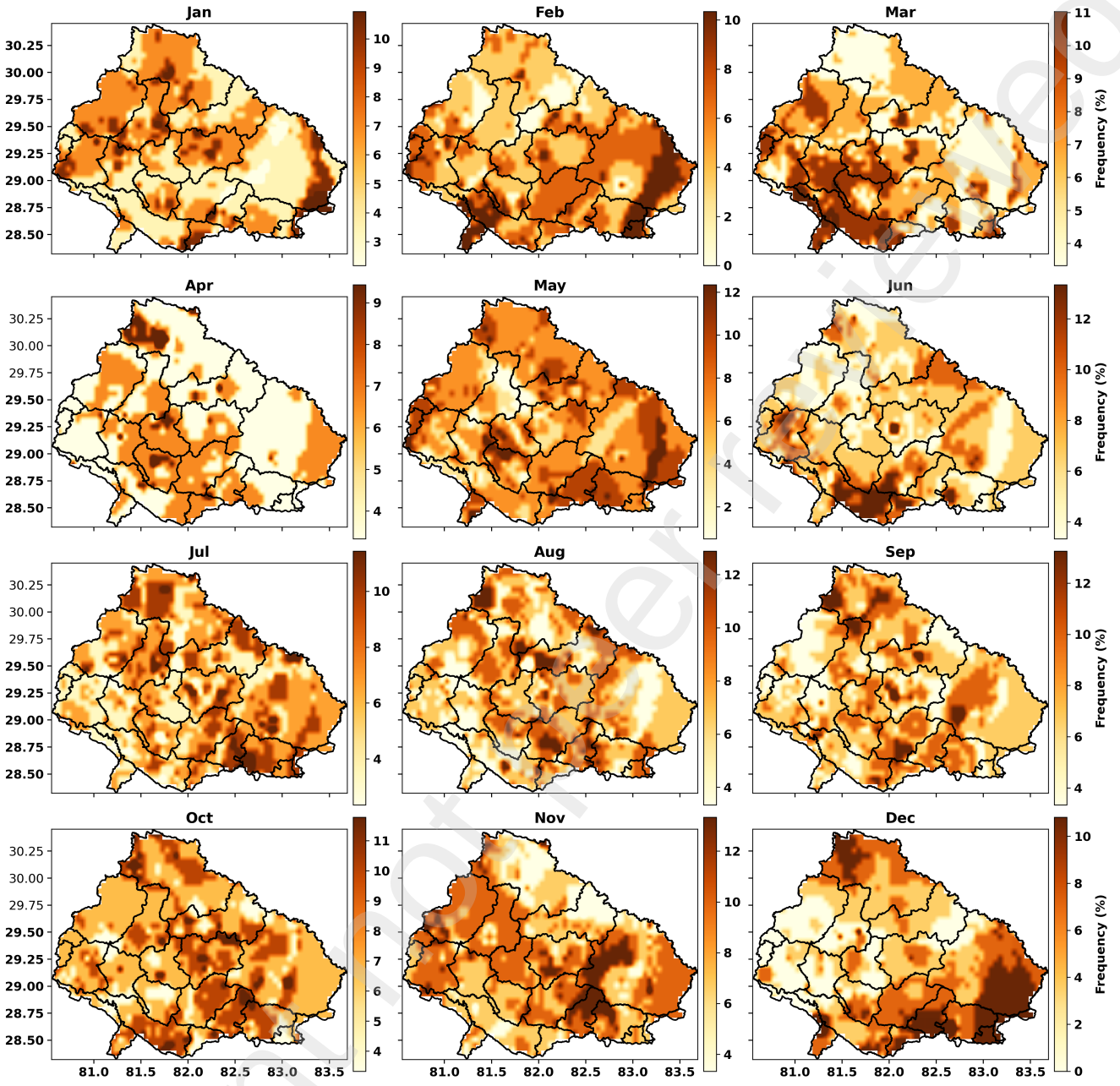

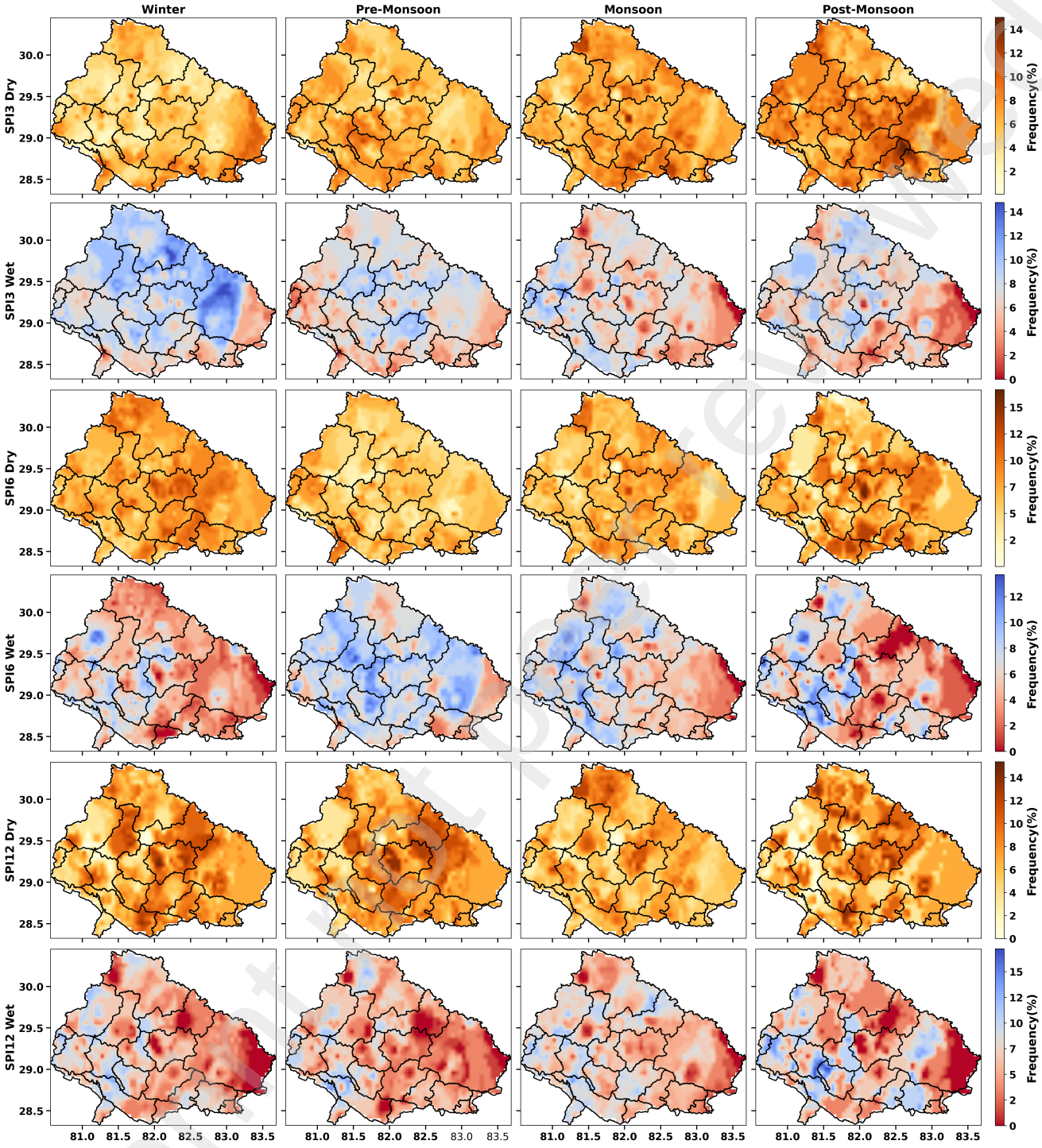

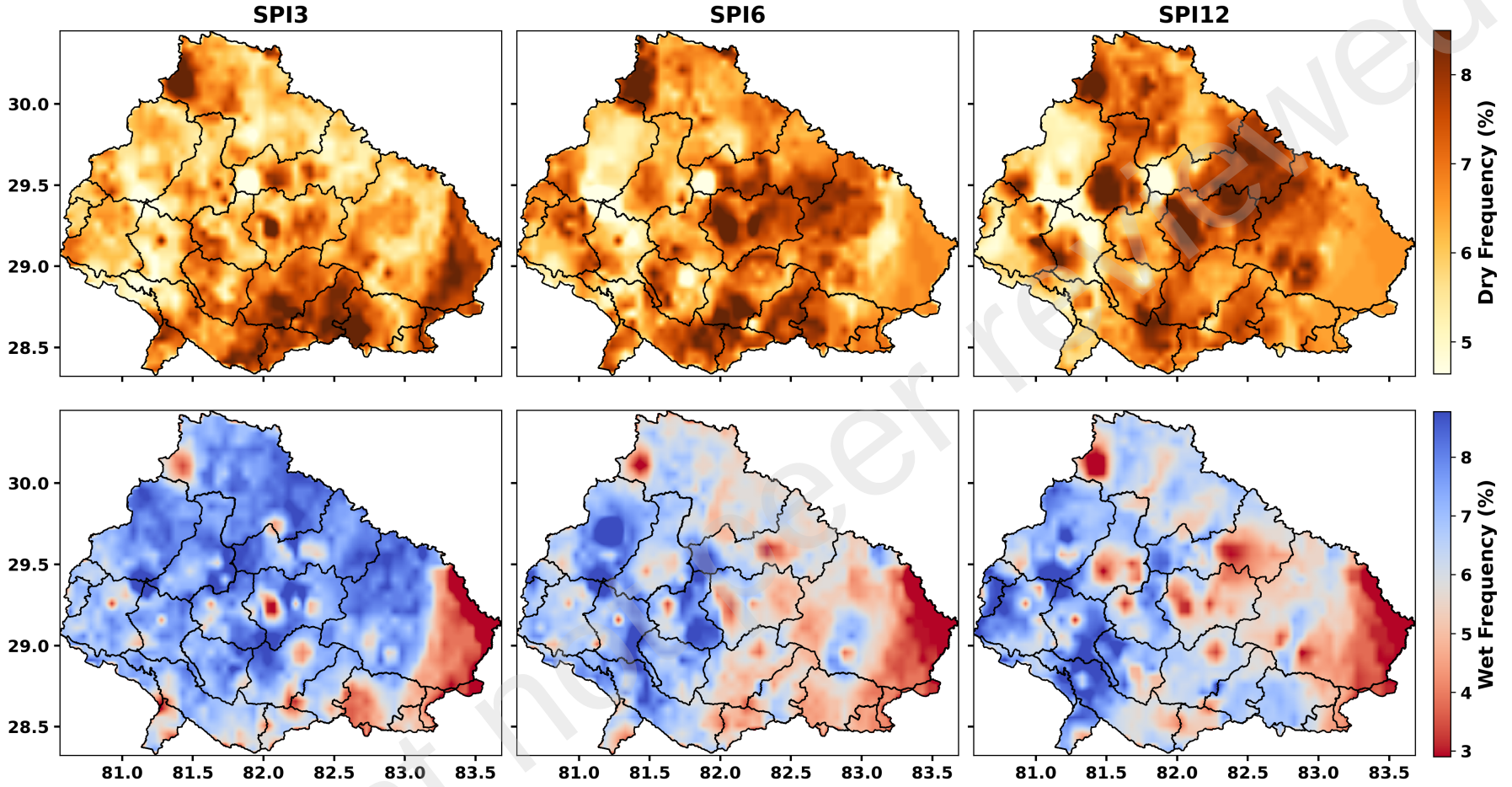

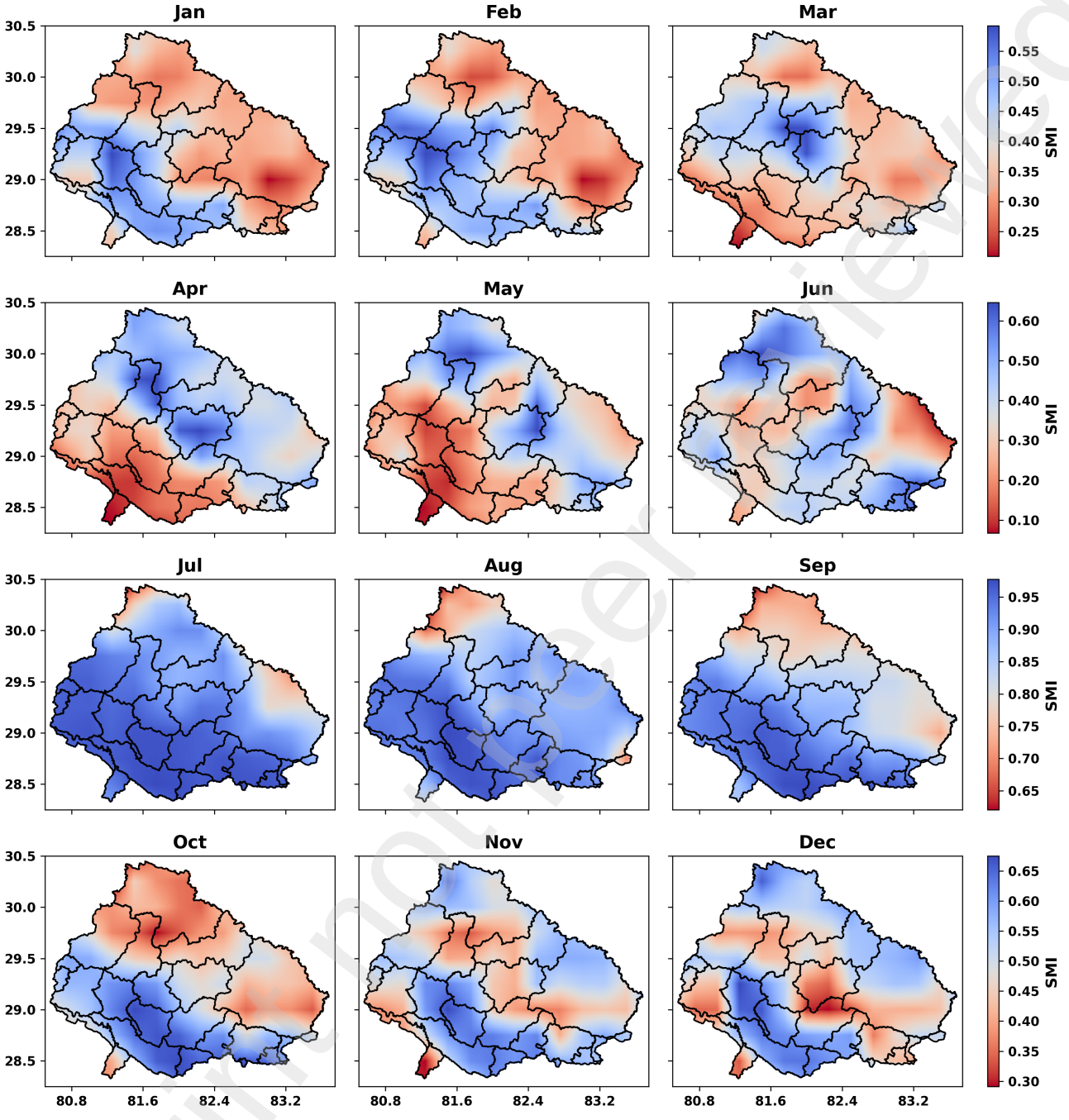

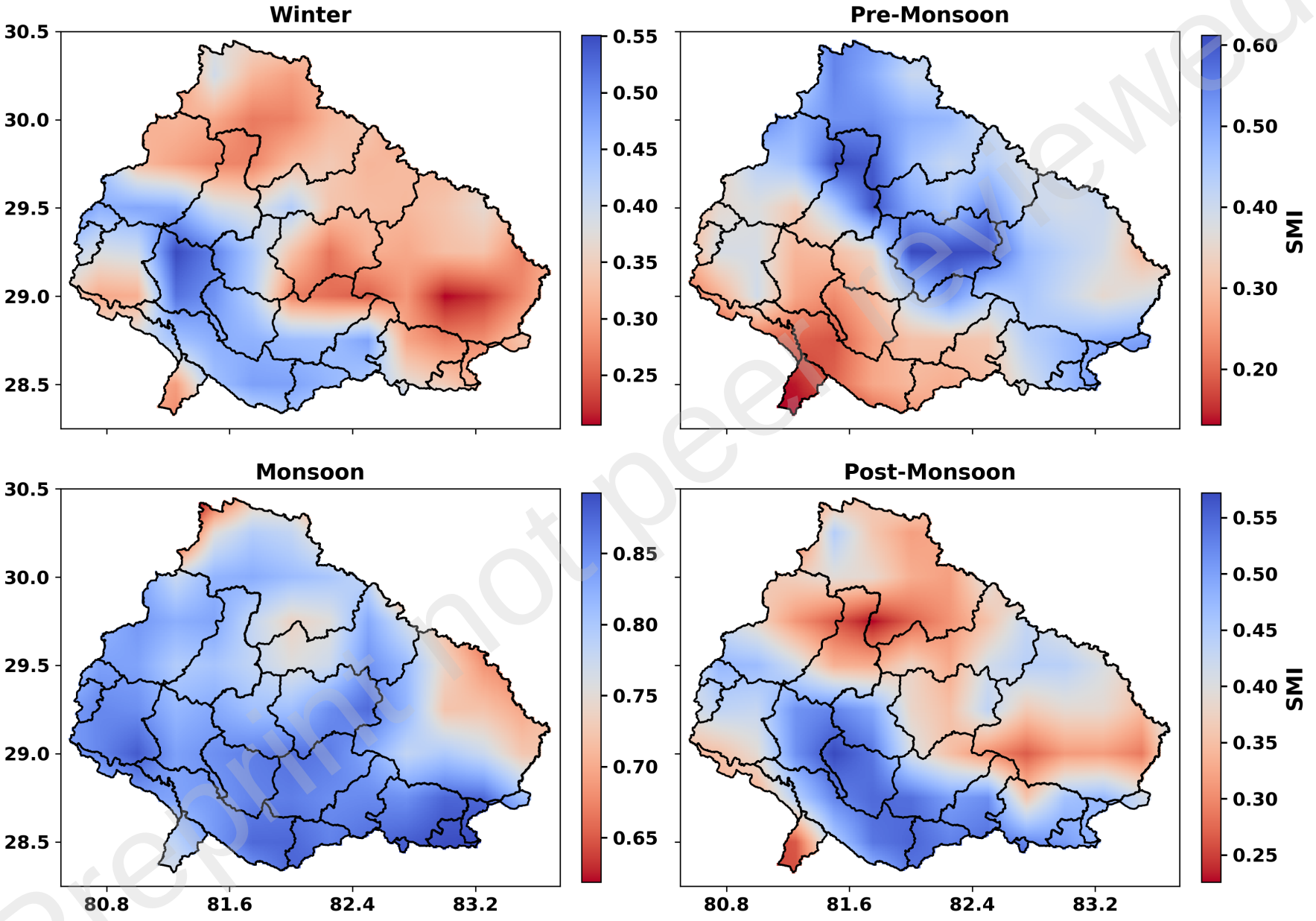

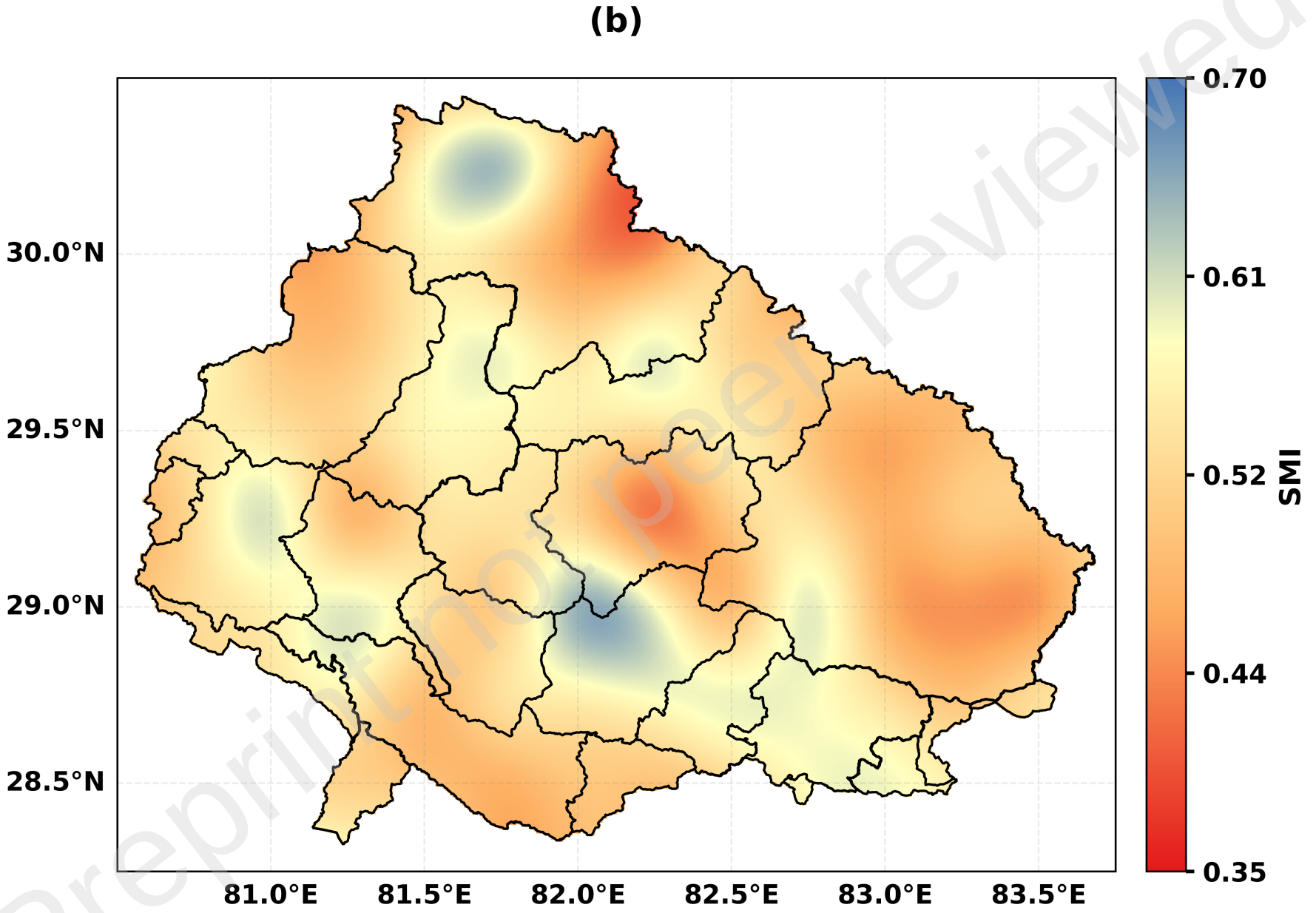

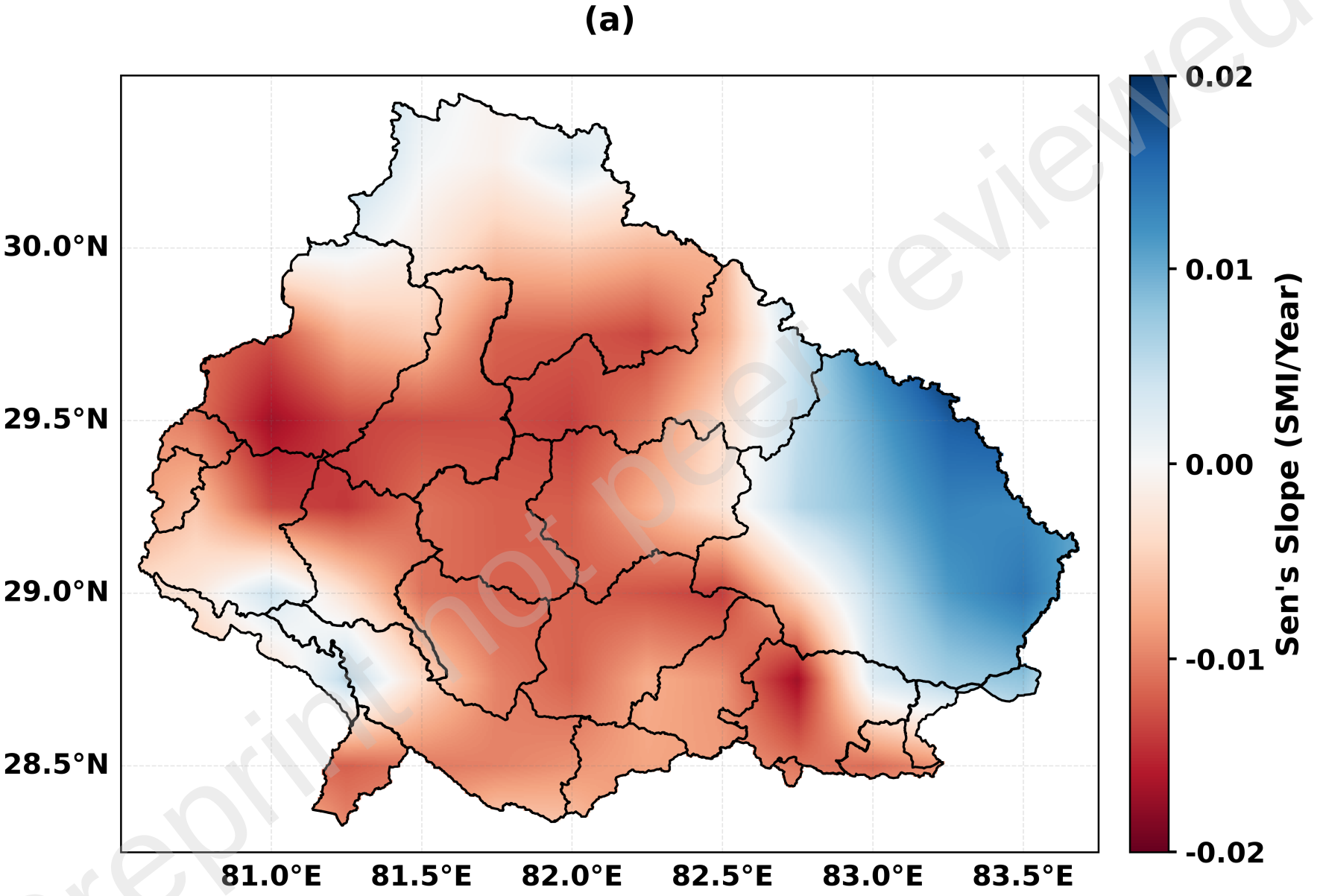

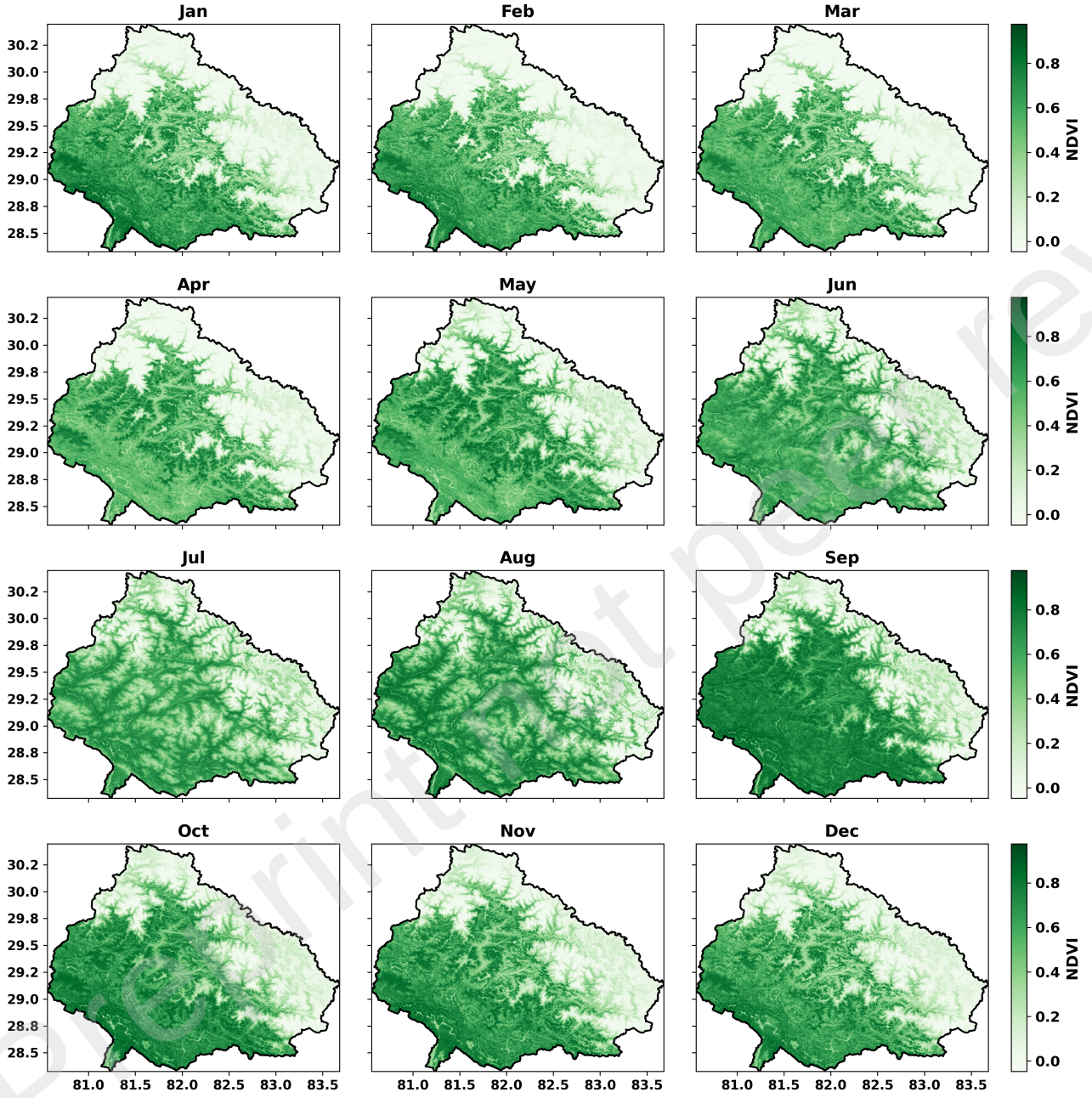

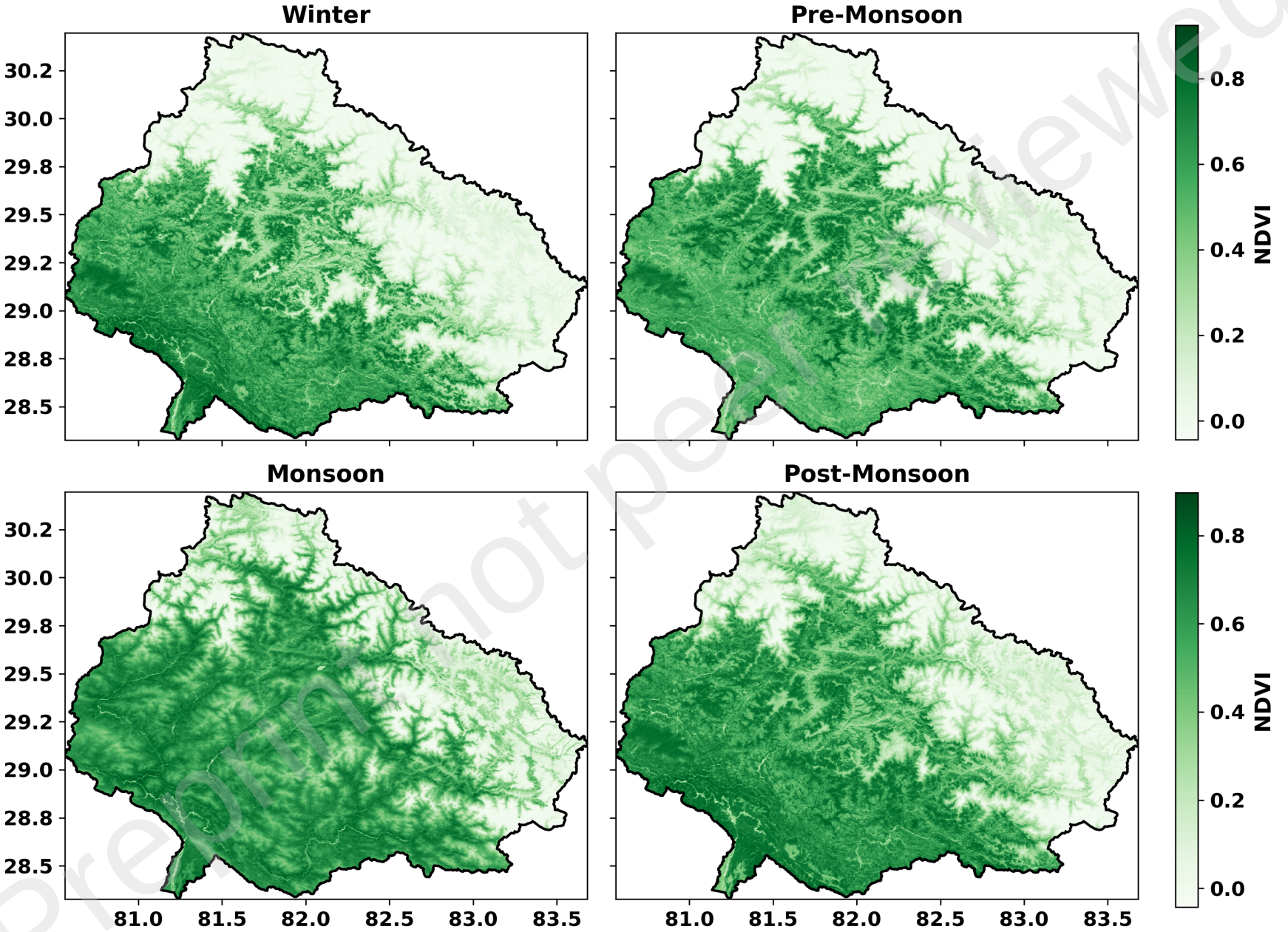

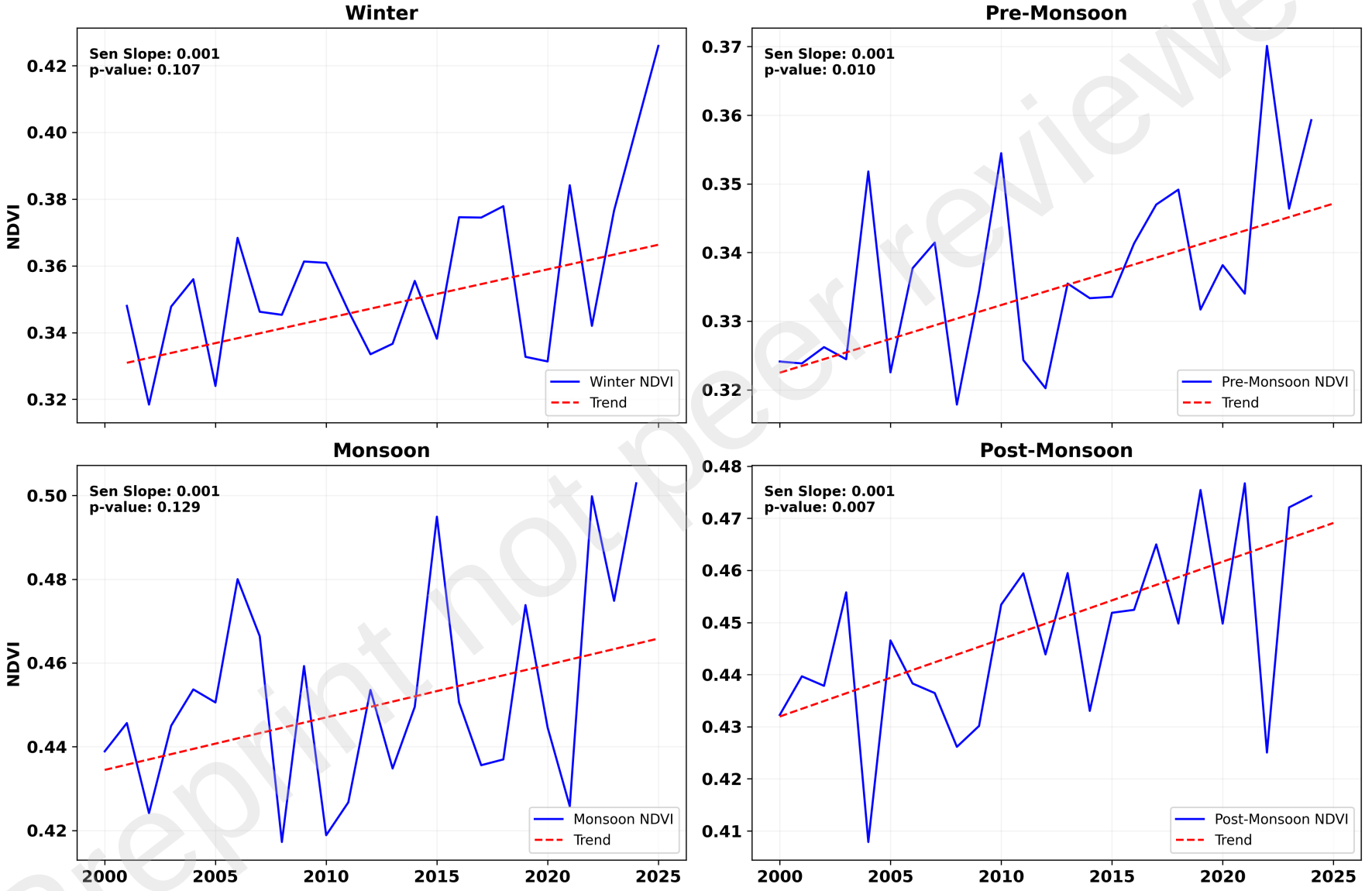

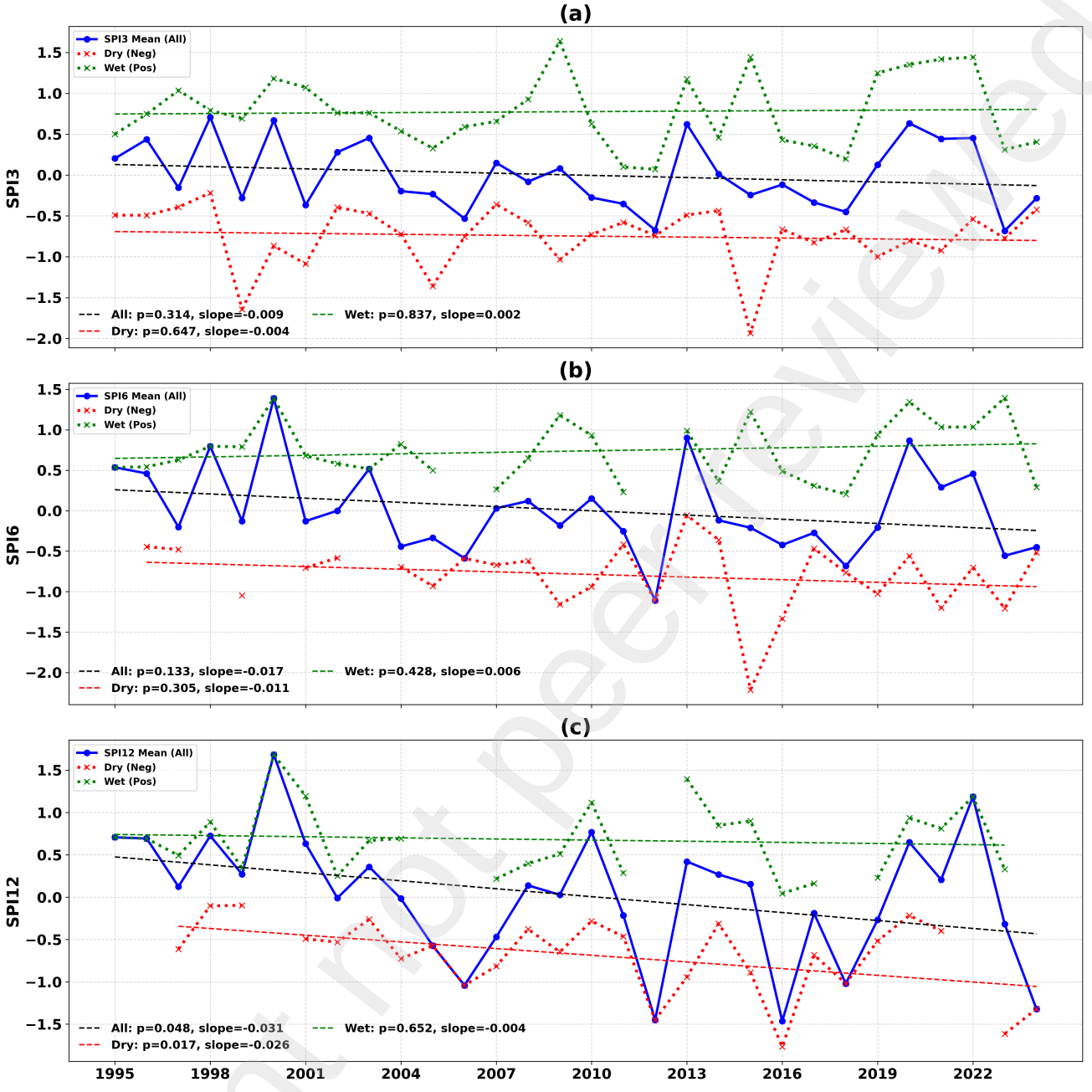

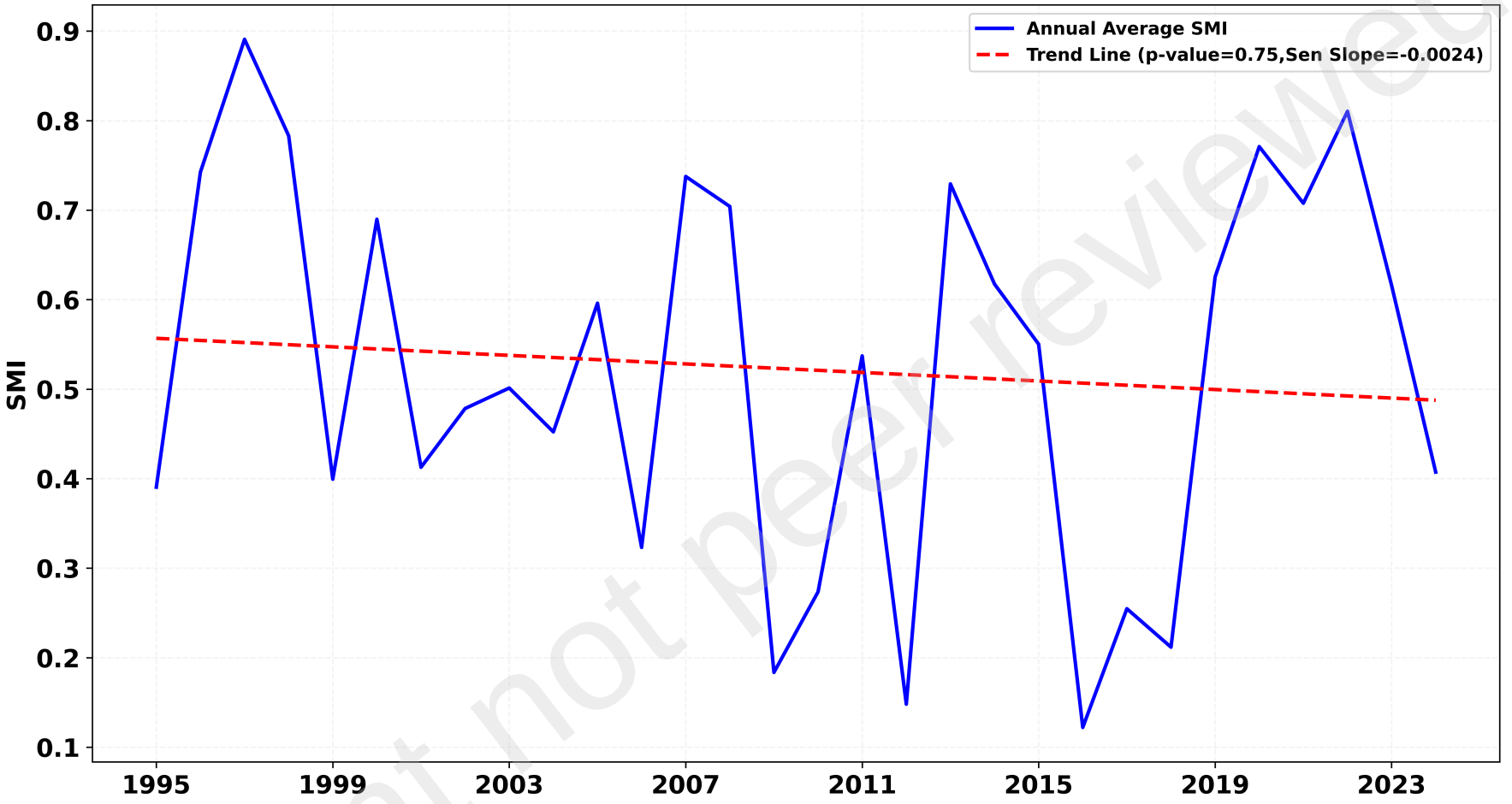

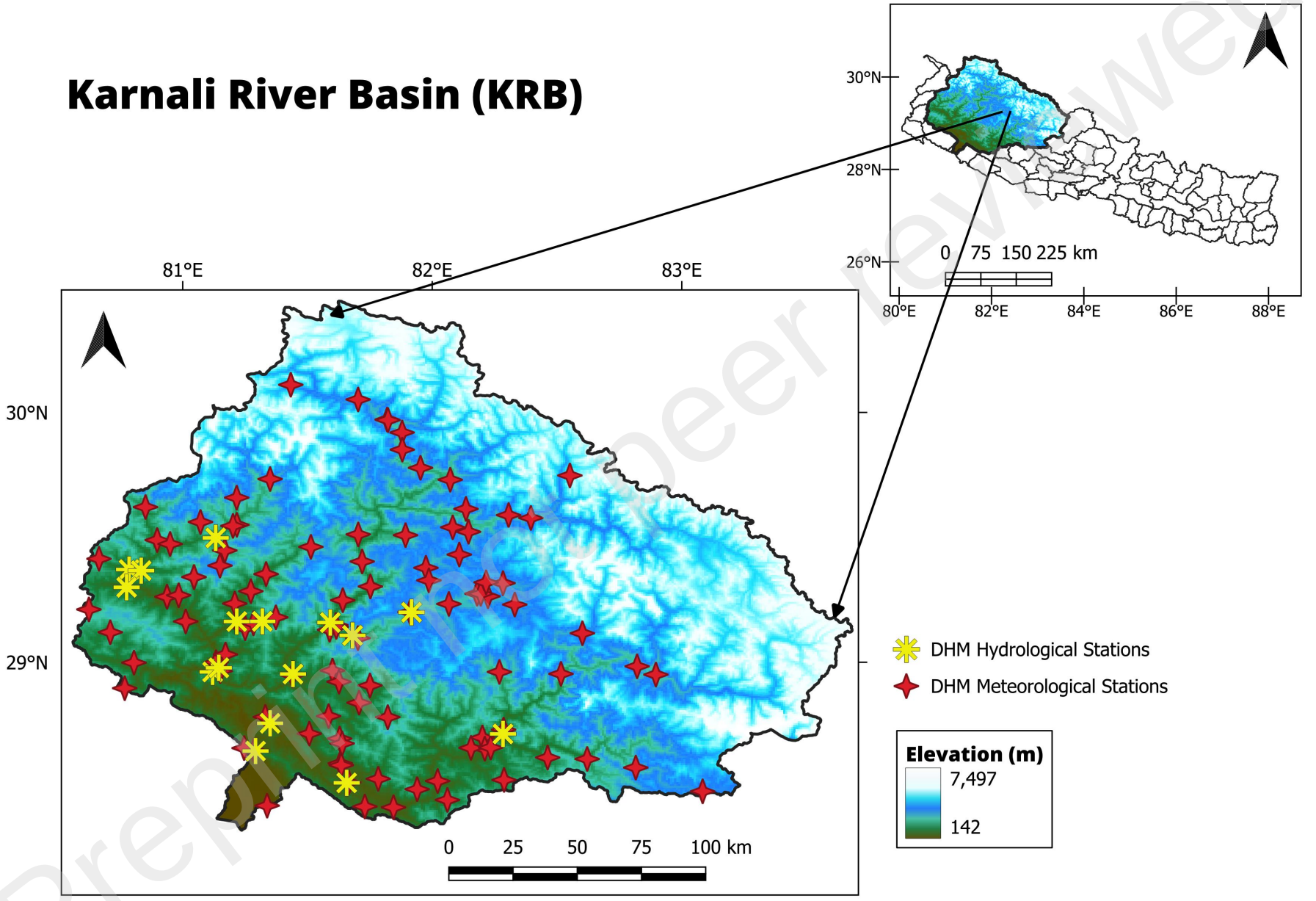

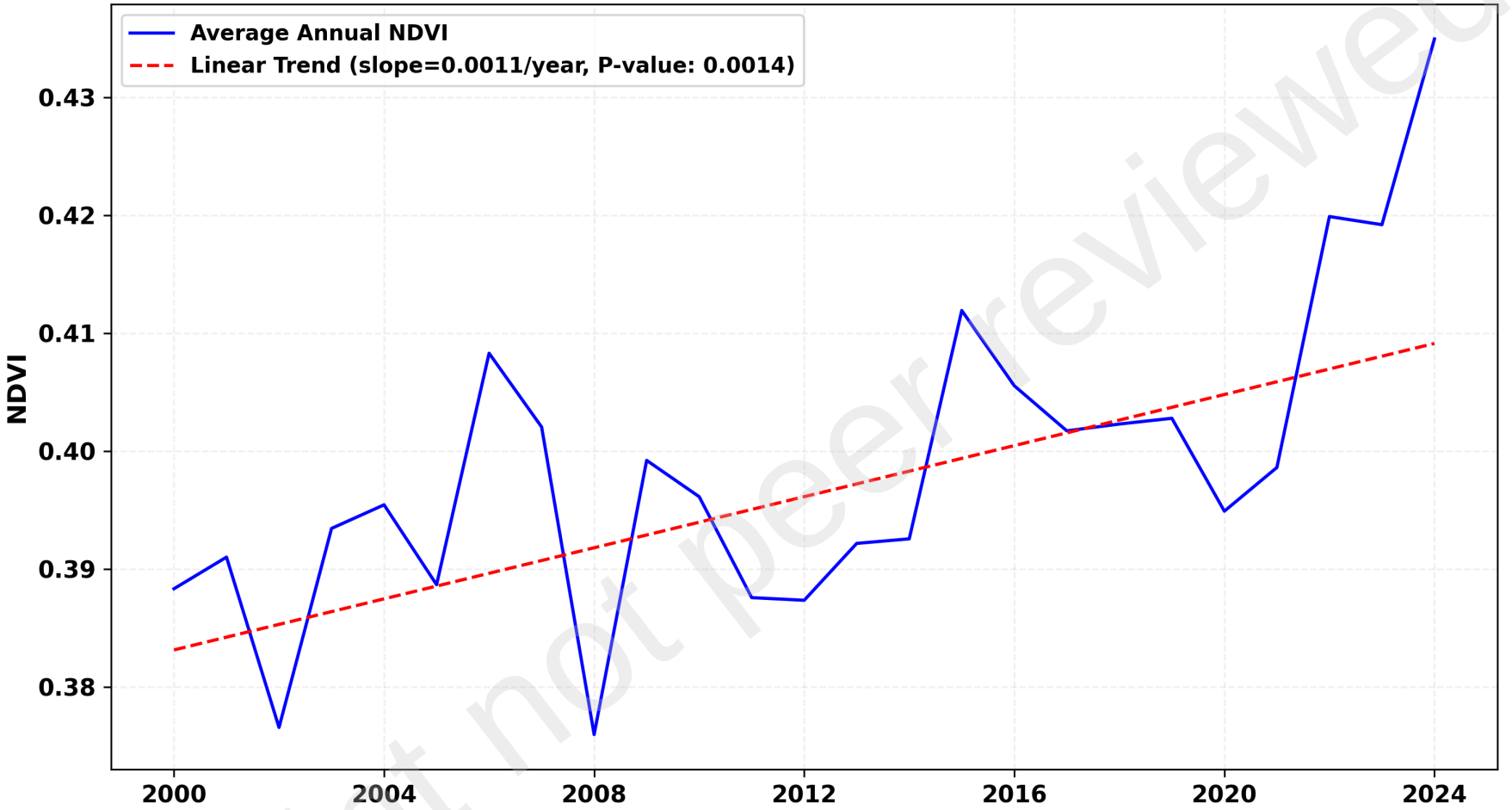

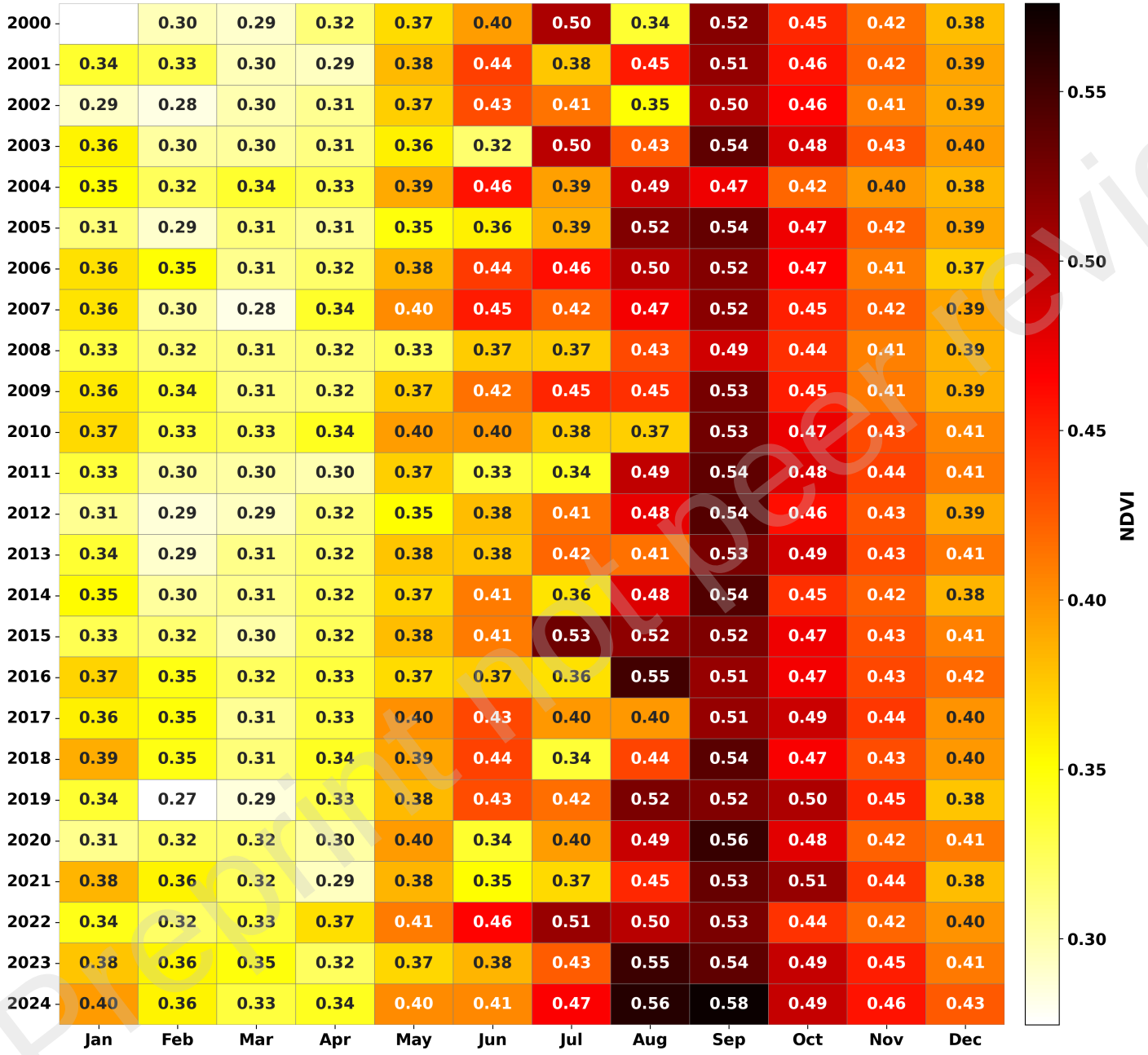

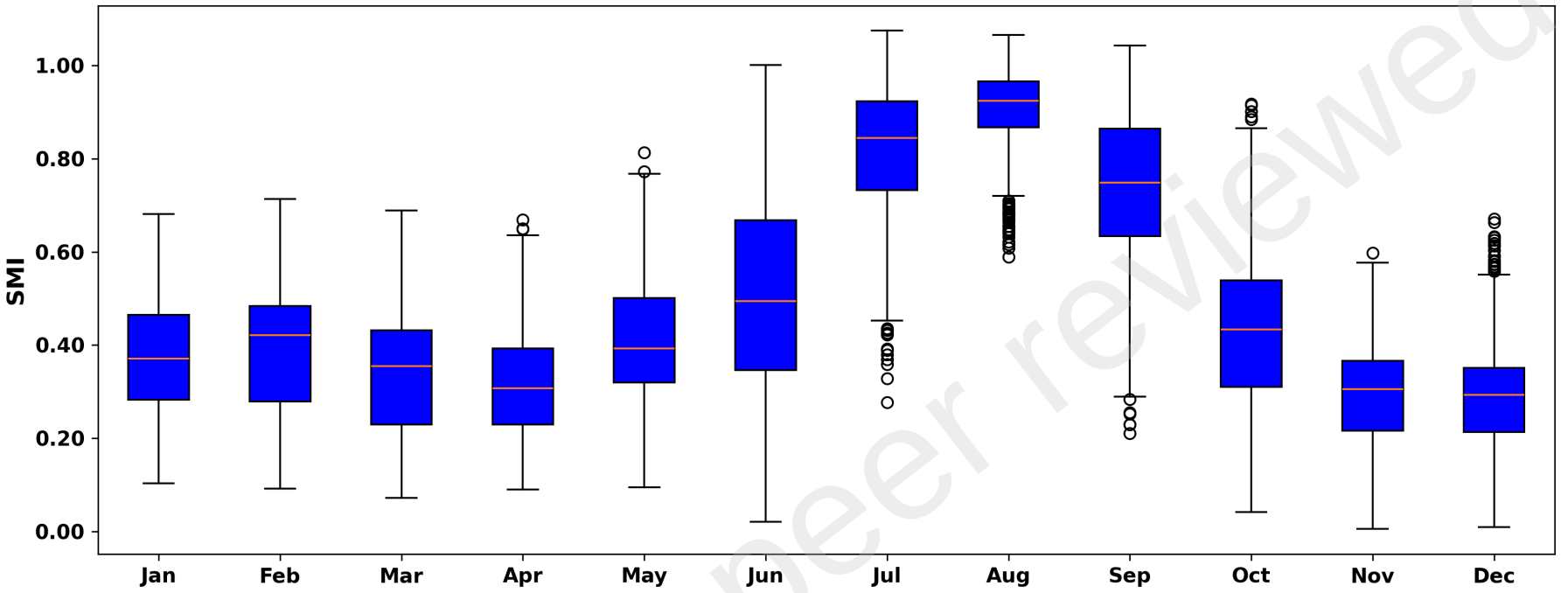

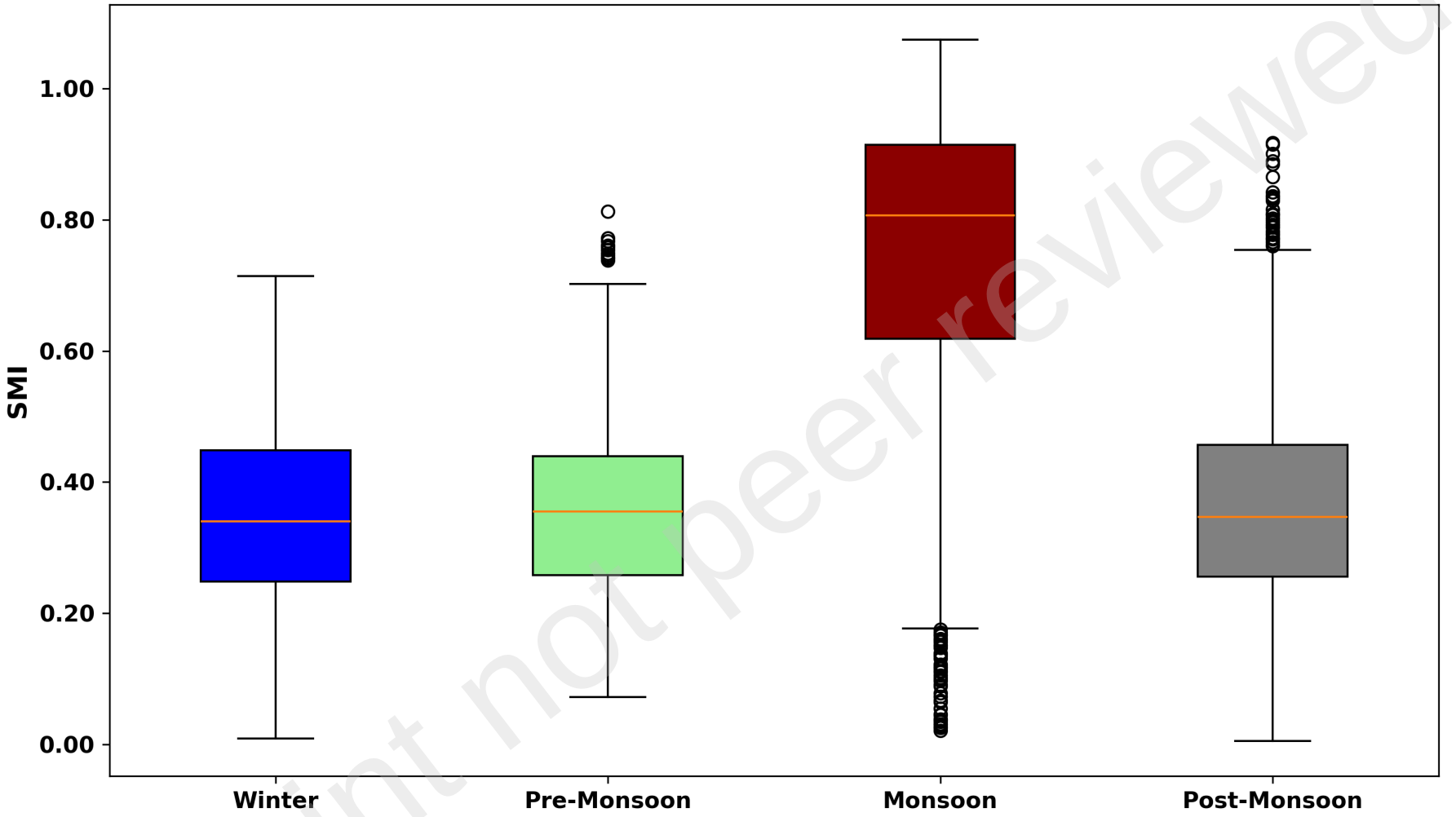

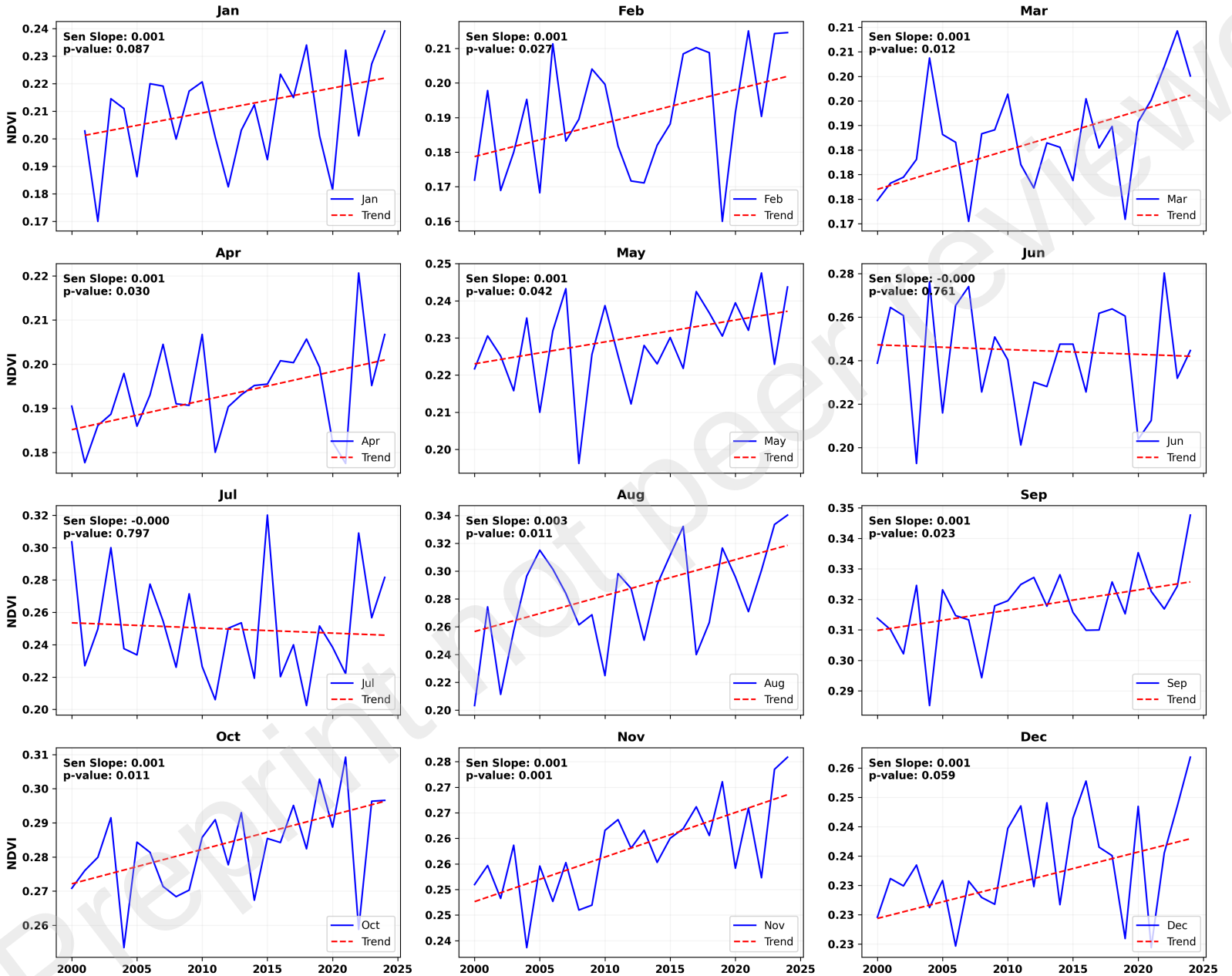

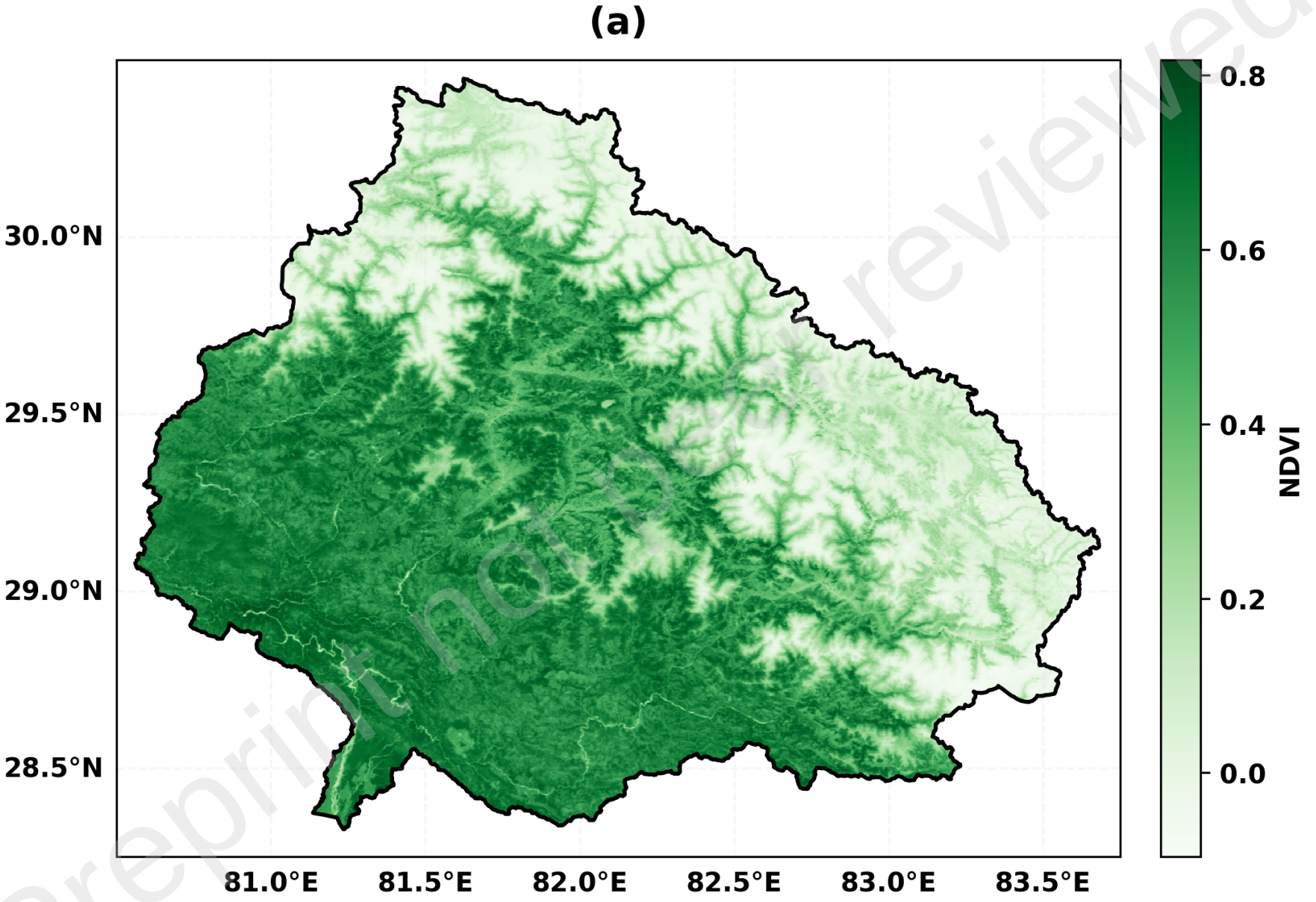

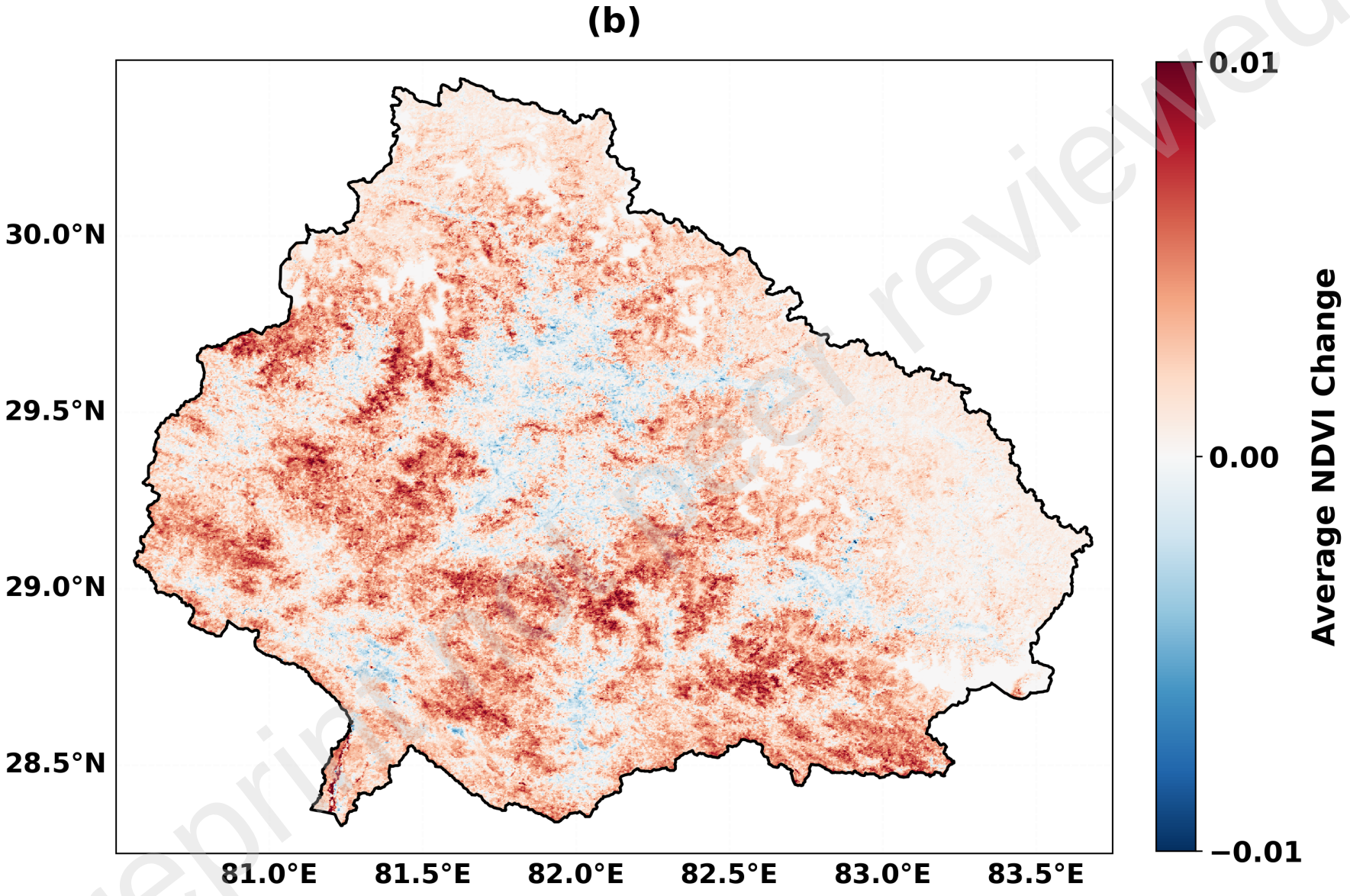

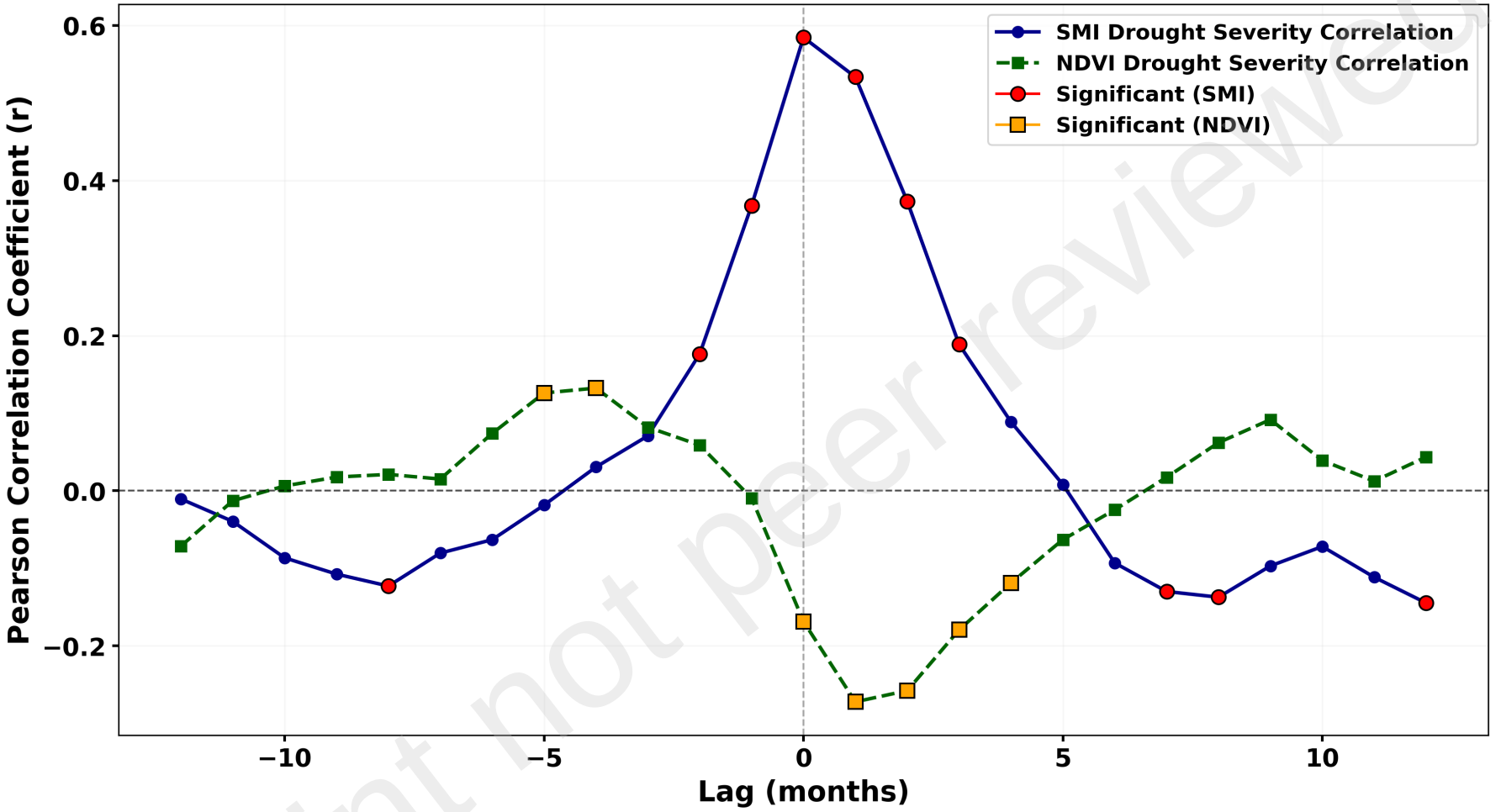

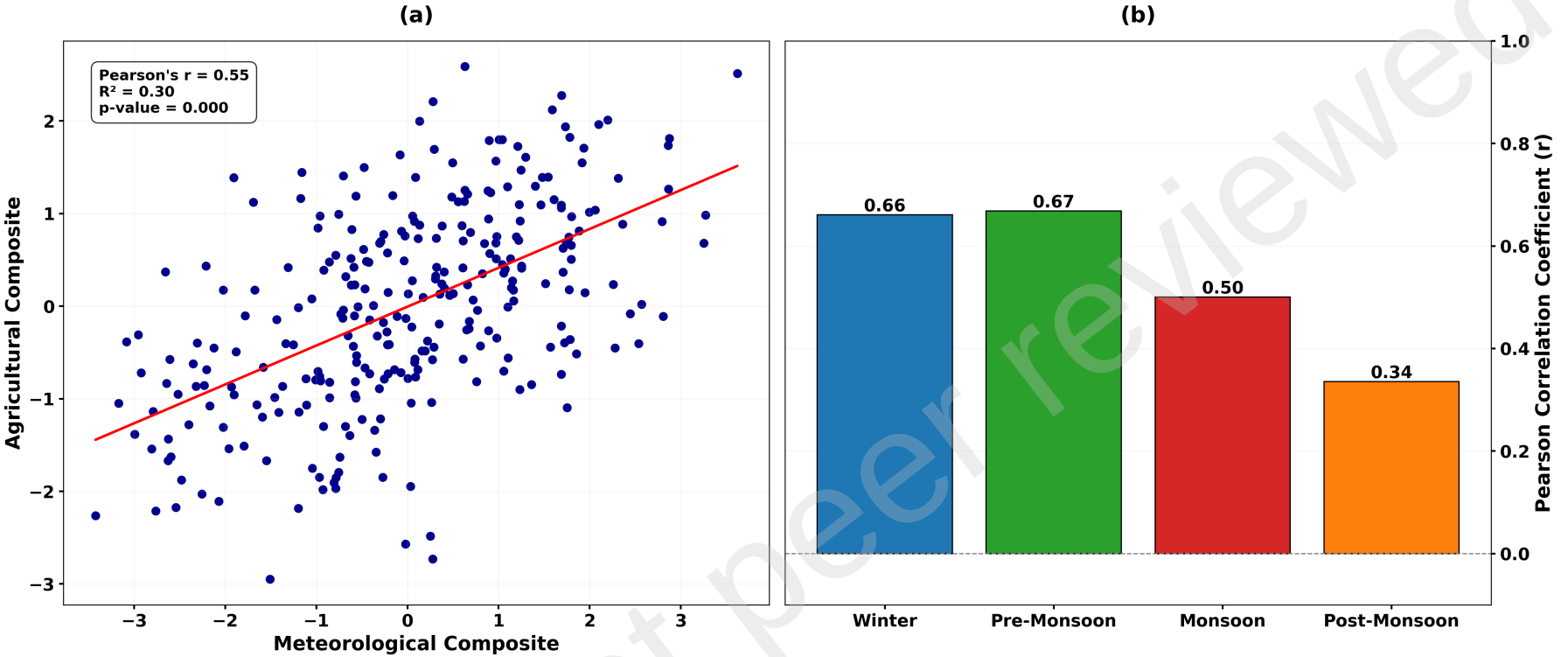

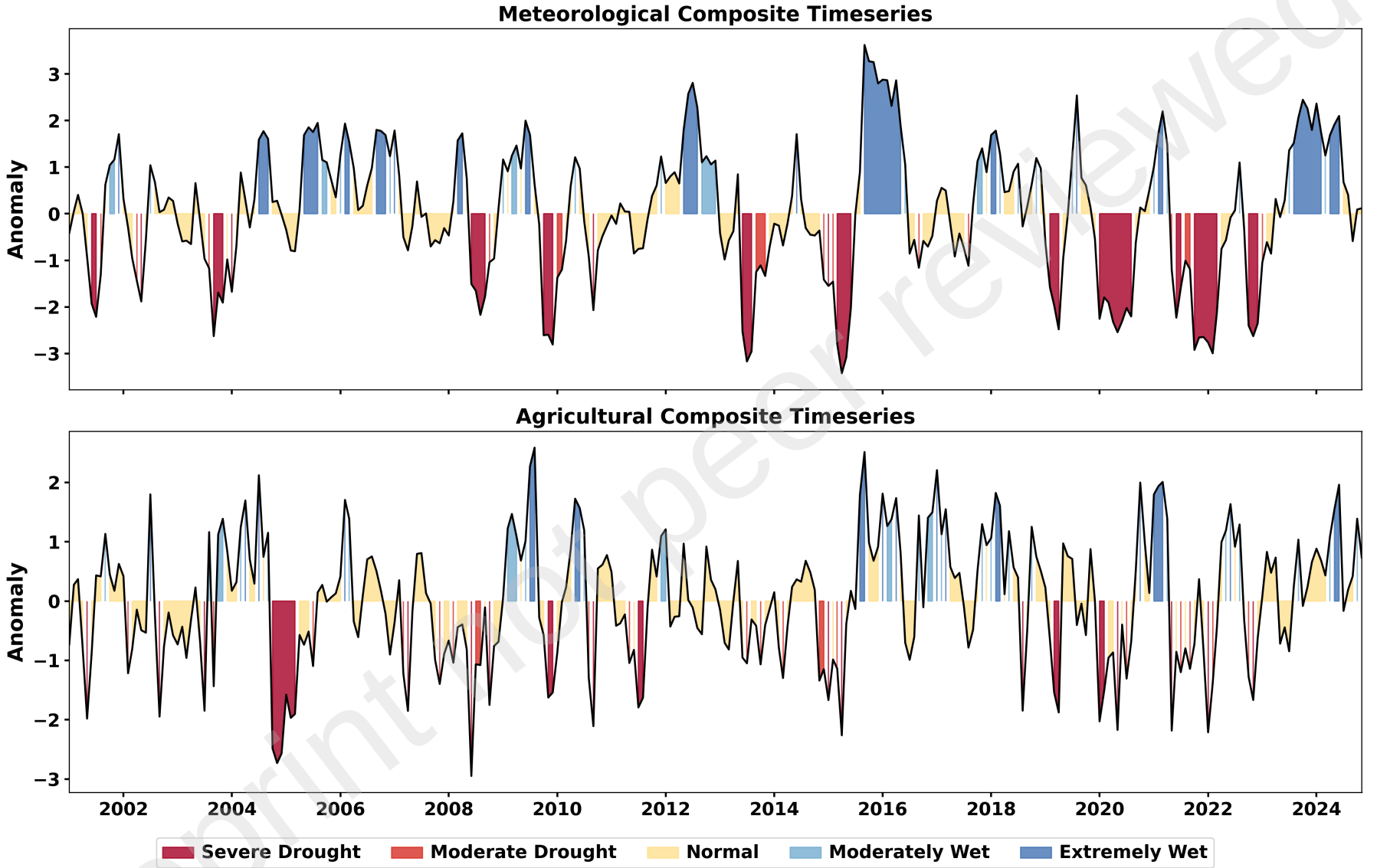

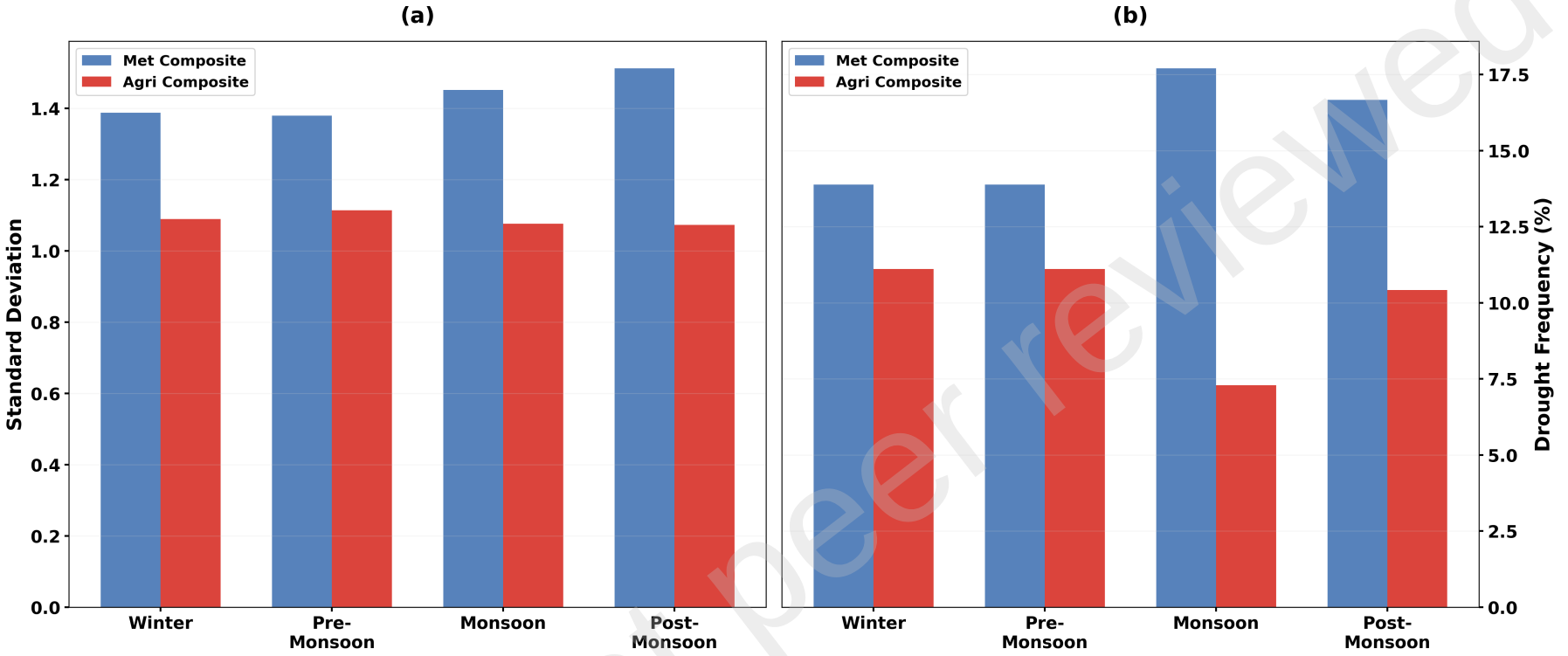

Dynamics of Meteorological and Agricultural Drought in the Karnali River Basin, Nepal

Kumar Aryal[1,2,*], Dhiraj Pradhananga[2], Deepak Aryal[1], Nir Krakauer[3], Rajesh Sigdel[4]

[1]Central Department of Hydrology and Meteorology, Tribhuvan University, Kathmandu

[2]Tri-Chandra Multiple Campus, Ghantaghar, Kathmandu

[3]Department of Civil Engineering, City College of New York, USA

[4]Institute of Forestry, Hetauda Campus, Chitwan

*Corresponding author: kumarandphd@gmail.com

Abstract

Drought poses significant threats to the Himalayan region, but comprehensive assessments incorporating meteorological, agricultural, and ecological dimensions are scarce. This work uses 30 years of observational and satellite data (1995-2024) to provide a multidimensional drought analysis for the Karnali River Basin in western Nepal. We created standardized drought indices based on ground station precipitation records, ERA5 reanalysis data, and MODIS NDVI products. Principal component analysis was used to develop composite meteorological and agricultural drought indices, for a more comprehensive assessment of drought propagation across domains. Long-term trends show large drops in precipitation (especially SPI12) and soil moisture during pre-monsoon and winter periods. However, there is a modest greening trend (+12% over 25 years). Spatial analysis shows mountainous regions as drought hotspots, with frequency surpassing 12%, whereas the Terai lowlands are more resilient. The temporal study found that vegetation responses lag soil moisture anomalies by about a month, indicating physiological buffering and crop phenology. The composite indices revealed that meteorological droughts are very volatile (52% normal conditions), but agricultural droughts evolve more slowly with greater permanence (64% normal conditions). The largest seasonal connection between meteorological and agricultural drought occurred in pre-monsoon ($r = 0.67$) and winter ($r = 0.66$) while the weakest was in monsoon ($r = 0.50$). These results indicate the growing drought threats in this basin and indicate how vital the development of integrated drought surveillance frameworks is as a key to the early warning systems, agricultural planning, and adaptive water resource management of mountain regions under changing climate.

Keywords: Drought monitoring, Composite indices, Karnali River Basin, PCA, Climate change adaptation

1. Introduction

One of the most widespread and damaging natural hazards worldwide is drought, which has extensive impacts on ecosystems, agricultural activities, water resources, and socioeconomic well-being (Vicente-Serrano et al., 2010; Wilhite & Pulwarty, 2017; IPCC, 2023). Unlike sudden disasters, drought develops gradually, and in most cases, it is hard to identify early and take appropriate measures to prevent the disaster in time (Wilhite & Glantz, 1985; Mishra & Singh, 2010). These issues are intensified in mountainous areas, where the topography and steep climatic slopes lead to high localization of drought symptoms (Karki et al., 2017; Ullah et al., 2023). In essence, drought is a silent hazard that emerges due to chronic water deprivation and has disastrous consequences on a community, in terms of agriculture, water supply, and the environment in its vicinity (Potopová et al., 2016; Dahal et al., 2024), leading to severe economic losses (Below et al., 2007; Wilhite et al., 2007; Sigdel & Ikeda, 2010). It has the potential to impact health, food security, energy systems, and environmental sustainability.

Despite growing concern, past studies in Nepal and particularly in the Karnali River Basin (KRB) region of western Nepal have largely relied on individual indicators, such as precipitation-based drought indices or vegetation metrics, which capture only one facet of drought (Aryal et al., 2022; Bagale et al., 2021; Baniya et al., 2019; Bista et al., 2021; Dahal et al., 2016, 2020; Hamal et al., 2020, 2021; Kafle, 2015; Khatiwada & Pandey, 2019). However, drought is a multi-dimensional phenomenon that unfolds across meteorological, hydrological, ecological, and agricultural domains (Ahady et al., 2025; Singh et al., 2024; Weaver et al., 2025).

To address this gap, this study uses a multi-index drought evaluation methodology. Standardized Precipitation Index (SPI) is used to describe meteorological drought at multiple timescales (3, 6, and 12 months), the Soil Moisture Index (SMI) is used based on reanalysis volumetric soil moisture to define hydrological and agricultural drought, and the Normalized Difference Vegetation Index (NDVI) is used to determine ecological and vegetation stress. Combining these indices gives a holistic understanding of drought and points to various aspects of water and vegetation feedback that cannot be described using any one of these individually.

The necessity to comprehend the long-term dynamics of droughts in Nepal is especially acute due to the high climate sensitivity of the Karnali River Basin and the significant role of rain-fed agriculture in the country Panthi, 2014; Bastakoti et al., 2017; Rimal et al., 2018; Bocchiola et al., 2019; Ghimire et al., 2020; Bista et al., 2021). The period 1995-2024 is an opportunity period that captures the historic variability of drought and recent aggravation of climate change, such as the major extended droughts of the 2010s (Bagale et al., 2021). It is necessary to examine the drought conditions on a monthly, seasonal, and annual basis to differentiate between short-term fluctuations and long-term, multi-year deficits. A spatially explicit approach allows for the identification of localized hotspots that may be overlooked in basin-wide averages. The overt analysis of both temporal and spatial variables at monthly, seasonal, and annual scales, mixed with frequency and categorical analysis, is what makes this study unique in the area.

The objectives of the overall study are to compute and standardize the SPI, SMI, and NDVI to gain a general statement of drought; to determine inter-annual and seasonal variability and location of spatial drought hotspots; to determine frequency, intensity, and category distributions of drought using standard thresholds; and to create decision-supportive visual products of drought monitoring in the Karnali River Basin. This spatially explicit drought assessment is a multi-index that is new in the KRB context, which offers a greater level of definition of drought properties, and it brings about actionable data in disaster preparedness, water resource planning, and climate adaptation.

2. Study area

Karnali River Basin (KRB) is located between 28.33 ° to 30.45 °N, and 80.55 ° to 83.68 °E (Figure 1) in a wide ecological zone between the high-altitude Himalayan areas and the mid-hills and plains in western Nepal. The basin covers a total of approximately 42,457 square kilometers in Nepal and is one of the largest in the country, centered on the Karnali River, which originates on the Tibetan Plateau. The altitude ranges from 142 m in the southern lowlands to 7,497 m in the higher mountains to the north in Nepal. Snow/glaciers and grasslands dominate the highlands of the KRB, and forests and agricultural lands dominate the lowlands.

Streamflow in the KRB is mostly rain-fed (Bookhagen & Burbank, 2010). The KRB climate is affected by the South Asian Summer Monsoon, the physiography of the area, and cold-season westerlies (Shrestha, 2000; Nayava et al., 2017). The mean annual precipitation in the basin is about 1479 mm, with high spatial, seasonal, and inter-annual fluctuations (Khatiwada et al., 2016). Stations in the region receive approximately 55 percent to 80 percent of annual precipitation in the summer season (June to September) (Shrestha, 2000). The highest part of the basin is the driest (with less than 300 mm in a year), but some pockets in mountainous regions receive over 2400 mm in a year (Palazzi et al., 2013). Precipitation events in summer dominate the river discharge, on top of the coupling of the baseflow with snow and glacier melt in spring and summer.

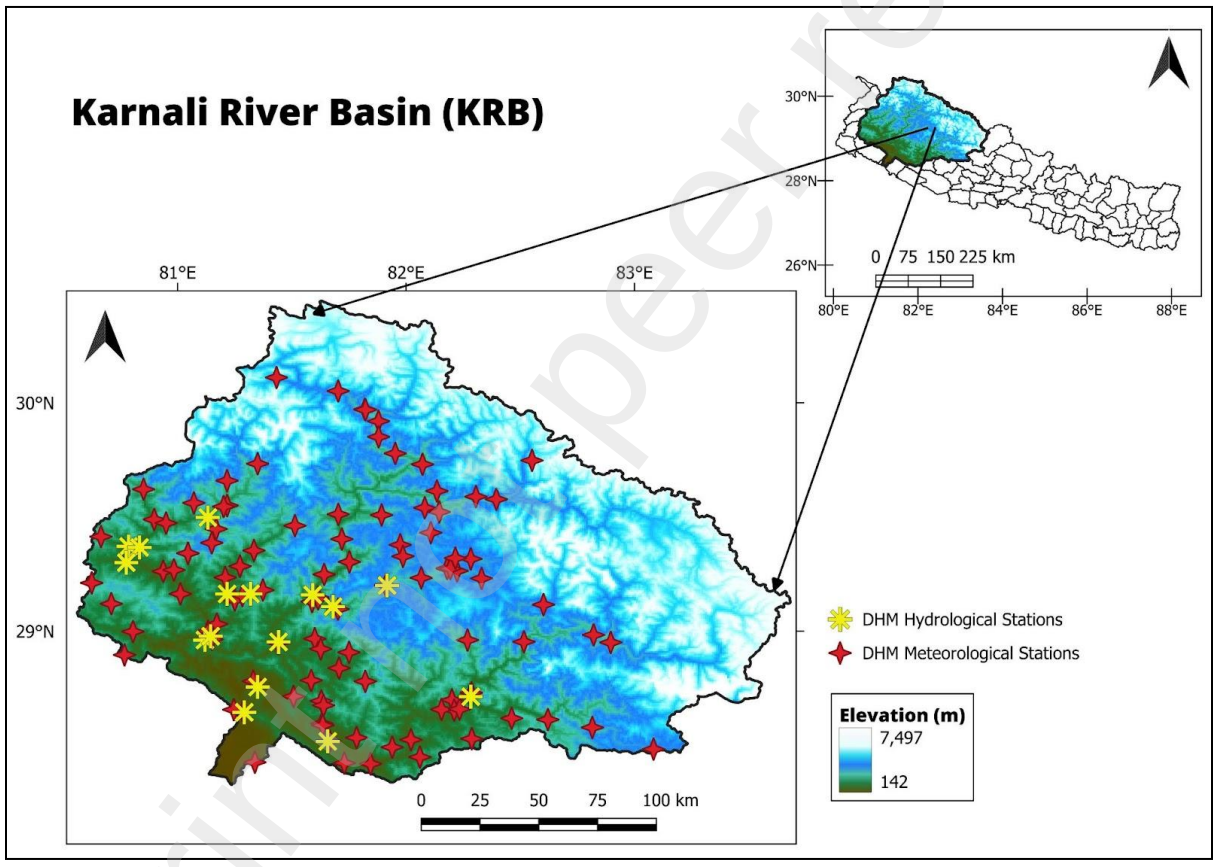

Figure 1: Karnali River Basin of Nepal with DHM Hydrological and Meteorological Stations

3. Materials and Methods

3.1. Data Sources

Daily precipitation data at 28 stations of the Department of Hydrology and Meteorology (DHM) for the study area were collected. After quality control using linear and spline interpolation, and the normal ratio method to fill the gaps (Paulhus & Kohler, 1952; Dyer & Dyer, 2001; Junninen et al., 2004; Silva et al., 2016; Huang, 2021), from the total of 102 stations in the region, only 28 were selected, based on requiring stations to have sufficiently long coverage (30 years) without large gaps (>20% missing data) or obvious quality problems. The daily data were summed to monthly totals, and spatial interpolation was done using the Inverse Distance Weighting (IDW) method to grids of 5km resolution (Franke & Nielson, 1980; Tung, 1983). The gridded data were then used to calculate the Standardized Precipitation Index (SPI).

For soil moisture, ERA5 reanalysis data of volumetric water content (0-7 cm depth) were obtained (Hersbach et al., 2020). The Normalized Difference Vegetation Index (NDVI) was obtained from the MODIS satellite instruments (MOD13Q1 product, 250 m resolution, 16-day composites), available from February 2000 onward (Didan, 2021). This NDVI product uses a "maximum value composite" approach over 16 days, which significantly reduces cloud contamination compared to raw daily data. These 16-day composite values were averaged to create simple monthly averages.

3.2. Drought Indices

This study employs three complementary drought indices, Normalized Difference Vegetation Index (NDVI), Standardized Precipitation Index (SPI), and Soil Moisture Index (SMI), to characterize ecological, meteorological, and agricultural drought conditions across the Karnali River Basin (KRB). These indices offer different perspectives on drought manifestation and, when combined, support a robust composite drought assessment framework.

3.2.1. NDVI (Ecological Drought Index)

The NDVI serves as a widely used indicator of vegetation health, derived from the differential reflectance of near-infrared (NIR) and red light. It is calculated as: $NDVI = \frac{NIR - Red}{NIR + Red}$

Where NIR is near-infrared reflectance and Red is red light reflectance. NDVI values range between -1 and +1, with higher values indicating denser and healthier vegetation (Didan, 2021; Zhang et al., 2018). Vegetation typically exhibits NDVI values between 0.2 and 0.9 (Alex et al., 2017; Krakauer et al., 2017; Baniya et al., 2018).

In order to address anomalies relative to the long-term distribution, NDVI was standardized into a z-score. The z score was calculated as: $Z_{NDVI} = \frac{NDVI_t - \mu}{\sigma}$

Where $NDVI_t$ is the value at time t, μ is the long-term mean, and σ is the standard deviation of the NDVI time series. This normalization allows comparison across regions and time by expressing deviations from the climatological average in units of standard deviation.

NDVI trends were analyzed across monthly, seasonal, and annual time scales to assess ecological drought conditions and vegetation response across spatial and temporal dimensions. The drought category, as defined by NDVI (Berhan et al., 2011; Aziz et al., 2018), is presented in Table 1.

Table 1: Drought Category based on NDVI z score

NDVI Value	Drought Category
> 0	No drought
0 to -0.99	Mild drought
-1.00 to -1.49	Moderate drought
-1.50 to -1.99	Severe drought
≤ -2.00	Extreme drought

3.2.2. SPI Calculation (Meteorological Drought Index)

The SPI is a statistical drought index that quantifies precipitation anomalies over various temporal scales. Its self-calibrating and multi-timescale nature is suited for drought monitoring in climatically variable regions such as the Himalayas (McKee et al., 1993). In this study, SPI was computed at 3-month, 6-month, and 12-month accumulation periods (SPI3, SPI6, and SPI12), capturing short-term, mid-term, and long-term drought events, respectively.

Monthly precipitation data were used to compute the SPI by fitting a gamma distribution to the cumulative precipitation values, which were then transformed into standardized z-scores (mean = 0, standard deviation = 1), following the method of McKee et al. (1993). The computations were performed using the climate-indices package in Python. SPI values were classified into drought categories (Table 2) using widely accepted thresholds (McKee et al., 1993; Sigdel & Ikeda, 2010; Aryal et al., 2022).

Table 2: Drought Category based on SPI

SPI Value	Drought Category
> 0	No drought
0 to -0.99	Mild drought
-1.00 to -1.49	Moderate drought
-1.50 to -1.99	Severe drought
≤ -2.00	Extreme drought

3.2.3. SMI Calculation (Hydrological Drought Index)

The SMI offers insight into agricultural and hydrological drought by measuring water availability in the root zone. It was derived from volumetric soil moisture data and standardized using the empirical cumulative distribution method to reflect drought severity based on percentiles. The SMI was calculated as: $SMI = \frac{SM - P_5}{P_{95} - P_5}$.

Where SM is the observed soil moisture at a given time, P_5 is the 5th percentile (representing dry conditions), and P_{95} is the 95th percentile (wet conditions) of the long-term soil moisture distribution (Wagner et al., 1999; Esch et al., 2018). SMI values range from near 0 (often approximating the wilting point) to 1 (often approximating field capacity). Both SMI values and their standardized anomalies were utilized to assess drought severity and contribute to the formation of the Agricultural Drought Indicator. Table 3 gives the values of SMI z scores and the drought category it defines.

Table 3: Drought Category based on SMI z score

SMI Value	Drought Category
> 0	No drought
0 to -0.99	Mild drought
-1.00 to -1.49	Moderate drought
-1.50 to -1.99	Severe drought
≤ -2.00	Extreme drought

3.2.4. Composite Agricultural and Meteorological Indices

A two-stage Principal Component Analysis (PCA) approach was used to develop Composite drought indices (Abdi & Williams, 2010; Greenacre et al., 2022). For the meteorological part, PCA was applied to derive a single composite representing precipitation variability from the standardized precipitation indices at different timescales (SPI3, SPI6, SPI12). For the agricultural domain, the optimal lag period was first identified by evaluating the temporal lag between soil moisture anomalies (SMI) and vegetation response (NDVI) through correlation. The lag-adjusted SMI and NDVI anomalies were then subjected to PCA to generate an agricultural composite. This process not only minimized the dimensionality but also represented the lagged soil-vegetation interactions and gave representative indices to be used in future drought analysis (Demšar et al., 2013).

3.3. Trend Analysis and Visualization

Trend analysis of SPI, SMI, NDVI, and the composite indices was conducted using the non-parametric Mann-Kendall test (Mann, 1945; Kendall, 1975) with Sen's slope estimator (Yue & Wang, 2004), both widely applied for detecting monotonic changes in hydroclimatic quantities that may not be normally distributed. Seasonal and monthly patterns were analyzed by grouping data into the four meteorological seasons of Nepal: winter (December-February), pre-monsoon (March-May), monsoon (June-September), and post-monsoon (October-November). Statistical significance for all trend analyses was determined at a 95% confidence level.

To analyze temporal trends, the NDVI was examined on annual, seasonal, and monthly scales. For the SMI, only the annual trend was displayed, as the seasonal and monthly trends did not show significant variations. Instead, box plots were created to illustrate the distribution patterns and variability in SMI values. In the case of the SPI, annual trends were analyzed separately for dry periods (indicated by negative SPI values), wet periods (indicated by positive SPI values), and the overall average. This disaggregated approach was adopted because analyzing wet and dry extremes separately avoids obscuring critical trends in precipitation and drought extremes.

For the spatial analysis of NDVI, the average difference in values between 2000 and 2024 was calculated for each grid cell. A difference map was produced to visualize these changes, along with spatially averaged NDVI plots at annual, seasonal, and monthly timescales across the KRB. For the SMI, spatial trends were computed for each grid cell over the entire study period, leading to the creation of an average spatial trend map for the KRB. Additionally, spatial distribution plots for SMI were developed at annual, seasonal, and monthly intervals to capture variations in time and space. For SPI, spatial anomaly frequency was calculated to see how often each grid cell experiences drought or wet anomalies at annual, seasonal, and monthly timescales. This method gives a clearer picture of extreme weather events by showing how frequently significant dry or wet conditions occur in each area.

3.4. Correlation Analysis

Correlation analysis was carried out among SPI, SMI, NDVI, and the composite indices to evaluate their degree of consistency and complementarity. Pearson correlation coefficients were computed at both grid and basin scales, and Fisher's Z-transformation was applied to estimate 95% confidence intervals. In addition, correlation was examined with lag adjustment to highlight the temporal relationships between vegetation stress and soil moisture anomalies.

4. Results

4.1. Long-Term Trends in Drought Indicators

Ecological drought indicator, NDVI, calculated per year in the KRB over 2000-2024 (Figure 2), reveals a consistent upward trend in greenness of the vegetation. The average NDVI increased to a high of 0.435 in 2024, which is about 12 percent higher than the 2000 level of 0.388. This long-term greening signal is reflective of a better ecological situation, which likely could be due to climate change, carbon dioxide fertilization, land-use change, or expansion of irrigation at the lower altitudes.

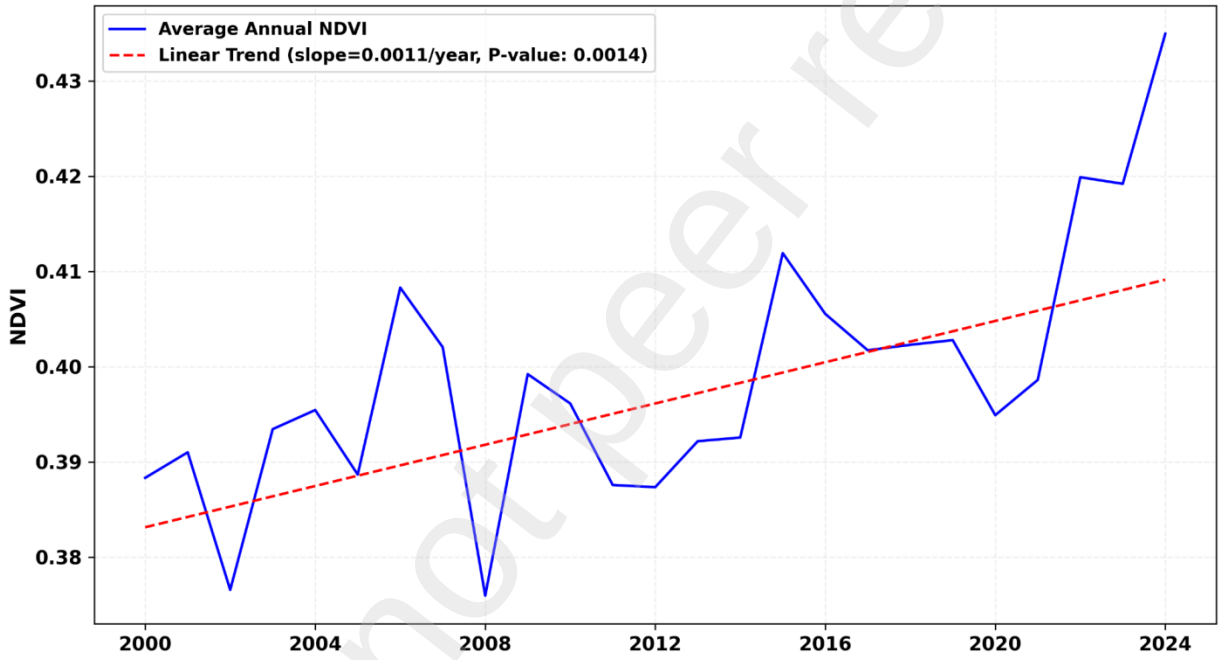

Figure 2: Mean annual NDVI from 2000 to 2024 of KRB

The NDVI shows a significant rise after 2014, with the values above 0.40 consistently high in the years that follow. In 2024, the mean NDVI was the highest (0.435), followed by 2022 (0.420) and 2023 (0.419). Conversely, the lowest annual averages were recorded in 2002 (0.376) and 2008 (0.376). The greening pattern is confirmed by the fact that Mann-Kendall trend analysis shows a statistically significant positive trend ($p < 0.05$) with Sen slope (0.0011/year), which is estimated annual rate of increase. However, interannual variations can be noted, which reflects ecological sensitivity to the seasonal droughts, especially in the pre- and post-monsoon seasons.

In the case of the hydrological drought indicator, a temporal pattern on the annual average SMI of 1995 to 2024 shows a dynamic pattern within the KRB (Figure 2b). The basin-average SMI shows an annual mean of 0.52, with high interannual fluctuation (standard deviation = 0.21). The basin exhibits a slight declining tendency in soil moisture with a Sen slope -0.0024/per year, although this trend is not statistically significant (p = 0.75). The temporal SMI, in general, indicates that the KRB has revealed a stable medium-soil moisture condition during the last three decades, with some drier years.

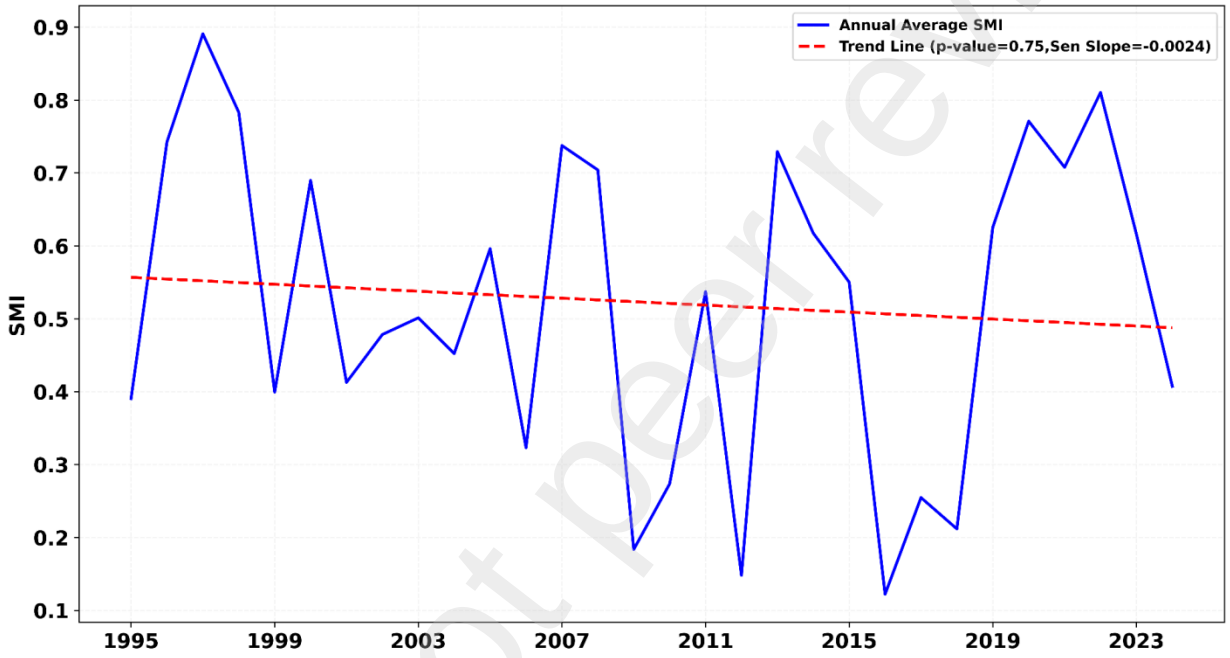

Figure 3: Annual SMI trend from 1995 to 2024 of KRB

Figures 4a-c indicate that the annual trends of the meteorological drought indicator, SPI at 3, 6, and 12-month time scales from 1995 to 2024 show a minor overall decrease. Mean annual SPI was found to have negative slopes of all timescales (-0.009 with SPI3, -0.017 with SPI6, and -0.031 with SPI12), though only SPI12 had statistical significance ($p < 0.05$). Separate wet and dry analyses showed a significant negative trend in the SPI12 dry series (slope = -0.026, p = 0.017), which is a strengthening of the severity of drought. In SPI3 and SPI6, the tendencies of dry periods and wet periods were decreasing and increasing, respectively, but not significantly.

Examination of the dry and wet series further highlights important structural differences across timescales. The disaggregated SPI3 remains continuous, confirming that every year contains both

positive and negative values. Conversely, SPI6 showed gaps in multiple years to either a lack of dry conditions (1995, 1998, 2000, 2003) or moist conditions (2006, 2012). The SPI12 record showed even more discontinuities, with years dominated entirely by persistent dryness (1995, 1996, 2000, 2022) or wetness (2005, 2006, 2012, 2018, 2024). As we might expect, shorter accumulation periods consistently capture dry-wet variability, whereas longer periods, despite smoothing short-term fluctuations, can mask one regime entirely when persistent anomalies dominate the annual cycle.

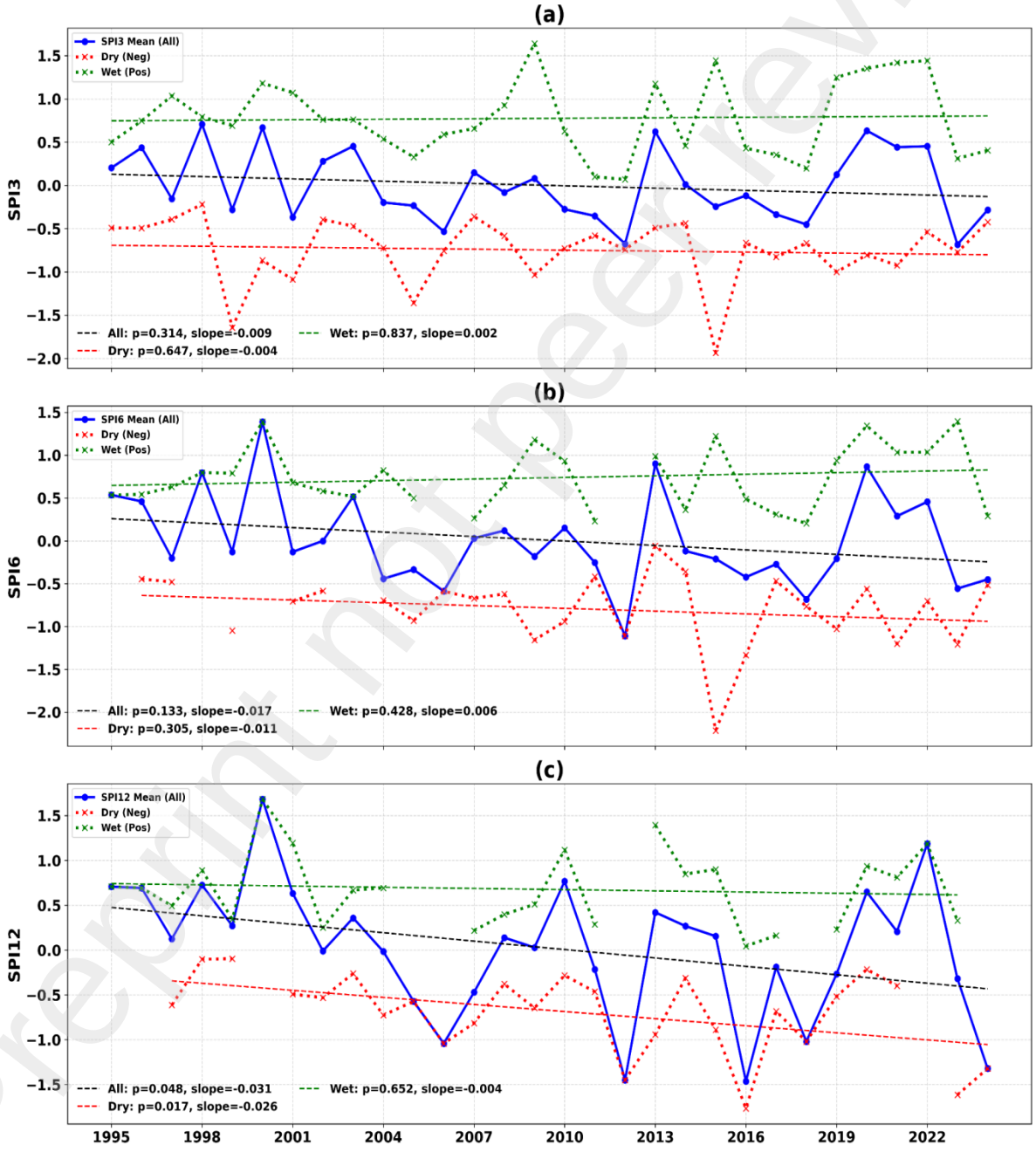

Figure 4: Annual trends for dry, wet, and all SPIs over KRB from 1995 to 2024

4.2. Seasonal Drought Dynamics

Seasonal analyses were conducted for pre-monsoon (Mar-May), monsoon (Jun-Sep), post-monsoon (Oct-Nov), and winter (Dec-Feb) seasons. The seasonal trends (Figure 5) indicate that NDVI is increasing in all seasons. Pre-monsoon and post-monsoon period marks a significant increasing trend ($p < 0.05$), whereas the trends in other seasons are not significant at 95% CI. It shows that NDVI peaks during the monsoon season, with gradual declines in post-monsoon and winter, but the lowest values are in the pre-monsoon period. A steep upward trend in the post-monsoon season suggests extended greening periods, likely due to delayed moisture availability or agricultural expansion.

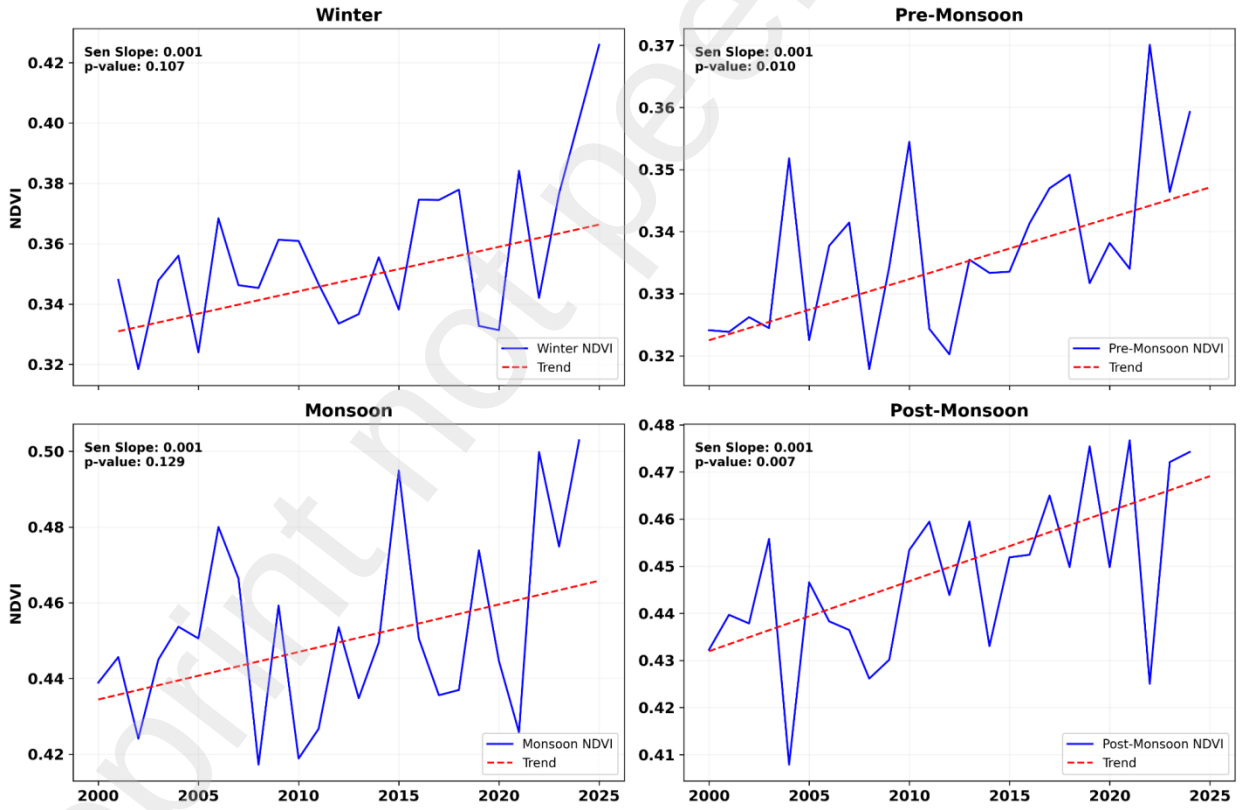

Figure 5: Seasonal NDVI trends from 2000 to 2024 of KRB

In the SMI analysis, the seasonal trends did not indicate any significant changes. However, the seasonal distribution of SMI reveals clear differences in both magnitude and variability across the

four seasons (Figure 6). The monsoon season exhibits the highest mean SMI value of 0.744 with the large variation (standard deviation 0.216), reflecting substantial moisture accumulation and variability during this period. Winter, pre-monsoon, and post-monsoon seasons show relatively lower mean SMI values of 0.346, 0.356, and 0.366, respectively, and correspondingly lower variability. A few statistical outliers are observed, particularly during the monsoon and post-monsoon seasons, indicating occasional extreme wet or dry events. Overall, the seasonal boxplot effectively captures the intra-seasonal variability in SMI, with the monsoon standing out as the most dynamic and moisture-rich period.

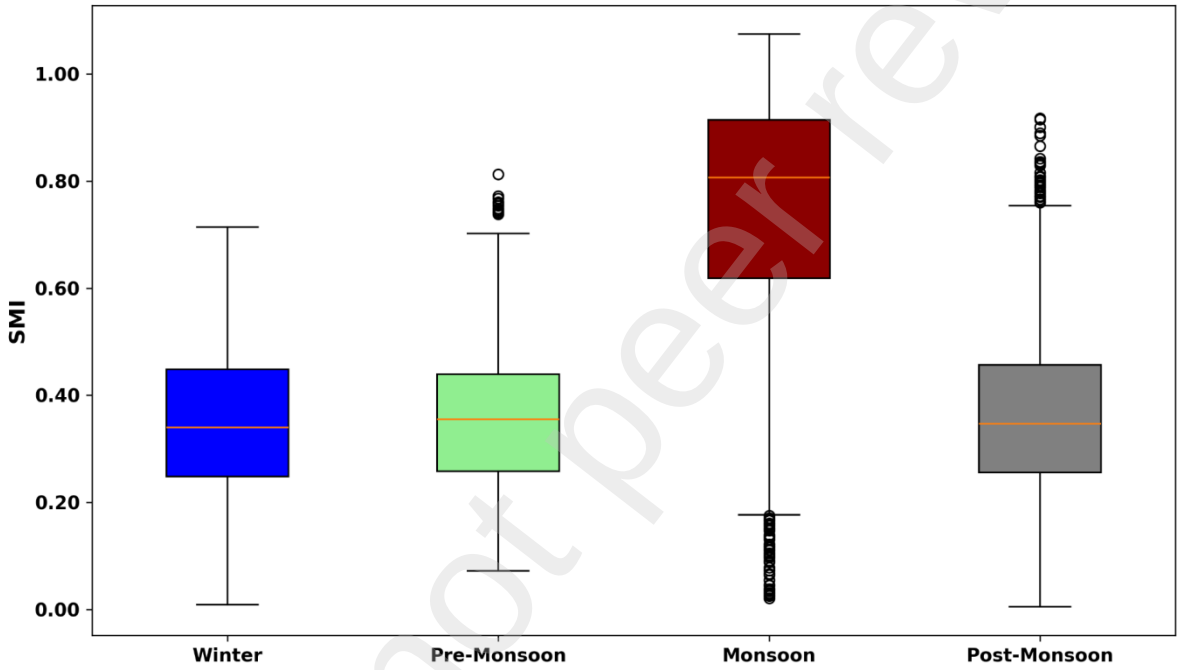

Figure 6: Seasonal distribution of SMI of KRB from 1995 to 2024

4.3. Monthly Drought Variability

The monthly analysis of the indices reveals more in-depth variations in the drought assessment. These indices are used for the temporal and spatial study of drought in the KRB. The analysis of NDVI (Figure 7) shows distinct intra-annual variations that align closely with the region's monsoonal climate cycle. NDVI values are lowest during the winter and early spring months (January to April), gradually increase through the pre-monsoon and monsoon periods, and peak during the late monsoon and early post-monsoon months.

The lowest vegetation activity is observed in March (0.312) and February (0.320), reflecting dry conditions and minimal canopy cover before the onset of pre-monsoon rains, which may also be influenced by low temperatures and snow cover at higher elevations. A sharp rise begins in May (0.378) and continues through June (0.400) and July (0.416), culminating in the highest average NDVI in September (0.526). This peak corresponds to the climax of the monsoon season, when vegetation is lush and soil moisture availability is at its maximum. After reaching its maximum, NDVI slowly decreases throughout October (0.469) and November (0.428), reflecting the aging of crops and vegetation as precipitation decreases. The mean NDVI in December (0.396) remains

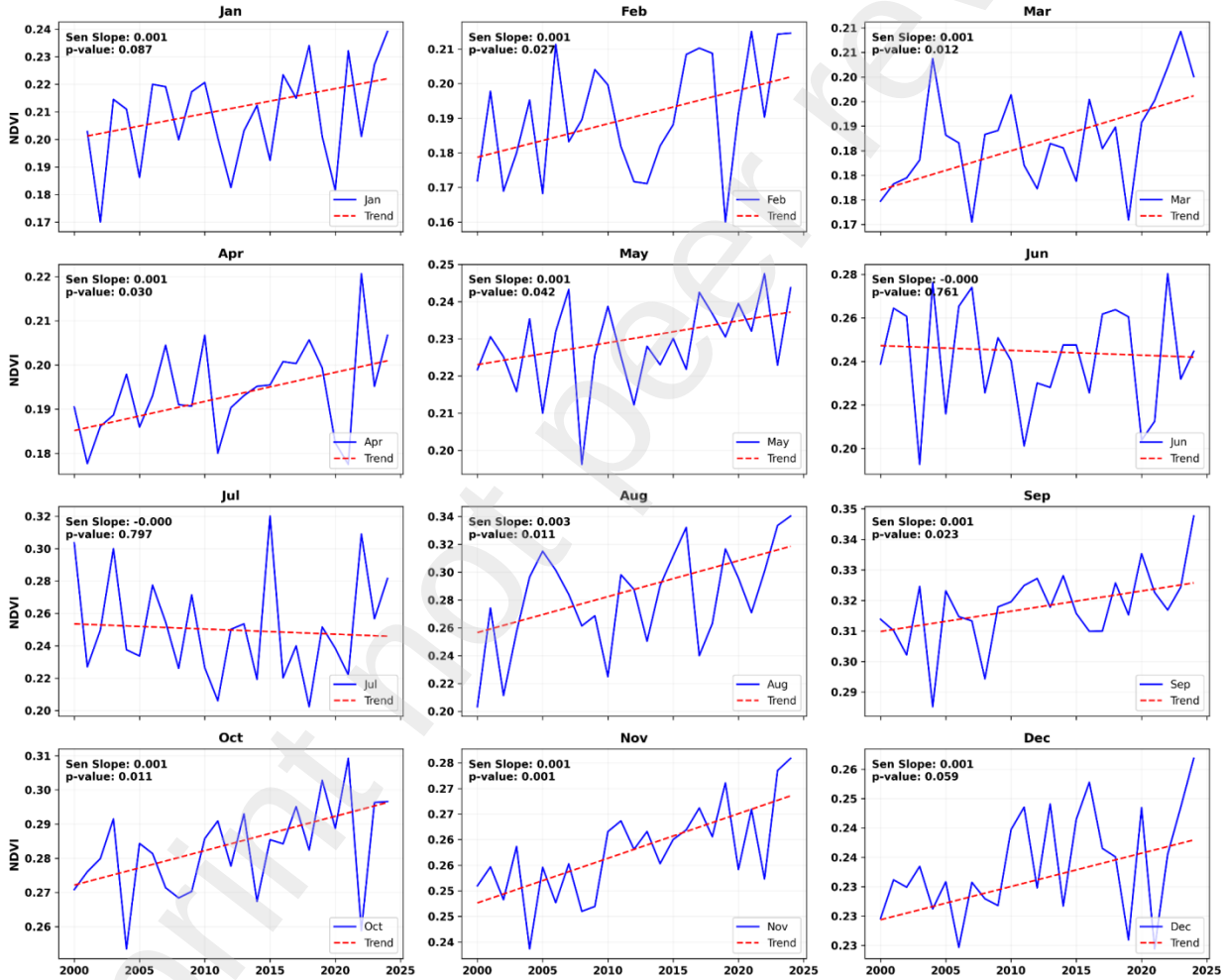

moderately high compared to the early dry months due to residual moisture and vegetation cover in the lowlands.

Figure 7: Monthly NDVI trends of KRB from 2000 to 2024

A heatmap representing the NDVI values across all months and years (Figure 8) further illustrates

seasonal cycles and interannual drought signals. Years such as 2002, 2004, and 2008 show reduced greenness during key growing months (Jun-Sep), aligning with reported drought episodes. Conversely, the post-2011 years tend to have particularly high NDVI.

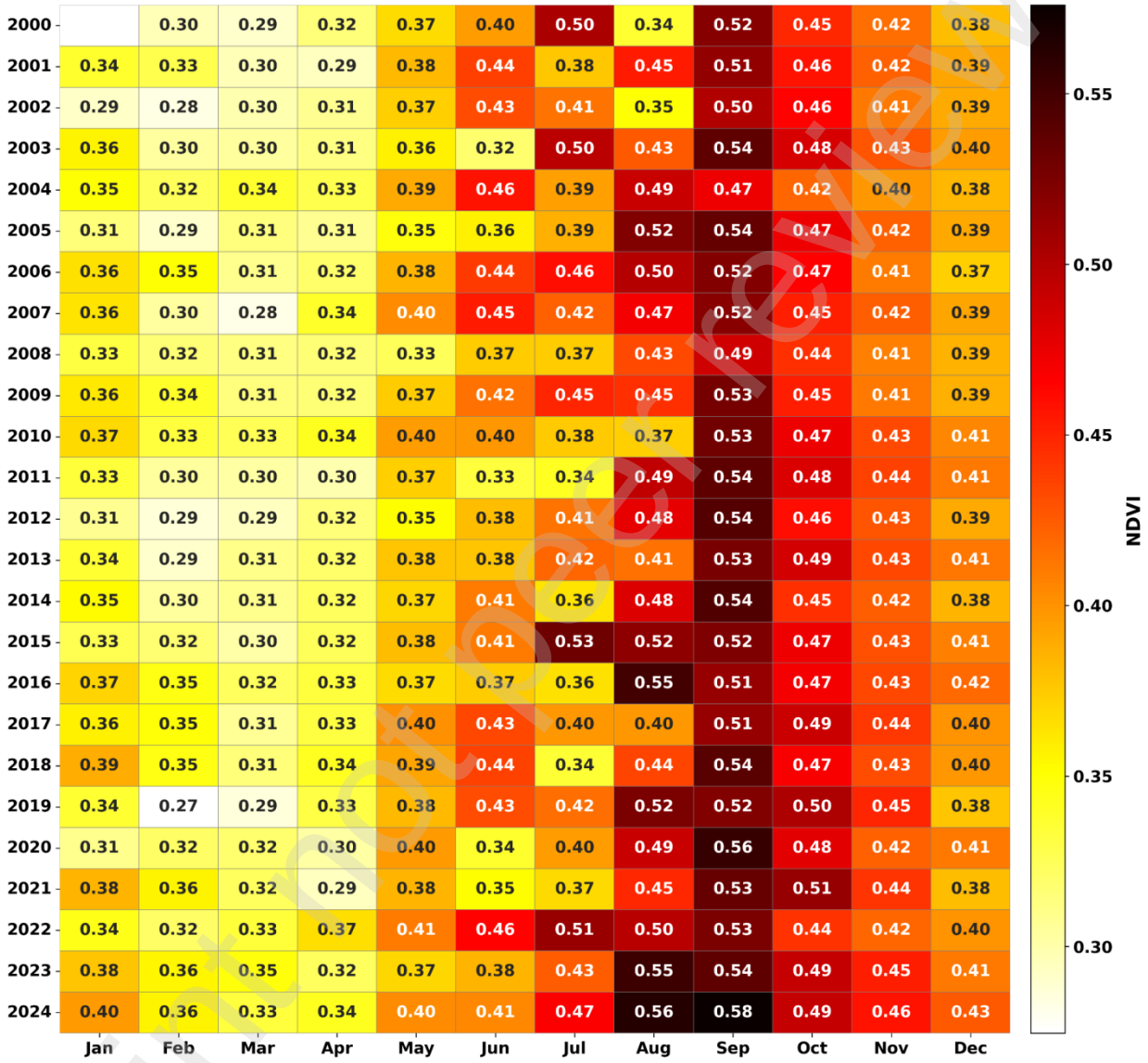

Figure 8: Heatmap of monthly NDVI values of KRB from 2000 to 2024

The monthly distribution of SMI (Figure 9) reveals a pronounced seasonal pattern, with peak values occurring during the core monsoon months of July (0.817) and August (0.909), succeeded by a gradual decline in the following months. The lowest mean SMI values are observed in November (0.296) and December (0.292), reflecting the dry conditions typical of the post-monsoon and early winter periods. Additionally, the standard deviation peaks in June (0.219),

indicating substantial variability in the onset of early monsoon rainfall. While some individual months display outliers in the boxplots, these variations are consistent with known climatic variability patterns. This monthly analysis emphasizes the distinct hydrological seasonality of the region, clearly distinguishing monsoon-driven moisture surpluses from pre- and post-monsoon deficits.

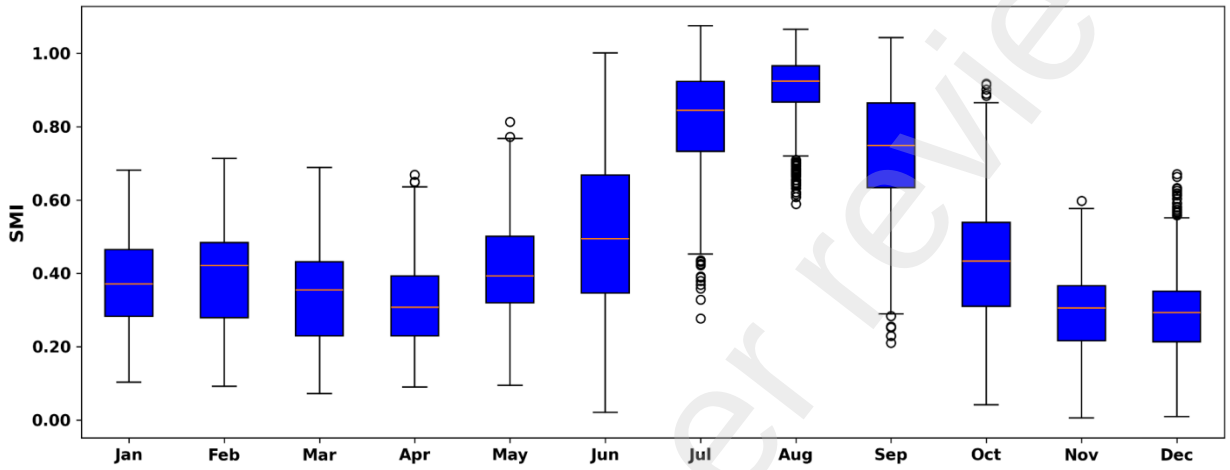

Figure 9: Monthly distribution of SMI of KRB from 1995 to 2024

4.4. Spatial Patterns of Drought

The spatial analysis of the three indicators is done to highlight gridwise drought variability and patterns. The spatial distribution of mean NDVI (Figure 10a) shows distinct patterns across elevation gradients. Higher NDVI values are consistently observed in the southern Terai plains and mid-hill regions, indicating dense and healthy vegetation cover. In contrast, the northern high-altitude areas exhibit persistently low NDVI values, generally below 0.2, corresponding to sparse alpine vegetation and snow-covered terrain. The mean NDVI values across the region range from a minimum of -0.10 to a maximum of 0.82, clearly highlighting the spatial heterogeneity in vegetation density and greenness.

The analysis of average annual NDVI change over the KRB for 2000-2024 indicates a slight overall increase in vegetation greenness, with a mean change of 0.0019 (Figure 10b). Spatially, the changes range from a minimum decrease of -0.0160 to a maximum increase of 0.0199, highlighting localized areas of vegetation loss and gain. The standard deviation (0.0022) suggests

that most of the basin experienced minor changes, with a few areas showing stronger variability (Figure 10b). Areas of positive NDVI changes dominate much of the basin, represented in red shades, while pockets of NDVI loss appear in blue tones, likely corresponding to areas facing land use change, water stress, or ecological degradation. This grid-level perspective enhances the temporal trend analysis by revealing localized patterns of vegetation recovery or stress that may not be evident from area-averaged data alone.

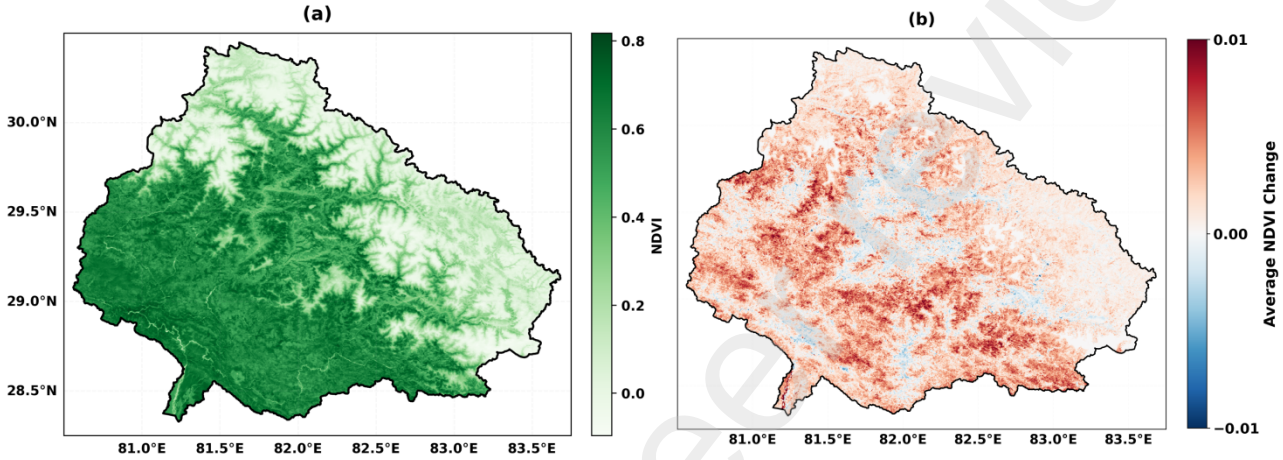

Figure 10: Spatial distribution of average NDVI (a) and its average change (b) from 2000 to 2024 over KRB

The spatial distribution of NDVI across the KRB shows a distinct seasonal pattern (Figure 11). During the monsoon season, there is a significant expanse of green coverage, which is then followed by the post-monsoon period. In contrast, the winter and pre-monsoon seasons exhibit relatively reduced vegetation due to limited precipitation. The post-monsoon season, in particular, shows dense vegetation, reflecting the delayed effects of monsoonal rainfall. As expected, high-altitude regions remain sparsely vegetated or non-vegetated throughout all seasons, due to cold temperatures and lack of moisture.

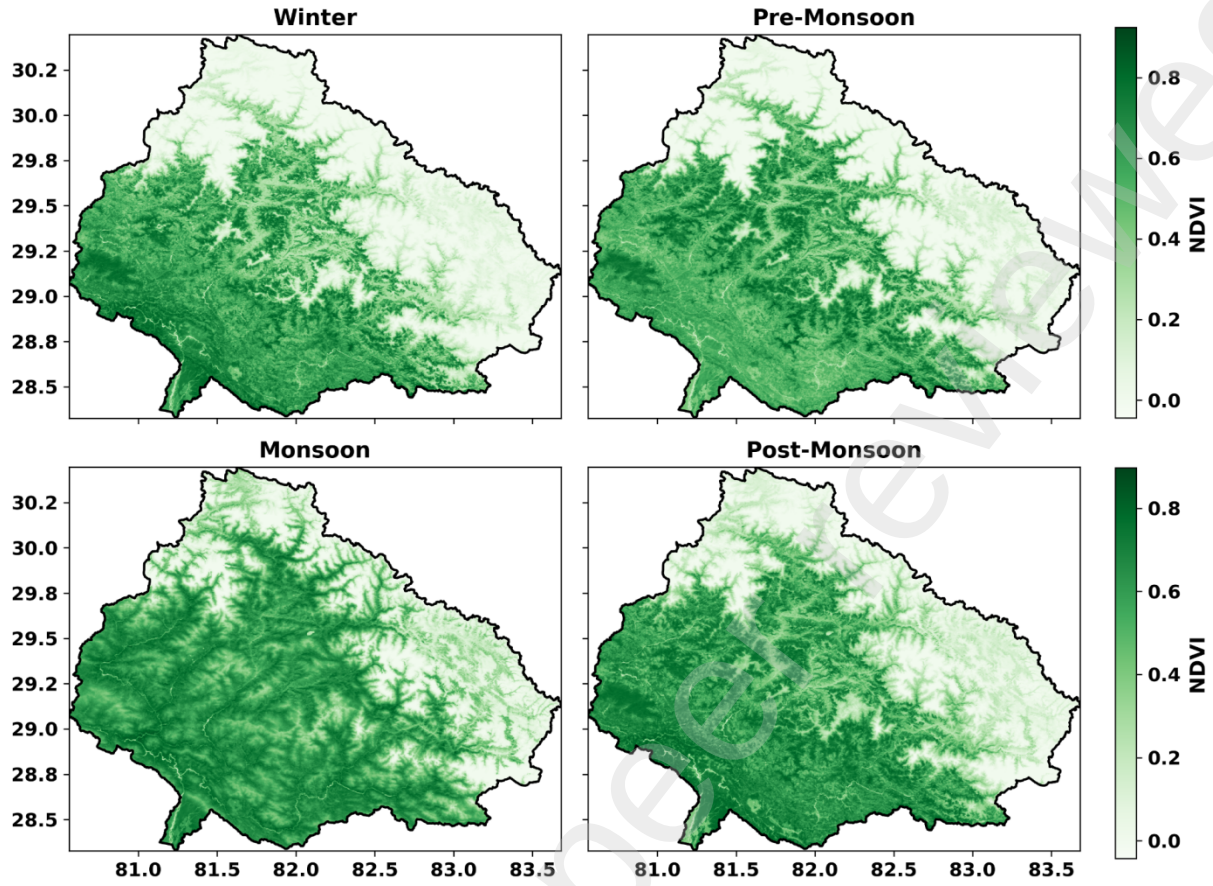

Figure 11: Spatial distribution of NDVI during different seasons of KRB from 2000 to 2024

The spatial maps for each month (Figure 12) similarly reveal pronounced eco-geographical gradients, with lower elevation Terai and mid-hills exhibiting strong monthly variation, while the high Himalayas maintain persistently low NDVI. This also illustrates the temporal coherence of NDVI patterns, highlighting September as a consistent peak month and February-March as periods of drought-induced stress.

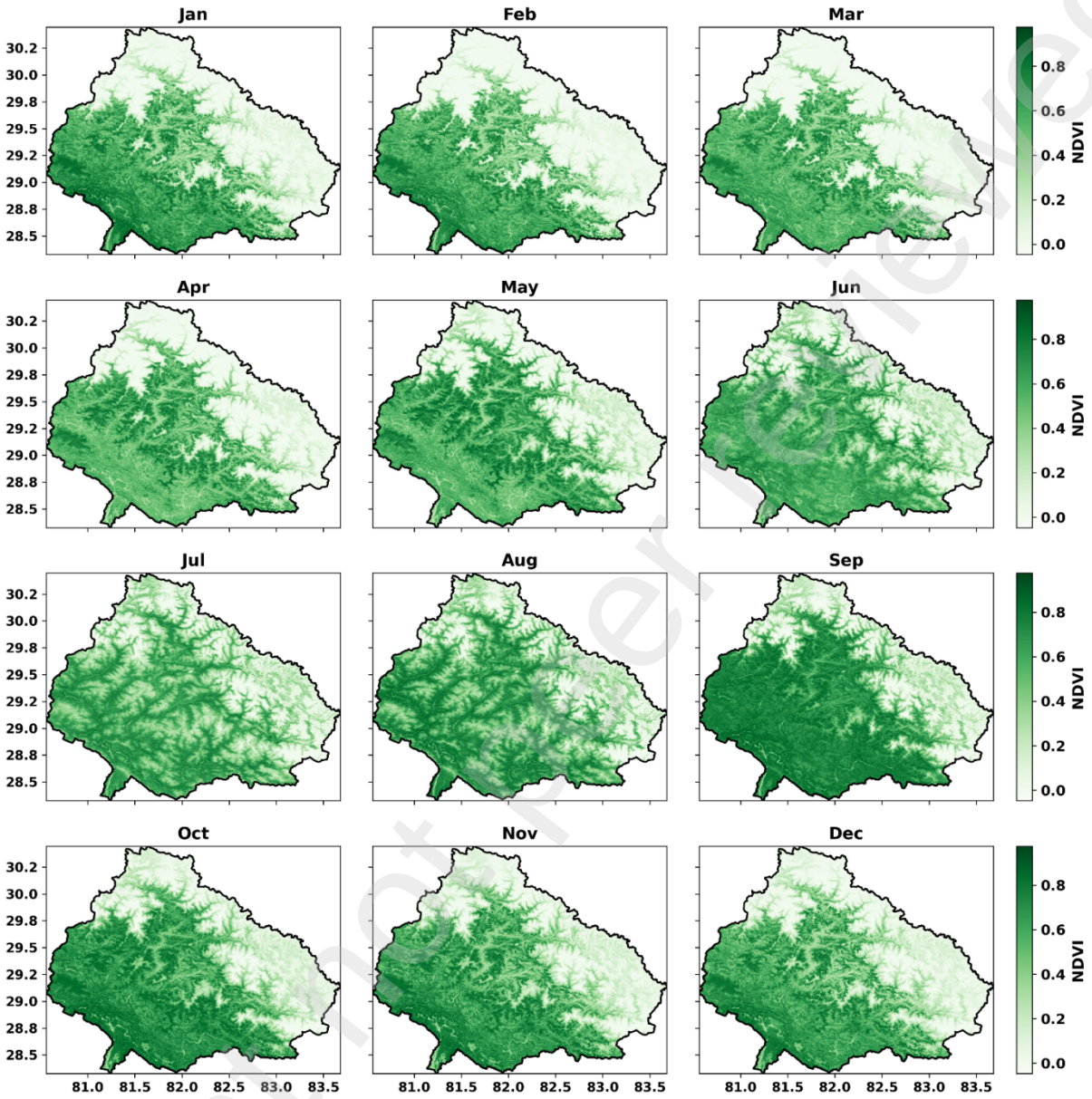

422 Figure 12: Spatial distribution of NDVI over KRB for representative months from 2000 to 2024

423

424 The spatial analysis of SMI trends across the grid cells from 1995 to 2024 highlights distinct
425 regional variations (Figure 13a). The spatial analysis across individual grid cells shows that most
426 areas exhibit small negative trends, with a mean Sen's slope of -0.0029 per year, and local slopes
427 ranging from -0.015 to 0.020 per year. The spatial distribution of trends is showing low spatial
428 variability (standard deviation = 0.008), highlighting that most of the basin is experiencing

consistent, minor reductions in soil moisture, reflecting general stability in overall basin hydrology despite some local variations.

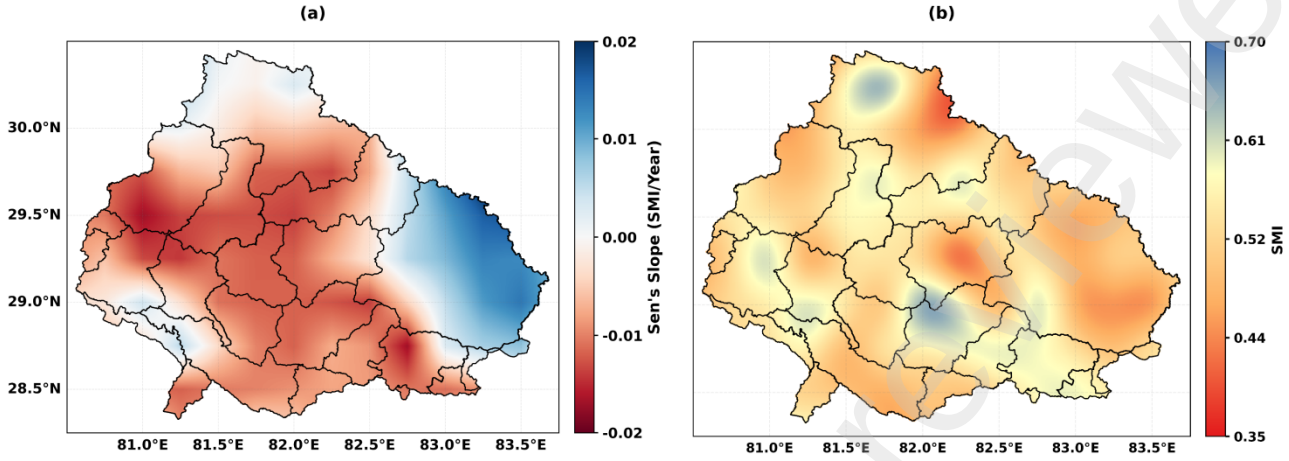

Figure 13: Spatial trend (a) and mean (b) of SMI over KRB from 1995 to 2024

Figure 13(b) shows the spatial distribution of the average SMI, which provides a general understanding of the typical soil moisture conditions across the KRB. The annual average SMI over the basin for 1995-2024 indicates moderate soil moisture conditions across the region, with a mean SMI of 0.532 and a median of 0.534. The minimum and maximum values (0.396 - 0.659) indicate localized variability, but the relatively low standard deviation (0.045) shows that most grid cells are clustered around the basin average.

SMI seasonal patterns analyzed spatially show that the monsoon months, spanning from June to September, exhibit notably higher soil moisture levels, indicating widespread wet conditions throughout the basin (Figure 14). In contrast, the pre-monsoon months, especially March and April, show lower SMI values with greater variability, reflecting the dry-season stress that precedes the arrival of monsoon rains. Unlike the NDVI results, the seasonal SMI data indicate that the post-monsoon period experiences relatively drier conditions compared to the pre-monsoon period. However, winter stands out as the driest season, with over half of the basin area registering values below approximately 0.35.

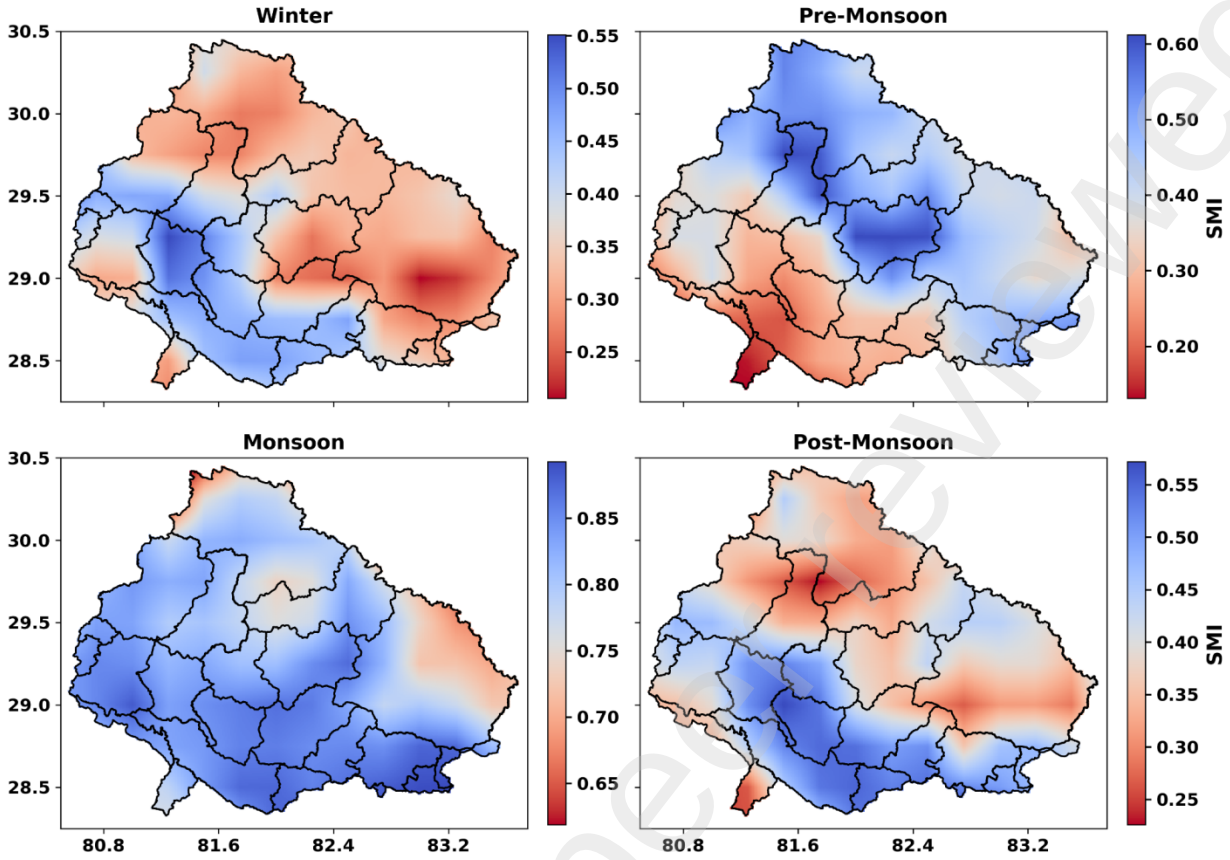

Figure 14: Seasonal distribution of SMI over KRB from 1995 to 2024

The monthly analysis of the SMI for the period 1995-2024 (Figure 15) shows clear seasonal fluctuations in moisture conditions across the KRB. The lowest mean SMI values are observed in December (0.296) and November (0.316), with minimum values reaching as low as 0.124 and 0.118, respectively. In contrast, the highest monthly mean values occur in August (0.933) and July (0.888), with maximum values reaching up to 0.977 and 0.978. These months also show higher central values, as indicated by median SMI values of 0.944 (August) and 0.930 (July). Standard deviations are lowest in August (0.039), indicating consistent high moisture conditions during the peak monsoon, and highest in May (0.176) and April (0.154), reflecting greater variability in the pre-monsoon period. Across all months, the data exhibit a gradual increase in SMI from March through August, followed by a steady decline toward the dry season.

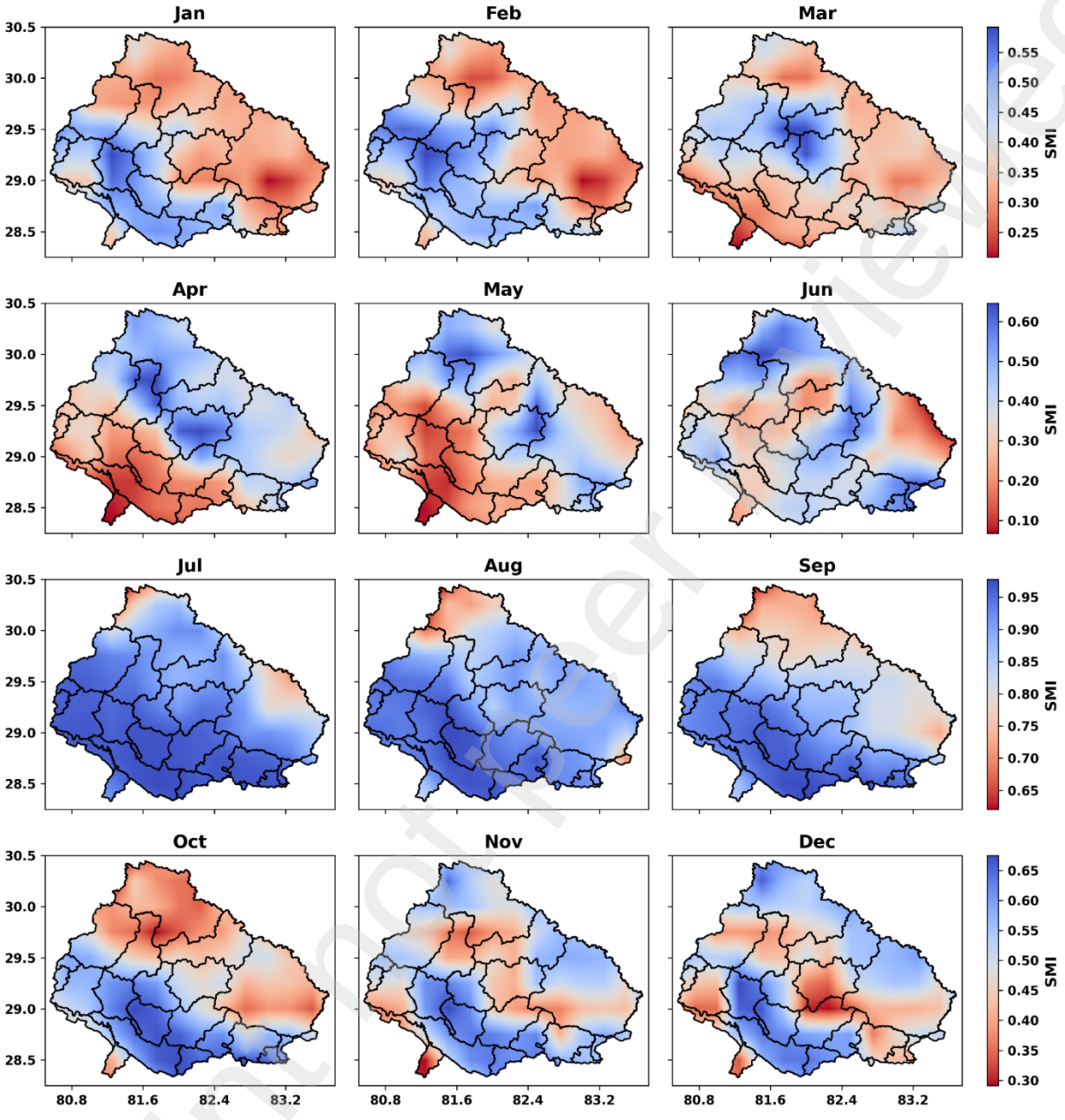

Figure 15: Monthly distribution of SMI over KRB from 1995 to 2024

For the spatial analysis of SPI over the KRB, the frequency of drought and wet anomalies was calculated on annual, seasonal, and monthly timescales. The resulting spatial maps (Figures 16, 17, 18) offer a more accurate representation of the frequency and distribution of dry and wet events across the basin.

The annual SPI drought and wet anomaly frequency analysis reveals that the frequency of extreme events remains relatively low on a yearly scale, typically between 5-7% across the SPI3, SPI6, and SPI12 timescales (Figure 17). For SPI3, the mean drought frequency is 6.43% and wet anomalies 6.87%, with a narrow variability (SD near 1). At longer accumulation periods, variability increases, particularly for SPI12, where dry and wet frequencies reach maximum values of 12.18% and 12.97% respectively. This indicates that, while annual drought and wet events are not widespread on average, prolonged accumulation periods (SPI12) capture stronger and more spatially extensive anomalies, consistent with the persistence of hydrological drought. The identified hotspots at SPI12 (with >12% frequency) highlight localized regions where drought and wet anomalies recur most frequently, underscoring their importance for water management.

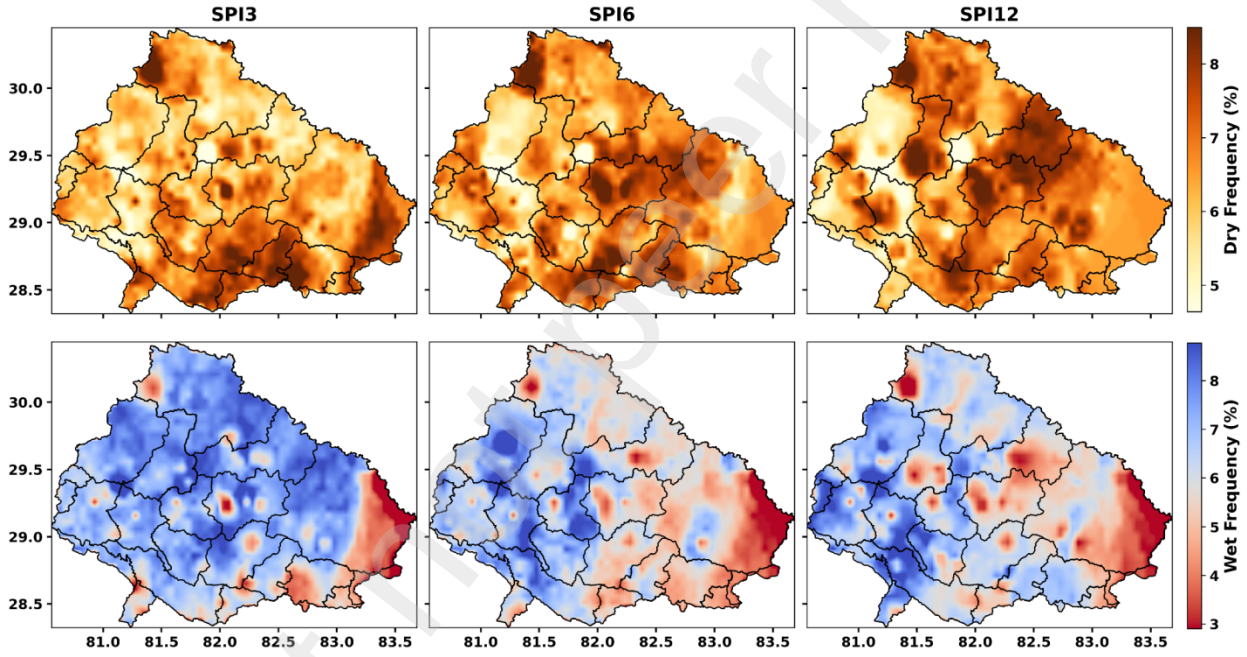

Figure 16: Annual Dry and Wet Anomaly Frequency over KRB from 1995 to 2024

The seasonal analysis reveals stronger intra-annual contrasts in drought and wet anomaly frequencies (Figure 17). In SPI3, dry anomalies are most frequent during the post-monsoon season (mean 7.91%), while wet anomalies peak in winter (mean 8.48%). SPI6 shows elevated drought frequencies in winter (mean 7.84%), whereas wet anomalies are more common in the pre-monsoon (mean 7.51%). For SPI12, both drought and wet anomalies display broader variability, with post-monsoon and winter seasons recording mean dry frequencies of around 7% and wet frequencies occasionally exceeding 6%. Importantly, variability (standard deviation) increases at longer

timescales, reaching up to 3.36 for wet anomalies in SPI12 post-monsoon. These findings suggest that drought and wet episodes exhibit clear seasonal dependency, with monsoon and post-monsoon conditions being particularly prone to extremes, while pre-monsoon and winter tend to capture more short-lived wet anomalies.

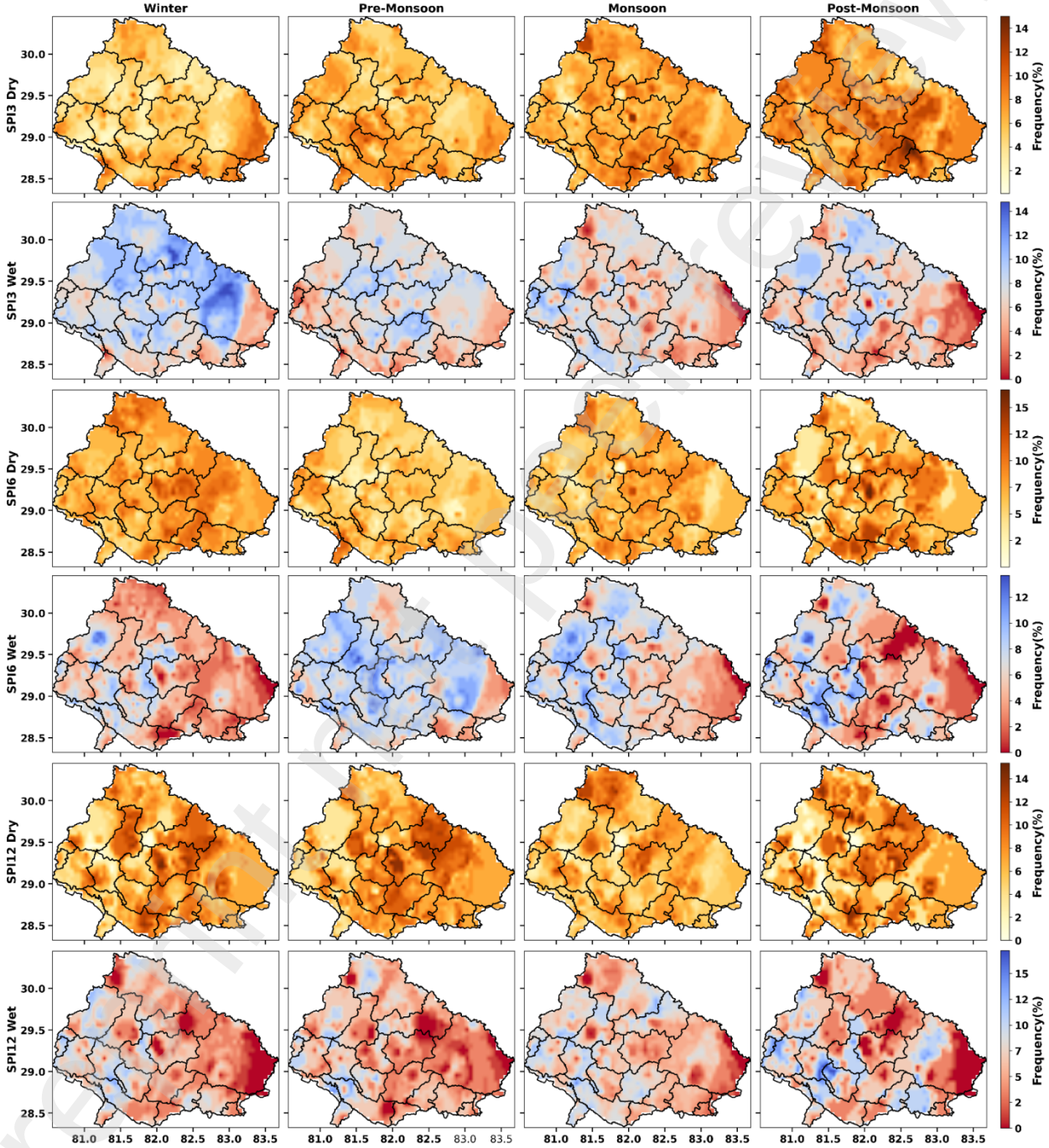

Figure 17: Seasonal Dry and Wet Anomaly Frequency from 1995 to 2024 of KRB

At the monthly scale, detailed statistics highlight peak drought and wet frequencies that are masked at broader temporal aggregations. In SPI3, November emerges as the driest month (8.35% mean drought frequency), while December is the wettest (10.66% mean wet frequency). For SPI6, drought conditions peak in February (8.38%) and wet anomalies in April (8.90%), consistent with early spring variability. SPI12 shows similar patterns, with February again recording the highest drought frequency (7.47%) and July emerging as the wettest month (6.97%), aligning with the monsoon onset. The monthly anomaly frequency spatial maps (Figure 18a-f) are provided in the supplementary material.

4.5. Categorical Classification of Drought

The category-based analysis of the monthly SMI for the KRB, as shown in Figure 19, suggests that the basin's soil moisture regime from 1995 to 2024 is predominantly characterized by near-normal to mildly dry conditions. The overall mean (0.003) and slightly negative median (-0.115) indicate moisture levels fluctuating around normal, with a tendency toward mild dryness. The mild drought category was the most frequent among others, occurring in 34.2% of months, followed by near-normal conditions at 26.7%. Wetter-than-normal conditions comprised approximately 19% of the recorded data. Severe drought was observed in only 0.6% of months, and no instances of extreme drought were observed, suggesting that while mild deficits are common, prolonged severe soil moisture stress is rarely encountered. Conversely, extremely wet months (2.2%) and severely wet months (6.1%) indicate that significant wet anomalies do occur occasionally. This distribution illustrates that soil moisture variability is primarily influenced by short-term deficits and surpluses, without persistent extreme drought conditions.

The monthly SMI z-score heatmap (Figure 20) further explains these trends by highlighting the temporal progression of dry and wet anomalies. Statistical properties support this distribution, with values ranging from a minimum of -0.841 to a maximum of 0.990, thereby covering nearly the entire theoretical range of the percentile-based index. The standard deviation of 0.490 underscores the considerable fluctuations observed across years, as well as the transitions between strongly negative (dry) and strongly positive (wet) anomalies. Overall, the heatmap emphasizes the significant impact of monsoonal rainfall, with distinct wet phases resulting in extremely high SMI

values, while extended non-monsoon periods typically exhibit mild to moderate droughts, reflecting the basin's sensitivity to seasonal hydrological dynamics.

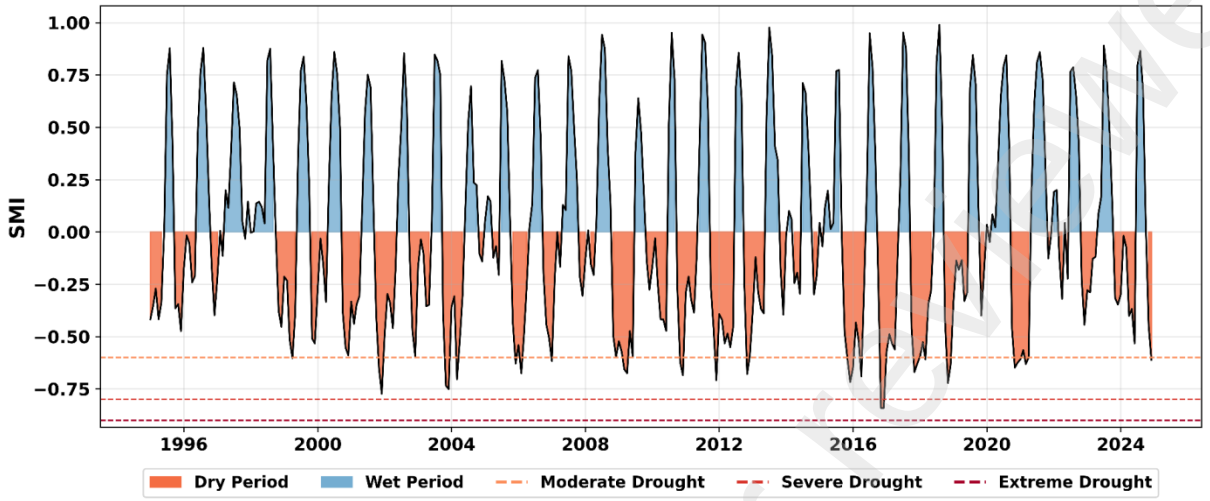

Figure 19: Monthly SMI Time series (category-based) of KRB from 1995 to 2024

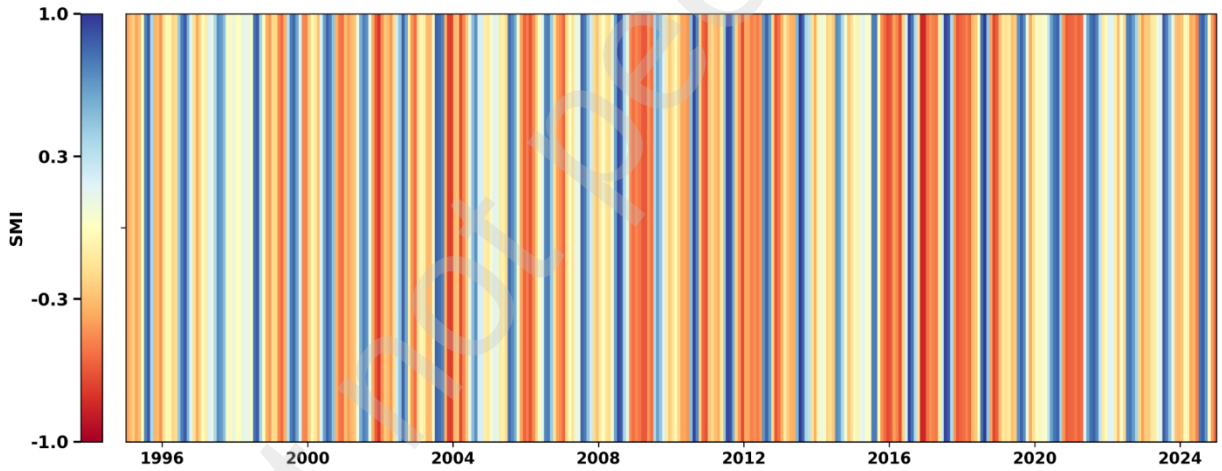

Figure 20: Heatmap of monthly time series for SMI of KRB from 1995 to 2024

The SPI heatmap (Figure 21) highlights alternating wet and dry phases, with notable severe droughts around 2000, 2016, and 2023, consistent across multiple timescales, suggesting periods of sustained hydroclimatic stress. Overall, these results indicate that both short- and long-term precipitation anomalies contribute to the occurrence of drought and wet events in the region, with long-term SPI capturing more extreme but less frequent anomalies.

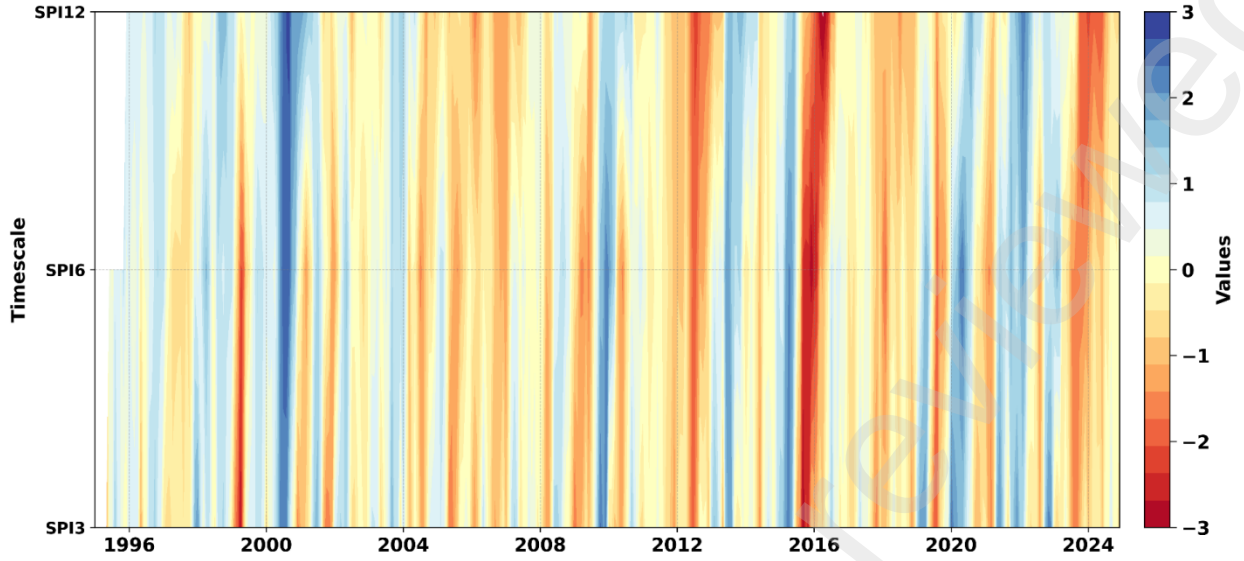

Figure 21: SPI time series heatmap of KRB from 1995 to 2024

The temporal analysis of standardized precipitation indices (SPI) at 3, 6, and 12-month timescales (Figure 22a-c) reveals distinct patterns of drought and wet conditions over the study period. SPI3, representing short-term precipitation variability, shows a mean near zero with a standard deviation of 1.0, indicating a generally balanced precipitation regime. Droughts (SPI < -1) occurred in 16.2% of months, with extreme droughts (SPI < -2) observed in 1.12% of months, while wet conditions (SPI > 1) were present in 15.6% of months and extreme wet events (SPI > 2) in 3.1%. At intermediate timescales (SPI6), the proportion of extreme drought months slightly increased to 2.25%, whereas wet events decreased marginally. Long-term precipitation variability (SPI12) shows fewer moderate drought months (14.6%) but a higher incidence of extreme droughts (2.87%), reflecting accumulated deficits over the year.

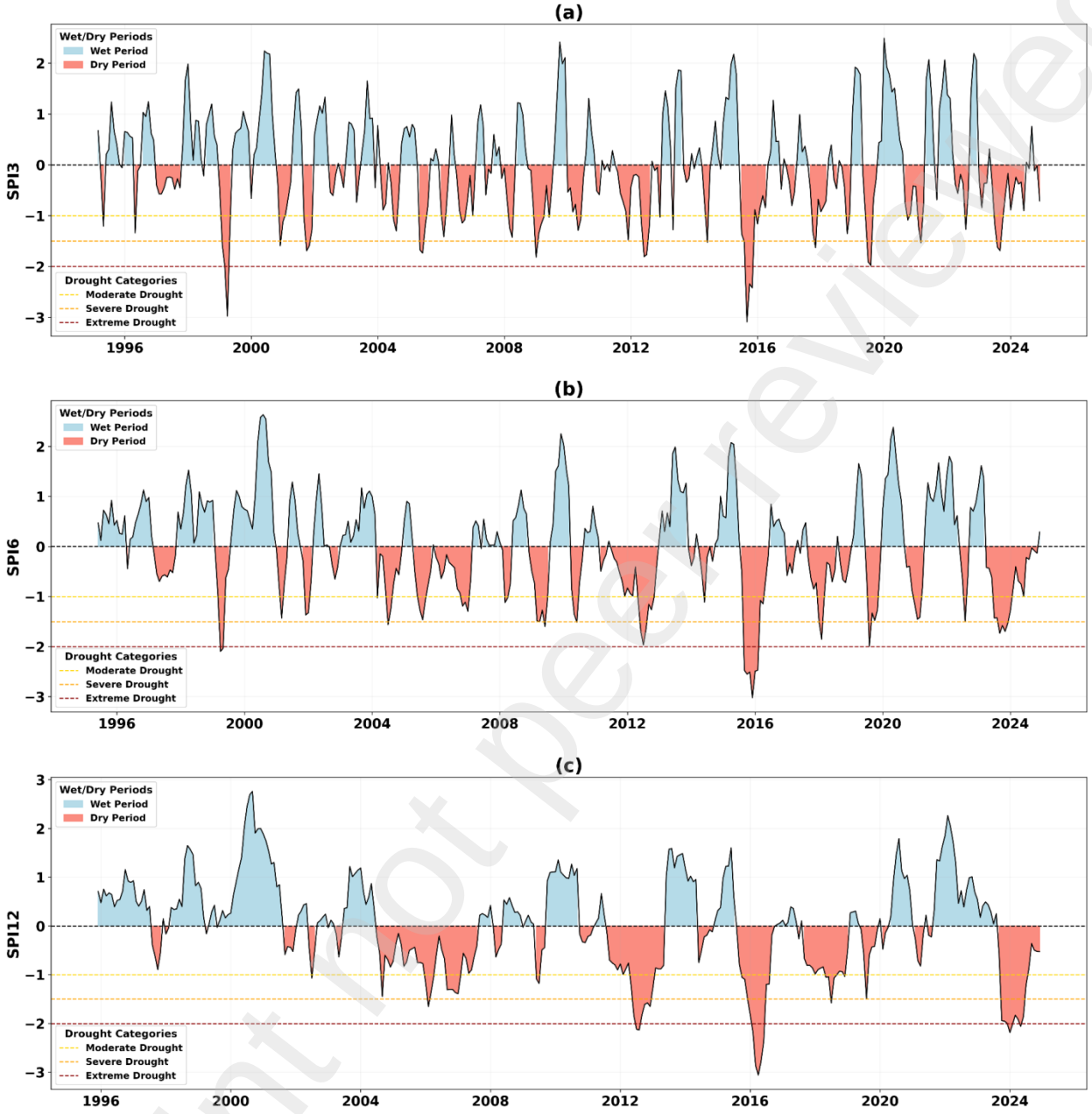

Figure 22: Categorical time series of drought in KRB from 1995 to 2024 based on SPIs

4.6. Meteorological and Agricultural Composites

4.6.1. Principal Component Analysis (PCA)

For the basin-average SPI, a single dominant principal component (PC1) was identified by the

PCA. This component accounts for 70.0 percent of the total variance; therefore, this component is in a position to represent most of the information contained in the three Standardized Precipitation Index (SPI) variables, as shown in Figure 23(a). In Figure 23(b), the cumulative variance plot, PC1 alone captures 70.0 percent of the variance, and a further addition of PC2 and PC3 captures a cumulative total of approximately 99.8 percent, meaning that a high level of information is represented by only three components. Likewise, PCA analysis of the agricultural data also provided one dominant component. Agricultural PC1 accounts for 61.2 percent of the total variance (Figure 23(a)). This component, though with a slightly reduced percentage than its meteorological counterpart, still contributes a large majority of the variance in the NDVI and SMI data.

The loadings plot (Figure 23c) further indicates that PC1 has strong positive loadings of all three variables of the SPI (SPI3, SPI6, and SPI12). This level of collinearity indicates that the three variables are very correlated among themselves, and they are the primary contributors to the same component. This positive correlation of strong values demonstrates that the meteorological PC1 could be viewed as a composite index that shows the general wetness or dryness situation at different time scales. Similarly, both NDVI and SMI showed a strong negative loading (-0.707) and a strong positive loading (0.707). This result indicates that the agricultural PC1 represents a contrast between vegetation health (NDVI) and soil moisture (SMI). This is a key finding because it indicates that low NDVI (poor vegetation health) periods are strongly connected with high SMI (wet soil), contrary to the intuitive idea, but can be reflected by certain conditions, such as rainy days that reduce the NDVI score but leave the ground moist. It also demonstrates the need to conduct further studies according to the elevation zones since the correlation between SMI and NDVI can be positive in the low-elevation and negative in the high-elevation areas.

The time series of both meteorological and agricultural PC1s were compared to assess their co-variability. The scatter plot in Figure 23(d) shows a positive correlation between the two composite indices, with a correlation coefficient (r) of 0.552. This moderate-to-strong positive relationship indicates that periods of high meteorological wetness (high positive values of meteorological PC1) are generally associated with conditions that favor the agricultural variables (high positive values of agricultural PC1), and vice versa.

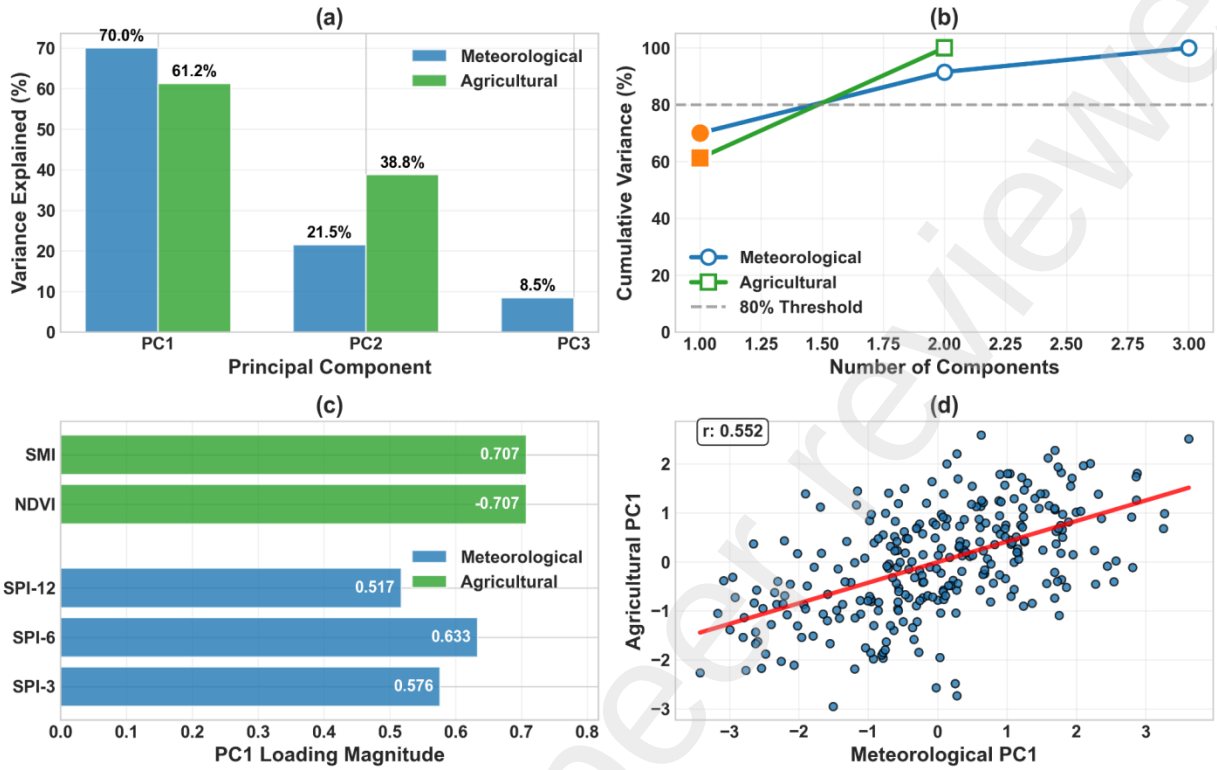

Figure 23: Barchart showing the percentage of variance explained by PCs for both meteorological and agricultural composites (a), Line plot showing the cumulative variance explained by increasing numbers of PCs for both composites (b). Horizontal bar chart illustrating the magnitude of the PC1 loading for each variable in both datasets (c), Scatter plot showing the correlation between the composite PC1 values for both composites with trendline (d).

4.6.2. Lag Analysis

The lag correlation analysis (Figure 24) highlights differences in how soil moisture and vegetation respond to meteorological drought conditions. The meteorological composite and SMI exhibit the highest correlation at 0-month lag, confirming an immediate response of soil moisture to precipitation anomalies. In contrast, the correlation between the meteorological composite and NDVI peaks at a 1-month lag, demonstrating a delayed vegetation response. This indicates that while soil moisture tracks rainfall deficits almost instantaneously, vegetation stress emerges after a short lag, reflecting both physiological delay and possible buffering by soil moisture availability.

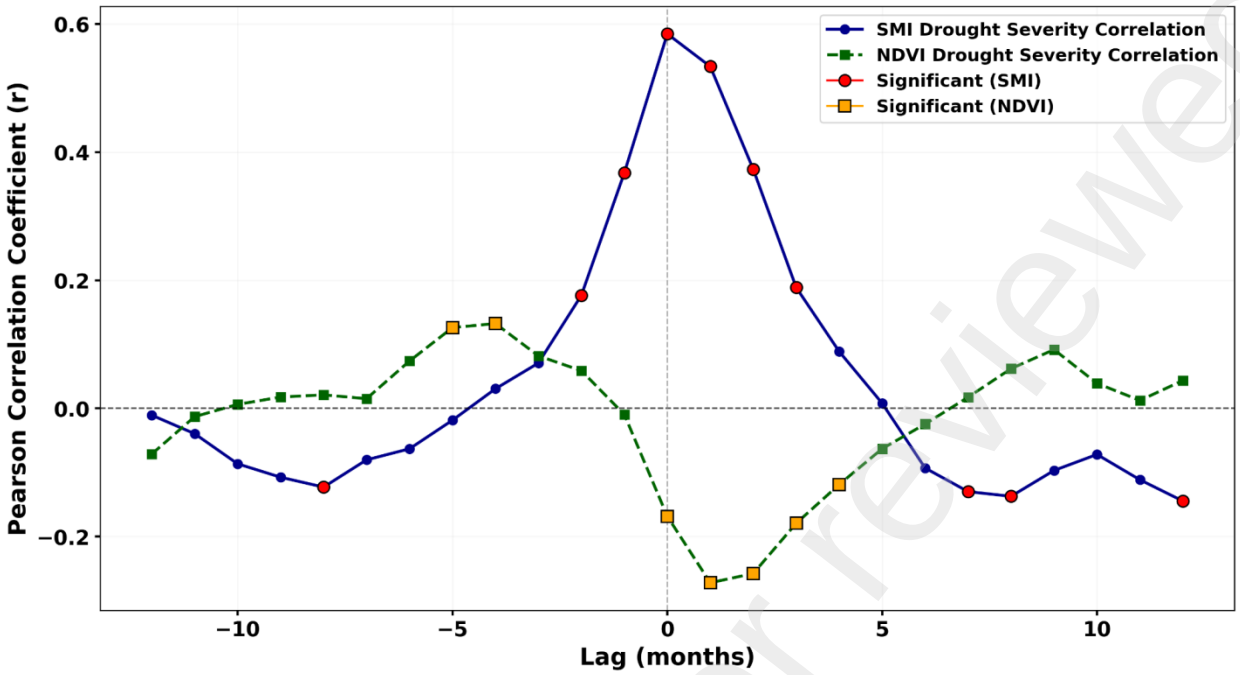

Figure 24: Lagged correlation between meteorological composite (SPI) and individual agricultural composite components (SMI and NDVI)

4.6.3. The Composite Correlation

The scatter plots (Figure 25a) show a moderate but significant relationship between the meteorological composite and the lag-adjusted agricultural composite ($r = 0.55$, $p < 0.05$, $R^2 = 0.30$). This suggests that about one-third of agricultural drought variability can be explained by meteorological anomalies after considering lag effects. The seasonal breakdown (Figure 24b) demonstrates clear differences in coupling strength: pre-monsoon ($r = 0.67$) and winter ($r = 0.66$) show the strongest relationships, while the link weakens during the monsoon ($r = 0.50$) and post-monsoon ($r = 0.34$) seasons. These results suggest that agricultural and ecological drought are most sensitive to meteorological deficits during typically water-stressed seasons (pre-monsoon, winter).

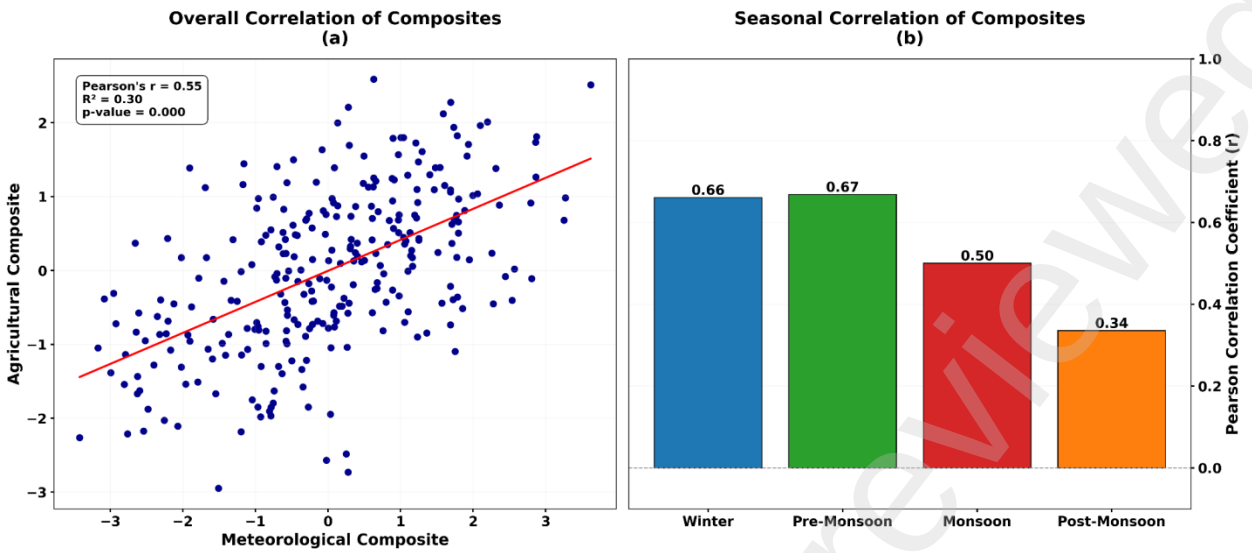

Figure 25: Correlation between composite indices, overall (a) and seasonal (b)

4.6.4. Time-series & Categorical Comparison

The time series (Figure 26) shows both composites generally following similar broad patterns from 2000-2024. However, important differences appear in their variability and drought expression. The meteorological composite (top) exhibits more pronounced fluctuations, featuring frequent and intense negative anomalies, reflecting the high instability of drought signals influenced by precipitation. On the other hand, the agricultural composite (bottom) appears more even, displaying fewer but more prolonged drought occurrences, aligning with the buffering role of soil moisture and vegetation in mediating short-term rainfall deficits.

The categorical representation strengthens these contrasts: the meteorological composite classified only about half the months as normal (52.26%), with relatively high proportions of severe (15.68%) and moderate (5.92%) droughts. By comparison, the agricultural composite showed a greater share of normal months (64.46%), fewer severe droughts (8.01%), but slightly more moderate droughts (10.45%). This divergence highlights that not all meteorological droughts translate into agricultural droughts, underlining the importance of monitoring both domains to capture the full drought continuum.

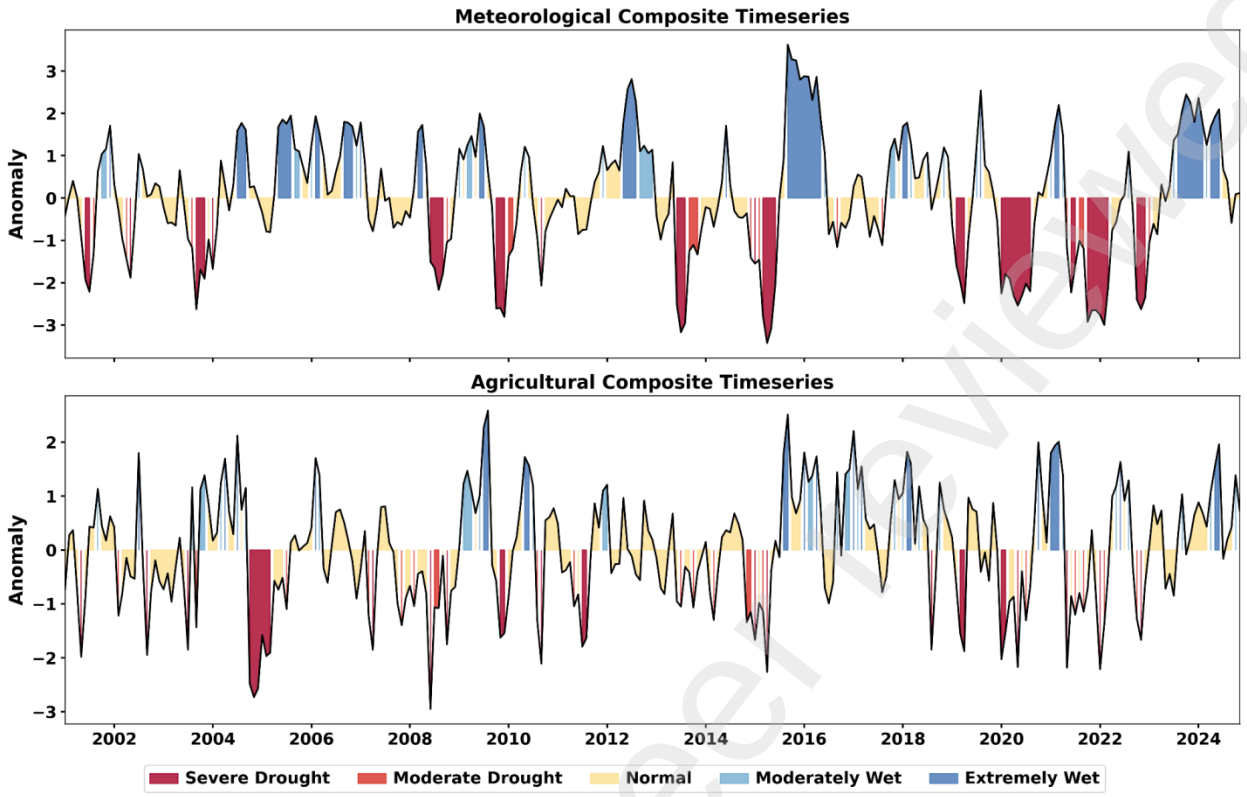

Figure 26: Categorical timeseries of meteorological and agricultural composite indices

4.6.5. Seasonal Variability & Drought Frequency

The seasonal variability analysis (Figure 27a) shows consistently higher standard deviation in the meteorological composite (1.4-1.5) compared to the agricultural composite (<1.2). This reflects the more volatile nature of precipitation-driven droughts relative to the smoother, lagged agricultural responses. Seasonal drought frequency (Figure 27b) shows some differences between indices. The meteorological composite has the highest drought frequency (>17.5%) during the monsoon, indicating recurrent meteorological anomalies even in the wettest season. By contrast, the agricultural composite peaks in winter (~10%), with the lowest drought frequency during the monsoon (~7.5%). This finding underlines that meteorological droughts are most common in the monsoon, but agricultural droughts are most critical in winter, when water availability is already low and vegetation is highly vulnerable.

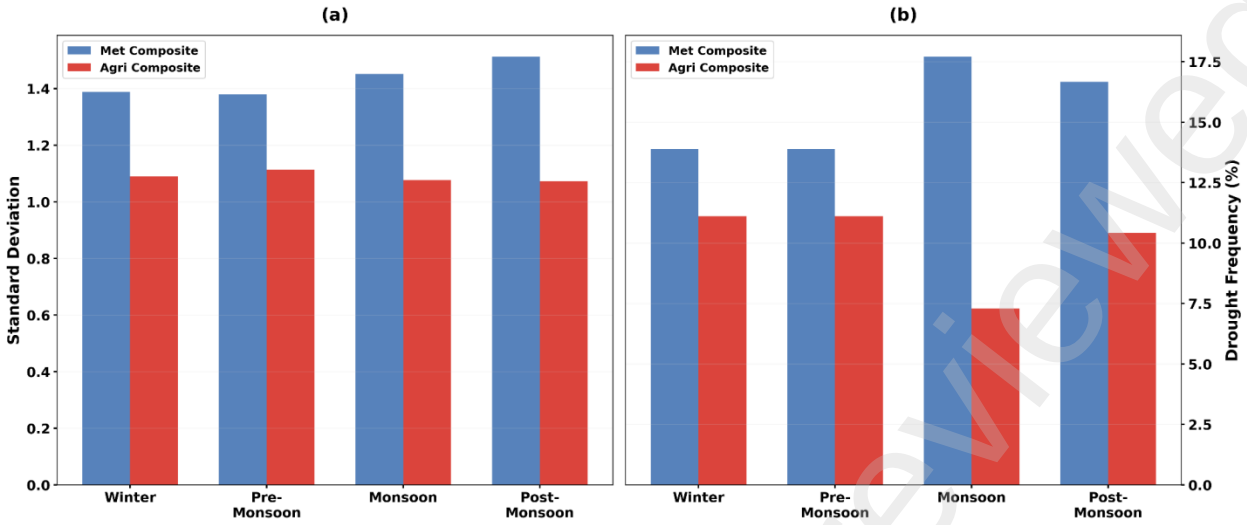

Figure 27: Seasonal variability (a) and drought frequency (b) of composites

5. Discussion and Conclusion

This paper presents a comprehensive framework of the Karnali River Basin (KRB) drought dynamics, as it merges meteorological, hydrological, and ecological views. Standardized indicators (SPI, SMI, and NDVI) were derived using precipitation records collected at in situ DHM stations, soil moisture estimates of ERA5, and vegetation indices of MODIS. The principal component analysis (PCA) was used to effectively correlate multi-scale precipitation variability with agricultural indicators. Trend analysis, spatial frequency mapping, categorical classification, and lagged vegetation responses were used to assess drought characteristics.

It was found that there was a significant decline in precipitation (SPI at longer accumulation periods), which is in agreement with previous researchers. According to Bagale et al. (2021), Nepal experienced higher drought frequency after the 1980s due to the weakening of monsoonal precipitation. Similarly, Aryal et al. (2022) reported the decreasing trends in precipitation in various basins, with the dry periods in the pre-monsoon and winter seasons intensifying significantly, which correlates well with these patterns. In the Karnali region, a recent study by Khatiwada & Pandey (2019) emphasizes the occurrence of recurrent meteorological droughts, particularly during the winter months. These droughts underscore the susceptibility of the region, as shown by short-term SPI anomalies. The study also demonstrates differences between seasons

and seasons, in terms of meteorological droughts being the most common in the monsoon season, and agricultural droughts being the most severe in winter. Similarly, Bista et al. (2021) found that winter drought was a major risk to the Sudurpashchim and Karnali provinces. Spatial heterogeneity shows that locations with mountain features experience more frequent drought events than Terai, which conforms to the results of Dahal et al. (2016) and Hamal et al. (2021), emphasizing the synergistic impacts of steep topography, shallow soils, and low irrigation.

There was no statistically significant long-term trend in the SMI, which indicated basin-scale hydrological stability in spite of decreasing precipitation. This is consistent with the findings of Dahal et al. (2020), who estimated water availability in the KRB in the future and highlighted the moderating impacts of snowmelt and irrigation. Similarly, Ghimire et al. (2020) discovered that crop productivity in western Nepal was able to endure reduced rainfall because of supplemental irrigation and traditional management practices. However, localized SMI declines determined in the spatial analysis coincide with Dahal et al.(2024) in the Koshi River Basin, where the soil moisture deficits caused yield losses in rain-fed agriculture. These underscore the fact that hydrological drought effects can be concealed at the basin level but still extreme in susceptible sub-regions. Moreover, the SMI is based on reanalysis climate, which requires more local data for evaluation and verification.

A modest but significant increasing trend in NDVI since 2000 was detected, with higher peaks during the monsoon and post-monsoon seasons. This supports findings by Baniya et al. (2018), who observed increases in vegetation health across Nepal using satellite-derived indices, particularly in irrigated and lowland areas. Krakauer et al. (2017) documented positive NDVI trends in mid-hill regions of Nepal, though stability or declines were noted at higher elevations, while Baniya et al. (2018) linked NDVI increases to rising temperatures and changing carbon dynamics. Collectively, these findings suggest that the positive NDVI trend in the KRB likely reflects both climatic variability and agricultural expansion in lowland areas, as previously proposed by Bocchiola et al. (2019).

PCA loadings revealed that agricultural drought variability was represented as a contrast between vegetation health and soil water availability, with NDVI showing a strong negative association

and SMI a strong positive association. This counterintuitive relationship, where low NDVI coincided with wet soils, may result from cloudy conditions suppressing vegetation signals despite sufficient soil moisture, or from the biases in the reanalysis SMI product. As well, the NDVI-SMI relationship may differ between lowlands and higher elevations.

A lag of about one month was observed in the response of NDVI to SMI, which is consistent with the study by Zhang et al. (2018). This reflects delayed vegetation response due to crop phenology and the buffering effects of soil. The immediate response of SMI to rainfall confirms its effectiveness as a hydrological drought indicator, while the delayed NDVI highlights the gradual onset of agricultural droughts. PCA-based composites revealed that meteorological droughts are highly volatile, whereas agricultural droughts develop more slowly. This difference underscores the buffering role of soil and vegetation, as observed by Weaver et al. (2025).

This result builds on earlier Nepal-focused studies by utilizing multiple drought indicators to provide a comprehensive framework for understanding the propagation of drought across meteorological, hydrological, and agricultural domains. The integrated approach aligns with recent recommendations for multi-scalar, integrated drought monitoring (IPCC, 2023; Ahady et al., 2025).

The findings emphasize the growing risks of drought in the Karnali River Basin (KRB), particularly during the pre-monsoon and winter seasons, when there is a decline in rainfall coupled with rising temperatures and increased agricultural water demand. The methodological framework employed in this study, utilizing multi-source data, anomaly-based indices, Principal Component Analysis (PCA) integration, and spatial-temporal analyses, establishes a transferable model for early warning systems, agricultural planning, and water resource management. Overall, these results underscore the significance of integrated drought monitoring frameworks in climate-vulnerable mountain basins and provide insights to guide adaptation strategies in response to escalating hydro-climatic variability in Nepal and other mountain regions.

6. Reference

Abdi, H., & Williams, L. J. (2010). Principal component analysis. *WIREs Computational Statistics*, *2*(4), 433–459. https://doi.org/10.1002/wics.101

Ahady, A. B., Klopries, E.-M., Schüttrumpf, H., & Wolf, S. (2025). Drought Analysis Methods: A Multidisciplinary Review with Insights on Key Decision-Making Factors in Method Selection. *Water*, *17*(15), 2248. https://doi.org/10.3390/w17152248

Alex, Ramesh, K., & Hari, S. (2017). *Alex, Elsu & Ramesh, K & Hari, Sridevi. (2017). Quantification and understanding the observed changes in land cover patterns in Bangalore. International Journal of Civil Engineering and Technology. 8. 597-603.* ResearchGate. https://www.researchgate.net/publication/316471841_Quantification_and_understanding_the_observed_changes_in_land_cover_patterns_in_Bangalore

Analyzing spatial patterns of meteorological drought using standardized precipitation index—Patel—2007—Meteorological Applications—Wiley Online Library. (n.d.). Retrieved July 13, 2025, from https://rmets.onlinelibrary.wiley.com/doi/10.1002/met.33

Aryal, Maharjan, M., Talchabhadel, R., & Thapa, B. R. (2022). Characterizing Meteorological Droughts in Nepal: A Comparative Analysis of Standardized Precipitation Index and Rainfall Anomaly Index. *Earth*, *3*(1), 409–432. https://doi.org/10.3390/earth3010025

Aziz, A., Umar, M., Mansha, M., Khan, M. S., Javed, M. N., Gao, H., Farhan, S. B., Iqbal, I., & Abdullah, S. (2018). Assessment of drought conditions using HJ-1A/1B data: A case study of Potohar region, Pakistan. *Geomatics, Natural Hazards and Risk*, *9*(1), 1019–1036. https://doi.org/10.1080/19475705.2018.1499558

Bagale, D., Sigdel, M., & Aryal, D. (2021). Drought Monitoring over Nepal for the Last Four Decades and Its Connection with Southern Oscillation Index. *Water*, *13*(23), Article 23. https://doi.org/10.3390/w13233411

Baniya, B., Tang, Q., Huang, Z., Sun, S., & Techato, K. (2018). Spatial and Temporal Variation of NDVI in Response to Climate Change and the Implication for Carbon Dynamics in Nepal. *Forests*, *9*(6), 329. https://doi.org/10.3390/f9060329

Baniya, B., Tang, Q., Xu, X., Haile, G. G., & Chhipi-Shrestha, G. (2019). Spatial and Temporal Variation of Drought Based on Satellite Derived Vegetation Condition Index in Nepal from 1982–2015. *Sensors*, *19*(2), 430. https://doi.org/10.3390/s19020430

Bastakoti, R. C., Bharati, L., Bhattarai, U., & Wahid, S. M. (2017). Agriculture under changing climate conditions and adaptation options in the Koshi Basin. *Climate and Development*, *9*(7), 634–648. https://doi.org/10.1080/17565529.2016.1223594

Below, R., Grover-Kopec, E., & Dilley, M. (2007). Documenting Drought-Related Disasters: A Global Reassessment. *The Journal of Environment & Development*, *16*(3), 328–344. https://doi.org/10.1177/1070496507306222

Berhan, G., Hill, S., Tadesse, T., & Atnafu, S. (2011). *Using Satellite Images for Drought Monitoring: A Knowledge Discovery Approach*.

Bista, N., Mahat, D., Manandhar, S., Regmi, B., Panday, U. S., & Karki, S. (2021). Analyzing Trend and Pattern of Agricultural Drought: A Case Study of Karnali and Sudurpashchim Provinces. *Journal on Geoinformatics, Nepal*, 1–8. https://doi.org/10.3126/njg.v20i1.39470

Bocchiola, D., Brunetti, L., Soncini, A., Polinelli, F., & Gianinetto, M. (2019). Impact of climate change on agricultural productivity and food security in the Himalayas: A case study in Nepal. *Agricultural Systems*, *171*, 113–125. https://doi.org/10.1016/j.agsy.2019.01.008

Bookhagen, B., & Burbank, D. W. (2010). Toward a complete Himalayan hydrological budget: Spatiotemporal distribution of snowmelt and rainfall and their impact on river discharge. *Journal of Geophysical Research: Earth Surface*, *115*(F3). https://doi.org/10.1029/2009JF001426

Dahal, N. M., Xiong, D., Neupane, N., Yuan, Y., Zhang, B., Zhang, S., Fang, Y., Zhao, W., Wu, Y., & Deng, W. (2024). Spatiotemporal assessment of drought and its impacts on crop yield in the Koshi River Basin, Nepal. *Theoretical and Applied Climatology*, *155*(3), 1679–1698. https://doi.org/10.1007/s00704-023-04719-3

Dahal, Shrestha, M. L., Panthi, J., & Pradhananga, D. (2020). Modeling the future impacts of climate change on water availability in the Karnali River Basin of Nepal Himalaya. *Environmental Research*, *185*, 109430. https://doi.org/10.1016/j.envres.2020.109430

Dahal, Shrestha, N. S., Shrestha, M. L., Krakauer, N. Y., Panthi, J., Pradhanang, S. M., Jha, A., & Lakhankar, T. (2016). Drought risk assessment in central Nepal: Temporal and spatial analysis. *Natural Hazards*, *80*(3), 1913–1932. https://doi.org/10.1007/s11069-015-2055-5

Demšar, U., Harris, P., Brunsdon, C., Fotheringham, A. S., & McLoone, S. (2013). Principal Component Analysis on Spatial Data: An Overview. *Annals of the Association of American Geographers*, *103*(1), 106–128. https://doi.org/10.1080/00045608.2012.689236

Didan, K. (2021). *MODIS/Terra Vegetation Indices 16-Day L3 Global 250m SIN Grid V061 [Data set]. NASA Land Processes Distributed Active Archive Center. Https://doi.org/10.5067/MODIS/MOD13Q1.061 Date Accessed: 2025-09-02* [Dataset]. Earth Science Data Systems, NASA. https://www.earthdata.nasa.gov/data/catalog/lpcloud-mod13q1-061

Dyer, S. A., & Dyer, J. S. (2001). Cubic-spline interpolation. 1. *IEEE Instrumentation & Measurement Magazine*, *4*(1), 44–46. https://doi.org/10.1109/5289.911175

Esch, S., Korres, W., Reichenau, T. G., & Schneider, K. (2018). Soil moisture index from ERS-SAR and its application to the analysis of spatial patterns in agricultural areas. *Journal of Applied Remote Sensing*, *12*(2), 022206. https://doi.org/10.1117/1.JRS.12.022206

Franke, R., & Nielson, G. (1980). Smooth interpolation of large sets of scattered data. *International Journal for Numerical Methods in Engineering*, *15*(11), 1691–1704. https://doi.org/10.1002/nme.1620151110

Ghimire, B., Maharjan, N., & Dotel, J. (2020). Drought assessment on barley and millet production in Karnali Province, Nepal. *Nepal Journal of Environmental Science*, *8*, 53–67. https://doi.org/10.3126/njes.v8i1.35729

Greenacre, M., Groenen, P. J. F., Hastie, T., D'Enza, A. I., Markos, A., & Tuzhilina, E. (2022). Principal component analysis. *Nature Reviews Methods Primers*, *2*(1), 100. https://doi.org/10.1038/s43586-022-00184-w

Hamal, K., Sharma, S., Khadka, N., Haile, G. G., Joshi, B. B., Xu, T., & Dawadi, B. (2020). Assessment of drought impacts on crop yields across Nepal during 1987–2017. *Meteorological Applications*, *27*(5), e1950. https://doi.org/10.1002/met.1950

Hamal, K., Sharma, S., Pokharel, B., Shrestha, D., Talchabhadel, R., Shrestha, A., & Khadka, N. (2021). Changing pattern of drought in Nepal and associated atmospheric circulation. *Atmospheric Research*, *262*, 105798. https://doi.org/10.1016/j.atmosres.2021.105798

Hersbach, H., Bell, B., Berrisford, P., Hirahara, S., Horányi, A., Muñoz-Sabater, J., Nicolas, J., Peubey, C., Radu, R., Schepers, D., Simmons, A., Soci, C., Abdalla, S., Abellan, X., Balsamo, G., Bechtold, P., Biavati, G., Bidlot, J., Bonavita, M., … Thépaut, J.-N. (2020). The ERA5 global reanalysis. *Quarterly Journal of the Royal Meteorological Society*, *146*(730), 1999–2049. https://doi.org/10.1002/qj.3803

Huang, G. (2021). Missing data filling method based on linear interpolation and lightgbm. *Journal of Physics: Conference Series*, *1754*(1), 012187. https://doi.org/10.1088/1742-6596/1754/1/012187

IPCC. (2023, March 19). *AR6 Synthesis Report: Climate Change 2023 — IPCC*. https://www.ipcc.ch/report/sixth-assessment-report-cycle/

Junninen, H., Niska, H., Tuppurainen, K., Ruuskanen, J., & Kolehmainen, M. (2004). Methods for imputation of missing values in air quality data sets. *Atmospheric Environment*, *38*(18), 2895–2907. https://doi.org/10.1016/j.atmosenv.2004.02.026

Kafle, H. (2015). Spatial and Temporal Variation of Drought in Far and Mid Western Regions of Nepal: Time Series Analysis (1982-2012). *Nepal Journal of Science and Technology*, *15*. https://doi.org/10.3126/njst.v15i2.12118

Karki, R., Hasson, S. ul, Schickhoff, U., Scholten, T., & Böhner, J. (2017). Rising Precipitation Extremes across Nepal. *Climate*, *5*(1), Article 1. https://doi.org/10.3390/cli5010004

Kendall. (1975). *Kendall: Rank correlation methods. - Google Scholar*. https://scholar.google.com/scholar_lookup?&title=Rank%20correlation%20methods&publication_year=1975&author=Kendall%2CM

Khatiwada, K. R., & Pandey, V. P. (2019). Characterization of hydro-meteorological drought in Nepal Himalaya: A case of Karnali River Basin. *Weather and Climate Extremes*, *26*, 100239. https://doi.org/10.1016/j.wace.2019.100239

Khatiwada, K. R., Panthi, J., Shrestha, M. L., & Nepal, S. (2016). Hydro-Climatic Variability in the Karnali River Basin of Nepal Himalaya. *Climate*, *4*(2), Article 2. https://doi.org/10.3390/cli4020017

Krakauer, N. Y., Lakhankar, T., & Anadón, J. D. (2017). Mapping and Attributing Normalized Difference Vegetation Index Trends for Nepal. *Remote Sensing*, *9*(10), Article 10. https://doi.org/10.3390/rs9100986

Mann, H. B. (1945). Nonparametric Tests Against Trend. *Econometrica*, *13*(3), 245–259. JSTOR. https://doi.org/10.2307/1907187

McKee, T. B., Doesken, N. J., & Kleist, J. (1993). *The relationship of drought frequency and duration to time scales*. *17*(22), 179–183.

Mishra, A. K., & Singh, V. P. (2010). A review of drought concepts. *Journal of Hydrology*, *391*(1), 202–216. https://doi.org/10.1016/j.jhydrol.2010.07.012

Nayava, J. L., Adhikary, S., & Bajracharya, O. R. (2017). Spatial and temporal variation of surface air temperature at different altitude zone in recent 30 years over Nepal. *MAUSAM*, *68*(3), Article 3. https://doi.org/10.54302/mausam.v68i3.649

Palazzi, E., von Hardenberg, J., & Provenzale, A. (2013). Precipitation in the Hindu-Kush Karakoram Himalaya: Observations and future scenarios. *Journal of Geophysical Research: Atmospheres*, *118*(1), 85–100. https://doi.org/10.1029/2012JD018697

Panthi, B. B. (2014). Analysis of Agricultural Drought and its Effects on Productivity at Different District of Nepal. *Journal of Institute of Science and Technology*, *19*, 106–110. https://doi.org/10.3126/jist.v19i1.13835

Paulhus, J. L. H., & Kohler, M. A. (1952). *INTERPOLATION OF MISSING PRECIPITATION RECORDS*. https://journals.ametsoc.org/view/journals/mwre/80/8/1520-0493_1952_080_0129_iompr_2_0_co_2.xml

Potopová, V., Boroneanţ, C., Boincean, B., & Soukup, J. (2016). Impact of agricultural drought on main crop yields in the Republic of Moldova. *International Journal of Climatology*, *36*(4), 2063–2082. https://doi.org/10.1002/joc.4481

Rimal, B., Zhang, L., & Rijal, S. (2018). Crop Cycles and Crop Land Classification in Nepal Using MODIS NDVI. *Remote Sensing in Earth Systems Sciences*, *1*(1), 14–28. https://doi.org/10.1007/s41976-018-0002-4

Shrestha, M. L. (2000). Interannual variation of summer monsoon rainfall over Nepal and its relation to Southern Oscillation Index. *Meteorology and Atmospheric Physics*, *75*(1), 21–28. https://doi.org/10.1007/s007030070012

Sigdel, M., & Ikeda, M. (2010). Spatial and Temporal Analysis of Drought in Nepal using Standardized Precipitation Index and its Relationship with Climate Indices. *Journal of Hydrology and Meteorology*, *7*(1), 59–74. https://doi.org/10.3126/jhm.v7i1.5617

Silva, R. P. D., Dayawansa, N. D. K., & Ratnasiri, M. D. (2016). *A comparison of methods used in estimating missing rainfall data | Journal of Agricultural Sciences – Sri Lanka*. https://doi.org/10.4038/jas.v3i2.8107

Singh, A., Solanki, H., & Sharma, P. J. (2024). Dynamic evolution of meteorological and hydrological droughts under climatic and anthropogenic pressures in water-scarce regions. *Hydrological Processes*, *38*(10), e15290. https://doi.org/10.1002/hyp.15290

Tung, Y.-K. (1983). Point Rainfall Estimation for a Mountainous Region. *Journal of Hydraulic Engineering*, *109*(10), 1386–1393. https://doi.org/10.1061/(ASCE)0733-9429(1983)109:10(1386)

Ullah, I., Ma, X., Yin, J., Omer, A., Habtemicheal, B. A., Saleem, F., Iyakaremye, V., Syed, S., Arshad, M., & Liu, M. (2023). Spatiotemporal characteristics of meteorological drought variability and trends (1981–2020) over South Asia and the associated large-scale circulation patterns. *Climate Dynamics*, *60*(7), 2261–2284. https://doi.org/10.1007/s00382-022-06443-6

Vicente-Serrano, S. M., Beguería, S., & López-Moreno, J. I. (2010). A Multiscalar Drought Index Sensitive to Global Warming: The Standardized Precipitation Evapotranspiration Index. *Journal of Climate*, *23*(7), 1696–1718. https://doi.org/10.1175/2009JCLI2909.1

Wagner, W., Lemoine, G., & Rott, H. (1999). A Method for Estimating Soil Moisture from ERS Scatterometer and Soil Data. *Remote Sensing of Environment*, *70*(2), 191–207. https://doi.org/10.1016/S0034-4257(99)00036-X

Weaver, S. M., Lupo, A. R., Hunt, S., & Aloysius, N. (2025). Refining Drought Assessment: A Multi-Dimensional Analysis of Condition Monitoring Observer Reports in Missouri (2018–2024). *Atmosphere*, *16*(4), 389. https://doi.org/10.3390/atmos16040389

Wilhite, D., Svoboda, M., & Hayes, M. (2007). Understanding the Complex Impacts of Drought: A Key to Enhancing Drought Mitigation and Preparedness. *Water Resources Management*, *21*, 763–774. https://doi.org/10.1007/s11269-006-9076-5

Wilhite, & Glantz, M. H. (1985). Understanding: The Drought Phenomenon: The Role of Definitions. *Water International*, *10*(3), 111–120. https://doi.org/10.1080/02508068508686328

Wilhite, & Pulwarty, R. S. (2017). Drought and Water Crises: Lessons Drawn, Some Lessons Learned, and the Road Ahead. In *Drought and Water Crises*. CRC Press.

Yue, S., & Wang, C. (2004). The Mann-Kendall Test Modified by Effective Sample Size to Detect Trend in Serially Correlated Hydrological Series. *Water Resources Management*, *18*(3), 201–218. https://doi.org/10.1023/B:WARM.0000043140.61082.60

Zhang, H., Chang, J., Zhang, L., Wang, Y., Li, Y., & Wang, X. (2018). NDVI dynamic changes and their relationship with meteorological factors and soil moisture. *Environmental Earth Sciences*, *77*(16), 582. https://doi.org/10.1007/s12665-018-7759-x